[redacted]

[redacted]

NASA TECHNICAL MEMORANDUM

NASA TM X-2618

NASA TM X-2618

INVESTIGATION AT NEAR-SONIC SPEED OF SOME EFFECTS OF HUMIDITY ON THE LONGITUDINAL AERODYNAMIC CHARACTERISTICS OF AN NASA SUPERCRITICAL WING RESEARCH AIRPLANE MODEL

[redacted]

by Frank L. Jordan, Jr.

Langley Research Center
Hampton, Va. 23365

NATIONAL AERONAUTICS AND SPACE ADMINISTRATION • WASHINGTON, D. C. • AUGUST 1972

[redacted]

INVESTIGATION AT NEAR-SONIC SPEED OF SOME EFFECTS OF HUMIDITY ON THE LONGITUDINAL AERODYNAMIC CHARACTERISTICS OF AN NASA SUPERCRITICAL WING RESEARCH AIRPLANE MODEL*

By Frank L. Jordan, Jr.
Langley Research Center

SUMMARY

An investigation has been conducted in the Langley 8-foot transonic pressure tunnel to determine the effects of humidity at near-sonic speed on the longitudinal aerodynamic characteristics and wing pressure distributions of an area-rule research airplane model with an NASA supercritical wing. Effects of dewpoint at the normal tunnel operating stagnation temperature of 48.9° C (120° F) and effects of stagnation temperature at a relatively high dewpoint of 15.6° C (60° F) were investigated. The test tunnel stagnation pressure was 101 325 N/m^2 (1 atmosphere).

The results demonstrated that condensation originating principally in the local expansion regions around the model before the occurrence of appreciable condensation in the free stream can cause significant effects on model test data at near-sonic speed. At moderate angles of attack the wing upper surface pressures were increased in the region of supersonic flow beginning near the leading edge. These effects on the wing pressures, believed to be caused by condensation originating principally in the local regions of supersonic flow over the wings, resulted in significant reductions in the lift coefficients.

Because of the extensive regions of supersonic flow over the wing upper surfaces at near-sonic speed, the lifting characteristics of supercritical wings may be particularly sensitive to wind-tunnel humidity at these speeds.

The occurrence of condensation in the free stream corresponded approximately to the onset of estimated free-stream saturation conditions. It was accompanied by an alteration in the test-section wall Mach number distributions, a reduction in the model base pressure, an increase in the model drag, a forward movement of the shock on the wing upper surface, and a further increase in the wing pressures that resulted in a decrease in lift coefficient.

---

*Title, Unclassified.

Decreasing the tunnel stagnation temperature resulted in humidity effects similar to those incurred by increasing the dewpoint, and increasing the temperature resulted in a reduction of these humidity effects.

INTRODUCTION

It is a well-established fact that humidity effects can invalidate wind-tunnel data (refs. 1 to 11). Condensation may be observed upstream of and in the test section or because of the higher local velocities and corresponding temperature reductions, may be seen originating only in the local expansion regions around the test model. In both cases test-section conditions and test measurements are affected.

The absence of visible condensation, however, is no guarantee that condensed moisture does not exist in the flow, particularly in the regions of rapid expansion over airfoils. If the pre-existing nuclei on which water particles can condense are too few or the rate of expansion is too large, the degree of supercooling (amount by which the local static flow temperature sinks below the saturation temperature in a given isentropic expansion of moist air) may become large enough to promote spontaneous nucleation. The particles produced in spontaneous nucleation may be so small as to be visible only by light scattering and not as fog.

Unfortunately, it is not possible to arrive at quantitative predictions of humidity effects on model testing. The effects on the various force and pressure coefficients will depend on a number of factors such as scale, Mach number, measurement procedures, stagnation temperature, dewpoint, and model geometry. Such quantitative predictions would require tests spanning the whole domain of realizable applicable parameters.

However, wind-tunnel investigations on the effects of humidity on the various aerodynamic data of representative test models can provide useful information on the nature of the effects which occur. Most previous investigations have been conducted in relatively small wind tunnels and because of the occurrence of condensation shocks, have been restricted to supersonic speeds. (See refs. 3, 5, and 7 to 10.) In addition, a limited amount of data has been obtained at high subsonic speeds, where, because of local regions of supersonic flow, condensation shocks may also occur (refs. 2 and 9).

With the recent development of the NASA supercritical airfoil (refs. 12 to 17), aircraft operational cruise speeds approaching a Mach number of unity have been demonstrated. Data on the effects of humidity on model testing at near-sonic speed however are limited. The present investigation, therefore, was performed in order to study some of the effects of humidity at near-sonic speed on a representative model incorporating an NASA supercritical wing.

SYMBOLS

Values are given in both SI and U.S. Customary Units. Measurements and calculations were made in U.S. Customary Units. All coefficients are based on the dimensions of the basic wing panel which does not include the leading-edge glove or the trailing-edge extension. (See fig. 1(a).) The total pitching-moment coefficients are referenced to the quarter-chord point of the mean geometric chord located at model station 99.45 cm (39.155 in.).

The terms, equations, and charts used to describe the properties of humid air can be found in the existing literature (refs. 1 to 3 and 7 to 11), and are not included in the present report.

Symbols used herein are defined as follows:

b wing span, 114.30 cm (45.0 in.)

C_D total drag coefficient, $\frac{\text{Drag}}{q_\infty S}$

C_L total lift coefficient, $\frac{\text{Lift}}{q_\infty S}$

C_m total pitching-moment coefficient, $\frac{\text{Pitching moment}}{q_\infty S\bar{c}}$

C_p pressure coefficient, $\frac{p - p_\infty}{q_\infty}$

$C_{p,b}$ base-pressure coefficient, $\frac{p_b - p_\infty}{q_\infty}$

c local streamwise chord of basic wing panel, cm (in.)

$\bar{c}$ wing-panel mean geometric chord, 18.09 cm (7.121 in.)

c_n wing-section normal-force coefficient, $\int_{\text{L.E.}}^{\text{T.E.}} \left(C_{p,l} - C_{p,u}\right) d\left(\frac{x}{c}\right)$

M Mach number

M_{sat} Mach number of a given isentropic expansion of moist air where static pressure and temperature of flow are equal to saturation pressure and temperature of water vapor (see ref. 11)

M_∞ free-stream Mach number

p	static pressure, N/m^2 (lb/ft^2)
p_b	base pressure, N/m^2 (lb/ft^2)
p_∞	free-stream static pressure, N/m^2 (lb/ft^2)
q_∞	free-stream dynamic pressure, N/m^2 (lb/ft^2)
S	wing area of basic panel including fuselage intercept, 0.193 $meter^2$ (2.075 ft^2)
s	tunnel test-section semispan at slot origin, 1.087 meters (3.563 ft)
T_{dp}	tunnel dewpoint measured at pressure of 101 325 N/m^2 (1 atmosphere), ^oC (^oF)
T_t	tunnel stagnation temperature, ^oC (^oF)
x	longitudinal location of pressure orifice, measured from test-section slot origin or from leading edge of local chord of basic wing panel, cm (in.)
y	spanwise distance from plane of symmetry, cm (in.)
α	angle of attack, referred to fuselage reference line, deg

Subscripts:

l	wing lower surface
u	wing upper surface

Abbreviations:

L.E.	leading edge
T.E.	trailing edge

APPARATUS AND PROCEDURES

Model

Geometric characteristics and photographs of the sting-supported 0.087-scale model are presented in figures 1 and 2, respectively. The model had fore-and-aft fuselage side fairings to improve the longitudinal development of cross-sectional area. It was also equipped with flow-through ducts, split at the base to allow room for the support sting.

The wing was in a high position with a root incidence angle of 1.5° and approximately 5° of twist (washout) between the root and tip chords. The basic (reference) panel had an aspect ratio of 6.8, a taper ratio of 0.36, and 42.24° of sweepback at the quarter-chord line. A detailed model description is contained in reference 16.

Wind Tunnel

The investigation was conducted in the Langley 8-foot transonic pressure tunnel (ref. 18). This single-return tunnel has a rectangular test section with slotted top and bottom walls to permit continuous operation through the transonic speed range with negligible choking and blockage effects. The cross-sectional area of the test region is approximately 4.65 meters^2 (50 ft^2). The open ratio of the slots (ratio of total slot width to width of top and bottom walls) was about 6 percent in the present test. Because of the relatively large size of the model (ratio of maximum model cross-sectional area to tunnel test-section cross-sectional area of approximately 0.005), wooden test-section sidewall inserts (fig. 1(c)) that were indented in the region of the model to reduce streamline distortion (ref. 16) were included. This facility has controls that allow for the independent variation of Mach number, stagnation pressure, temperature, and specific humidity.

Measurements

An internal six-component electrical strain-gage balance housed within the fuselage cavity was used to measure overall forces and moments on the model. A differential pressure transducer referenced to free-stream static pressure was used to measure the pressure at the model base.

Static-pressure orifices were distributed in streamwise rows over the right-wing upper surface and the left-wing lower surface. The wing orifice locations are diagramed and tabulated in figure 1(b). Because the basic wing panel includes neither the glove nor inboard trailing-edge extension, there are values of x/c both greater than 1.0 and less than 0 for the two innermost wing orifice rows. One rearward-facing pressure orifice was included in the wing trailing edge at semispan station 0.480 to measure the trailing-edge pressure near the wing midsemispan.

Wing surface pressures were measured by means of differential pressure scanning valves mounted in the fuselage nose. Wing-section normal-force coefficients were obtained by numerical integration (based on the trapezoidal method) of the local pressure coefficients measured at each orifice multiplied by an appropriate weighting factor (incremental area). In addition to the pressure orifices on the model, there were two streamwise rows of static-pressure orifices distributed along the test-section walls. These wall pressures were also measured by means of differential pressure scanning valves. The tunnel stagnation pressure and the reference pressure in the chamber surrounding the test section were measured by means of absolute pressure manometers.

Corrections and Accuracy

The model support sting was designed to minimize sting interference at near-sonic Mach number (ref. 19). Corrections have been made to the measured angle of attack for model support sting and balance deflections due to aerodynamic loads on the model. Further corrections to the measured angle of attack have been made for tunnel airflow angularity (determined from comparisons of results of tests with upright and inverted models) and for first-order boundary-induced lift-interference effects. These boundary-induced lift-interference corrections, based on the theory of reference 20, amounted to reductions in the measured angle of attack of 0.09 times the normal-force coefficient.

Drag results have been adjusted to correspond to a condition of free-stream static pressure acting over the balance cavity and model base.

Since no free-stream Mach number surveys have been made under the humidity conditions of the present investigation, no attempt was made to correct the tunnel Mach number calibration for possible humidity effects.

It is estimated that the model balance was capable of measuring normal force within ±56 newtons (±12.5 lb), axial force within ±4 newtons (±1.0 lb), and pitching moment within ±2 m-N (±1.5 ft-lb). The differential pressure gage used to measure the pressure at the model base had a range of 17.2 kN/m^2 (2.5 lb/in^2) and an estimated accuracy of 0.5 percent of the full range. The differential pressure scanning valves used to measure the model wing and tunnel wall pressures had ranges of 86.2 kN/m^2 (12.5 lb/in^2) and 6.9 kN/m^2 (1.0 lb/in^2), respectively, and estimated accuracies of 1 percent of the full ranges. The model angle of attack was measured to an estimated accuracy of $\pm 0.05^o$.

Test Conditions

Tests were conducted at Mach numbers of 0.95, 0.98, and 1.00 at a tunnel stagnation pressure of 101 325 N/m^2 (1 atmosphere). Data were taken at dewpoints of -17.8^o C (0^o F), -6.7^o C (20^o F), 4.4^o C (40^o F), and 15.6^o C (60^o F) at a stagnation temperature

of 48.9° C (120° F), and at stagnation temperatures of 43.3° C (110° F) and 57.2° C (135° F) at a dewpoint of 15.6° C (60° F). The model angle-of-attack range was from 0° to 10°.

RESULTS AND DISCUSSION

Wind-Tunnel Mach Number Calibration

The effects of humidity on the Mach number distributions axially along the top and side walls of the test section are presented in figures 3 and 4. These data were taken with the tunnel at a nominal Mach number of 0.980, and the model at an angle of attack of 3.30°. Also included in figures 3 and 4 is the estimated saturation Mach number M_{sat} for each humidity condition.

Shown in figure 3 are the effects of dewpoint variation at the normal tunnel operating stagnation temperature. These data indicate that only small effects of humidity are introduced in the wall Mach number distributions with the model at this angle of attack for dewpoints of 4.4° C (40° F) or less. When the dewpoint is increased to 15.6° C (60° F), however, the Mach number distributions along both the top and side walls are appreciably altered. A more positive Mach number gradient is indicated at this dewpoint relative to the data unaffected by humidity. Since the model data have not been corrected for the horizontal buoyancy changes related to these effects, the measured drag coefficients may be increased at this relatively high dewpoint. At this dewpoint the view of the model was obscured by thick clouds of condensed moisture originating well upstream of the model and filling the test section. Since estimated free-stream saturation conditions are not reached at a dewpoint of 4.4° C (40° F) (note that the nominal free-stream Mach number is less than the estimated saturation Mach number at this dewpoint), the existence of condensed phase would be unlikely in the undisturbed flow field ahead of the model at this humidity condition. However, at a dewpoint of 15.6° C (60° F), the estimated saturation Mach number has dropped below the nominal free-stream Mach number, and the moist air in the free stream ahead of the model would be supersaturated without the formation of condensed phase. Because visual observation confirmed that extensive condensation was, in fact, occurring in the undisturbed flow field upstream of the model at a dewpoint of 15.6° C (60° F), and because the occurrence of condensation in wind-tunnel flow is accompanied by a reduction in the stagnation pressure in the condensation regions (refs. 2 and 3), the true free-stream Mach number at this dewpoint may be somewhat less than that obtained from the tunnel calibration.

The effects of stagnation temperature variation at a relatively high dewpoint are given in figure 4. The data taken at a dewpoint of -6.7° C (20° F) are included in this figure for comparison since these data are considered to be negligibly affected by humid-

ity. As expected, figure 4 shows that humidity effects on the Mach number distributions become more severe with cooling and are reduced by heating. However, the heating capability of the tunnel (57.2° C (135° F)) was inadequate for eliminating the effects of humidity incurred in the wall Mach number distributions at this relatively high dewpoint. Thin clouds of condensed moisture originating well upstream of the model could be seen passing through the test section at this stagnation temperature.

It is interesting that in the present investigation the introduction of condensation effects in the wall Mach number distribution and the first signs of condensed moisture in the test-section flow correspond approximately to the onset of estimated free-stream saturation conditions. (Note that at a dewpoint of 15.6° C (60° F) and a stagnation temperature of 57.2° C (135° F) the nominal free-stream Mach number only slightly exceeds the estimated saturation Mach number.) This result suggests that slow condensation (fog formation) may be occurring on particles already present in the airstream. According to reference 4, in a continuous-circuit tunnel, such as the Langley 8-foot transonic pressure tunnel, the possibility exists that the solid or liquid particles carried around in the airstream may be sufficiently numerous to provide nuclei for condensation. Also, the rates of temperature change in such a large nozzle may be sufficiently small to allow slow condensation (fog formation) on these nuclei. Under these conditions the condensation process may approximate a saturated equilibrium expansion, and the large degree of supercooling and subsequent spontaneous nucleation (rapid condensation), which is characteristic of condensation processes in relatively small induction-type high-speed wind tunnels (see refs. 3, 5, and 7 to 10), may not occur.

Model Base Pressure

Shown in figure 5 are the humidity effects on base-pressure coefficient with the model at an angle of attack of 0°. The effects of dewpoint variation at the normal tunnel operating stagnation temperature are indicated by the faired data. These data show the effects of dewpoint on the base-pressure coefficient to be negligible for dewpoints of 4.4° C (40° F) or less, but indicate an appreciable decrease in base pressure at a dewpoint of 15.6° C (60° F). The decrease in base-pressure coefficient with increase in dewpoint for subsonic Mach numbers is in agreement with the results of reference 9 and affords further evidence to support the possibility that the true free-stream Mach number may be less than the value indicated by the tunnel calibration at this relatively high dewpoint. The effects of stagnation temperature variation at a relatively high dewpoint are indicated by the ticked data. Here again, as expected, humidity effects become more severe with cooling and are ameliorated by heating. But, as with the test-section wall pressure distributions, the available tunnel heating was insufficient for eliminating the effects of humidity at this dewpoint. In fact, at a Mach number of unity, very little reduction in the effects is noted. Since the humidity effects at the base of the model may extend

to points further upstream and thus are not amenable to correction, these results imply that an increase in drag may be incurred when testing at relatively high dewpoints.

Model Longitudinal Aerodynamic Characteristics

In figure 6 are shown the effects on the longitudinal aerodynamic characteristics of dewpoint variation at the normal tunnel operating stagnation temperature. These data indicate that the effects of dewpoint on the longitudinal aerodynamic characteristics are generally negligible only at dewpoints of -6.7° C (20° F), or less. Further increases in dewpoint tend to cause an appreciable decrease in the lift coefficient at moderate angles of attack, an effect that is most pronounced at a Mach number of 0.98 where a notable decrease occurs even at the lower angles of attack. The reduction in lift coefficient with increasing dewpoint is associated with the effect of humidity on the wing upper surface pressure distributions and will be discussed later. Only a slight effect of dewpoint on drag coefficient as a function of angle of attack is seen although some increase is evident at the lower angles of attack and a relatively high dewpoint. The plot of drag coefficient against lift coefficient indicates, in general, large increases in drag coefficient for the higher dewpoints. However, it is clear from consideration of the data previously discussed that this effect is due primarily to the reduction in lift. The effects of dewpoint on pitching-moment coefficient are generally small, except at the highest lift coefficients where a large reduction in pitching moment occurs at the higher dewpoints.

The effects on the longitudinal aerodynamic characteristics of stagnation temperature variation at a relatively high dewpoint are presented in figure 7. The data taken at a dewpoint of -6.7° C (20° F) are included in this figure for comparison since these data are considered to be negligibly affected by humidity. Here again, as expected, humidity effects become more severe with cooling and are ameliorated by heating. But, as with the results previously considered, the available tunnel heating was insufficient for eliminating the effects of humidity for this relatively high dewpoint. Also, as has been noted regarding the base-pressure coefficient, less reduction in the effects occurs at a Mach number of unity.

Model Wing Pressure Distributions

In figures 8 to 13 are presented the effects of dewpoint variation at the normal tunnel operating stagnation temperature on representative wing streamwise-chord pressure profiles and resultant span-load characteristics at selected angles of attack. The data at a tunnel Mach number of 0.98 are shown since the largest humidity effects on the lift-force characteristics occur at this Mach number. The humidity effects on the wing pressure distributions, of course, do have a tendency to vary somewhat with Mach number.

The data of figures 8, 10, and 12 indicate that humidity effects on the lower surface pressure distributions are generally small for the dewpoint range and angle-of-attack range of the present investigation. The upper surface pressure distributions, however, are altered at all higher test dewpoints relative to the distributions obtained at the lowest test dewpoint. Therefore, the dewpoint necessary to insure negligible humidity effects in the pressure data cannot be determined from the test results of the present investigation.

The humidity effects which are typical of the effects that occur in the wing-pressure and span-load distributions at moderate angles of attack are shown in figures 8 and 9, respectively. At the higher dewpoints the pressures are increased in the region of supersonic flow beginning near the leading edge. The loss of lift which is apparent over the forward part of the wing is shown in the span-load distribution (fig. 9) and is consistent with the lift-force data which were discussed previously.

Humidity effects at a lower angle of attack are shown in figures 10 and 11. At dewpoints of 4.4° C (40° F) and less, the differences seen between the data at the test dewpoints vary greatly with span location. At the outboard spanwise stations, differences in the shock position amounting to about 10 percent of the local chord are seen. The tendency for the humidity effects to vary at this angle of attack with spanwise location is shown in the span-load distribution. (See fig. 11.) Although the differences in the pressure data obtained at the lowest two dewpoints are appreciable, the random nature of the effects accounts for the negligible differences seen in the force data at these two dewpoints. At the highest dewpoint the pressures are increased in the region of supersonic flow beginning near the leading edge and a forward movement of the shock occurs. This shock movement is consistent with the increase in drag previously noted.

Humidity effects at near-cruise lift coefficient for this configuration are presented in figures 12 and 13. The effects are similar to those shown at the lower angle of attack, but demonstrate the tendency for the random differences between the data at the lowest dewpoints to diminish with increase in angle of attack.

A design feature of the NASA supercritical airfoil (refs. 12 to 17) is the existence of extensive local regions of supersonic flow over the upper surface when operating at near-sonic speed. Because an effect of humidity, mentioned above, is to increase the pressures in the regions of supersonic flow over the upper surface of the wing, the lifting characteristics of NASA supercritical wings may be particularly sensitive to wind-tunnel humidity at near-sonic speed.

Effects of Local Condensation

An important observation to be made from the data presented herein is that significant humidity effects appear in the model force and pressure coefficients although no evidence suggests that appreciable condensation is occurring in the free stream. At a

nominal Mach number of 0.98, for instance, the wing upper surface pressures are significantly affected by humidity at a dewpoint of -6.7° C (20° F), and the model lift and pitching-moment coefficients are affected at a dewpoint of 4.4° C (40° F). At this Mach number the free stream is estimated to be unsaturated at these dewpoints, and no humidity effects appear in either the tunnel-wall Mach number distributions or the model base-pressure coefficients.

It is a well-established fact that because of the higher local velocities, and therefore increased supercooling, extensive condensation can occur in the expansion regions around a test model for less severe humidity conditions than it does in the free stream itself.

Thus, in the present investigation, condensation originating in the local expansion regions around the model, particularly in the local regions of supersonic flow over the upper surfaces of the wings, is felt to be mainly responsible for the humidity effects seen in the model force and pressure data at dewpoints of 4.4° C (40° F) and less. Condensation that occurs in the free stream and causes a possible reduction in the true free-stream Mach number is felt to account for the large humidity effects seen in the model force and pressure data at a dewpoint of 15.6° C (60° F).

CONCLUDING REMARKS

An investigation has been conducted in the Langley 8-foot transonic pressure tunnel to determine the effects of humidity at near-sonic speed on the longitudinal aerodynamic characteristics and wing pressure distributions of an area-rule research airplane model with an NASA supercritical wing. Effects of dewpoint at the normal tunnel operating stagnation temperature of 48.9° C (120° F) and effects of stagnation temperature at a relatively high dewpoint of 15.6° C (60° F) were investigated. The test tunnel stagnation pressure was 101 325 N/m^2 (1 atmosphere).

The results demonstrated that condensation originating principally in the local expansion regions around the model before the occurrence of appreciable condensation in the free stream can cause significant effects on model test data at near-sonic speed. At moderate angles of attack the wing upper-surface pressures were increased in the region of supersonic flow beginning near the leading edge. These effects on the wing pressures, believed to be caused by condensation originating principally in the local regions of supersonic flow over the wings, resulted in significant reductions in the lift coefficients.

Because of the extensive regions of supersonic flow over the wing upper surfaces at near-sonic speed, the lifting characteristics of supercritical wings may be particularly sensitive to wind-tunnel humidity at these speeds.

The occurrence of condensation in the free stream corresponded approximately to the onset of estimated free-stream saturation conditions. It was accompanied by an alteration in the test-section wall Mach number distributions, a reduction in the model base pressure, an increase in the model drag, a forward movement of the shock on the wing upper surface, and a further increase in the wing pressures that resulted in a decrease in lift coefficient.

Decreasing the tunnel stagnation temperature resulted in humidity effects similar to those incurred by increasing the dewpoint, and increasing the temperature resulted in a reduction of these humidity effects.

Langley Research Center,
National Aeronautics and Space Administration,
Hampton, Va., July 5, 1972.

REFERENCES

1. Oswatitsch, Kl.: Formation of Fog in Wind Tunnels and Its Influence on the Investigation of Models. Reports and Translations 459, British M.A.P. Völkenrode, June 1946.

2. Pearcey, H. H.: The Effect of the Condensation of Atmospheric Water Vapour on Total Head and Other Measurements in the N.P.L. High-Speed Tunnels. R. & M. No. 2249, Brit. A.R.C., 1951.

3. Lukasiewicz, Julius; and Royle, J. K.: Effects of Air Humidity in Supersonic Wind Tunnels. R. & M. No. 2563, Brit. A.R.C., 1953.

4. Ritchie, Virgil S.; Wright, Ray H.; and Tulin, Marshall P.: An 8-Foot Axisymmetrical Fixed Nozzle for Subsonic Mach Numbers up to 0.99 and for a Supersonic Mach Number of 1.2. NACA RM L50A03a, 1950.

5. Cawthon, J. A.: Water Vapor Condensation Effects in the Ordnance Aerophysics Laboratory Supersonic Wind Tunnel. OAL Rep. 340-1 (Contract NOrd-16126), Convair Div., General Dynamics Corp., Aug. 1, 1956. (Available from DDC as AD 140 799.)

6. Matthews, Clarence W.: An Investigation of the Adaptation of a Transonic Slotted Tunnel to Supersonic Operation by Enclosing the Slots With Fairings. NACA RM L55H15, 1955.

7. Burgess, Warren C., Jr.; and Seashore, Ferris L.: Criterions for Condensation-Free Flow in Supersonic Tunnels. NACA TN 2518, 1951.

8. Raney, D. J.; and Beastall, D.: Criteria for Condensation Free Flow in the R.A.E. No. 18 (9 in. × 9 in.) Supersonic Tunnel. C.P. No. 164, Brit. A.R.C., 1954.

9. Christensen, Daphne S.: Condensation Effects in Wind Tunnel Flow. Rep. No. AL-1821, North American Aviation, Inc., June 26, 1953.

10. Monaghan, R. J.: Tests of Humidity Effects on Flow in a Wind Tunnel at Mach Numbers Between 2.48 and 4. C.P. No. 247, Brit. A.R.C., 1956.

11. Wegener, P. P.; and Mack, L. M.: Condensation in Supersonic and Hypersonic Wind Tunnels. Advances in Applied Mechanics, Vol. V, H. L. Dryden and Th. von Kármán, eds., Academic Press, Inc., 1958, pp. 307-447.

12. Whitcomb, Richard T.; and Clark, Larry R.: An Airfoil Shape for Efficient Flight at Supercritical Mach Numbers. NASA TM X-1109, 1965.

13. Blackwell, James A., Jr.: Aerodynamic Characteristics of an 11-Percent-Thick Symmetrical Supercritical Airfoil at Mach Numbers Between 0.30 and 0.85. NASA TM X-1831, 1969.

14. Harris, Charles D.: Wind-Tunnel Investigation of Effects of Trailing-Edge Geometry on a NASA Supercritical Airfoil Section. NASA TM X-2336, 1971.

15. Harris, Charles D.; and Blackwell, James A., Jr.: Wind-Tunnel Investigation of Effects of Rear Upper Surface Modification on an NASA Supercritical Airfoil. NASA TM X-2454, 1972.

16. Harris, Charles D.; and Bartlett, Dennis W.: Wind-Tunnel Investigation of Effects of Underwing Leading-Edge Vortex Generators on a Supercritical-Wing Research Airplane Configuration. NASA TM X-2471, 1972.

17. Harris, Charles D.: Aerodynamic Characteristics of Two NASA Supercritical Airfoils With Different Maximum Thicknesses. NASA TM X-2532, 1972.

18. Schaefer, William T., Jr.: Characteristics of Major Active Wind Tunnels at the Langley Research Center. NASA TM X-1130, 1965.

19. Lee, George; and Summers, James L.: Effects of Sting-Support Interference on the Drag of an Ogive-Cylinder Body With and Without a Boattail at 0.6 to 1.4 Mach Number. NACA RM A57I09, 1957.

20. Wright, Ray H.; and Barger, Raymond L.: Wind-Tunnel Lift Interference on Sweptback Wings in Rectangular Test Sections With Slotted Top and Bottom Walls. NASA TR R-241, 1966.

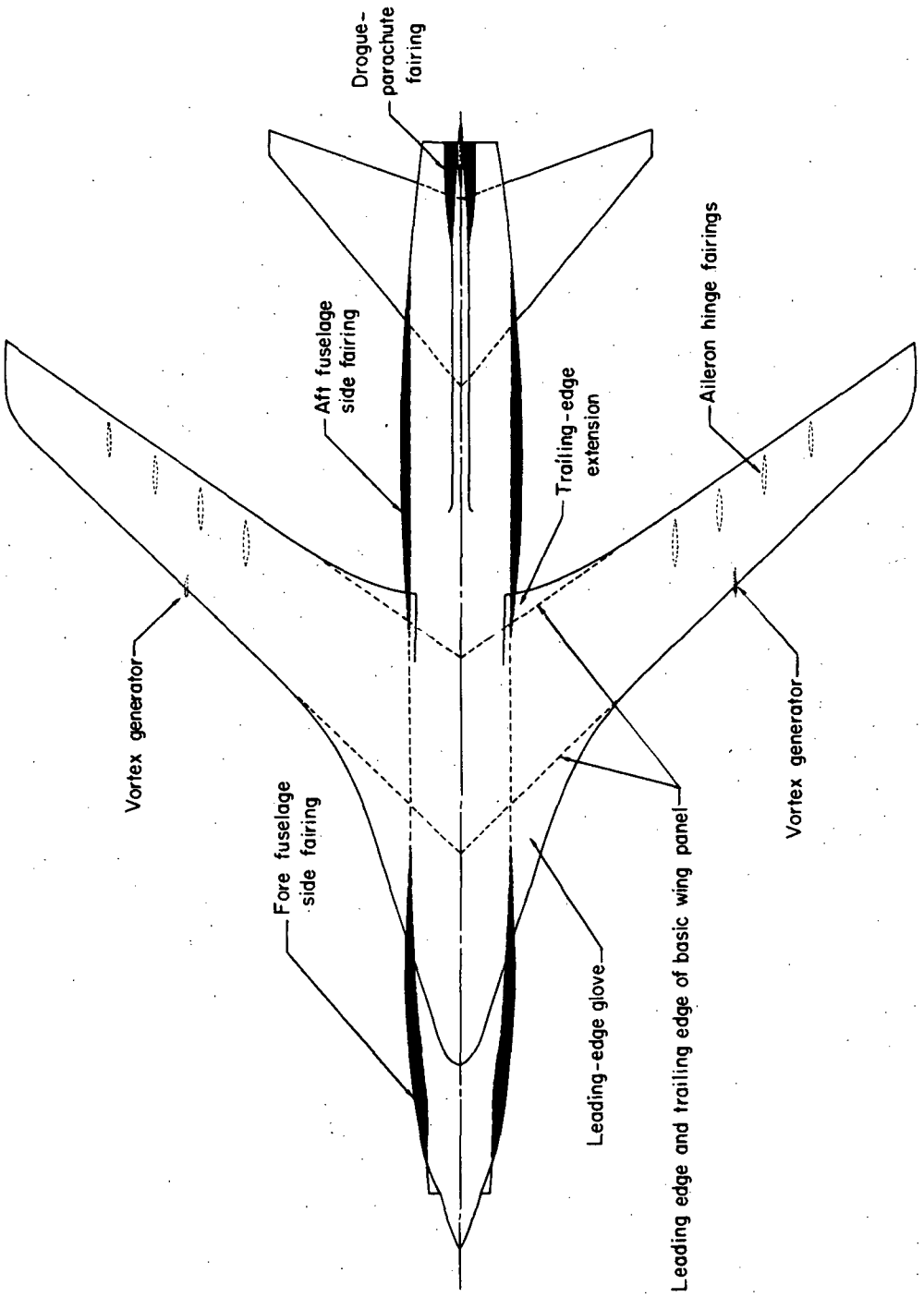

(a) General planform arrangement of the 0.087-scale model.

Figure 1.- Model details. Dimensions are in centimeters (inches).

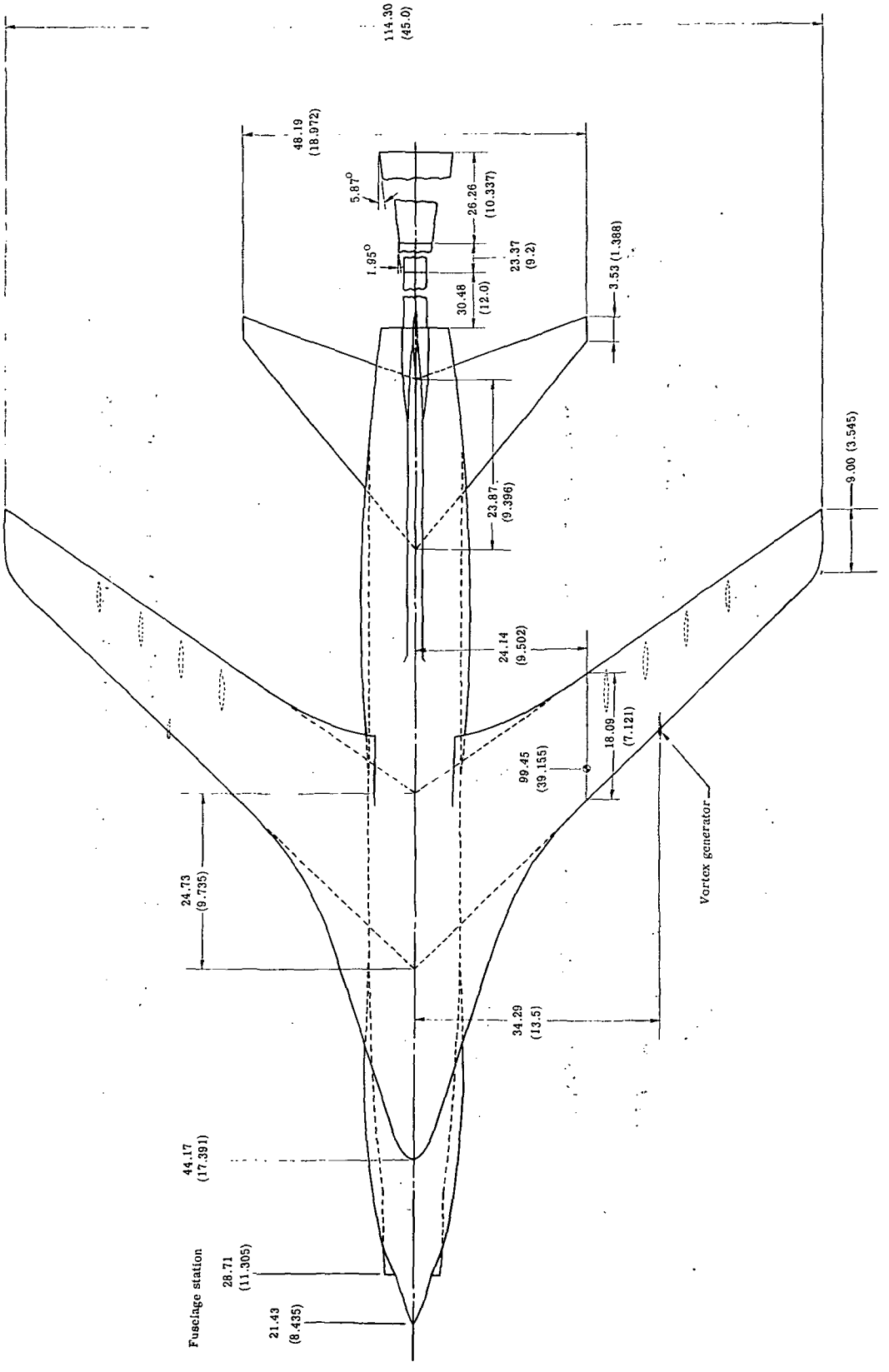

(a) General planform arrangement of the 0.087-scale model. Concluded.

Figure 1.- Continued.

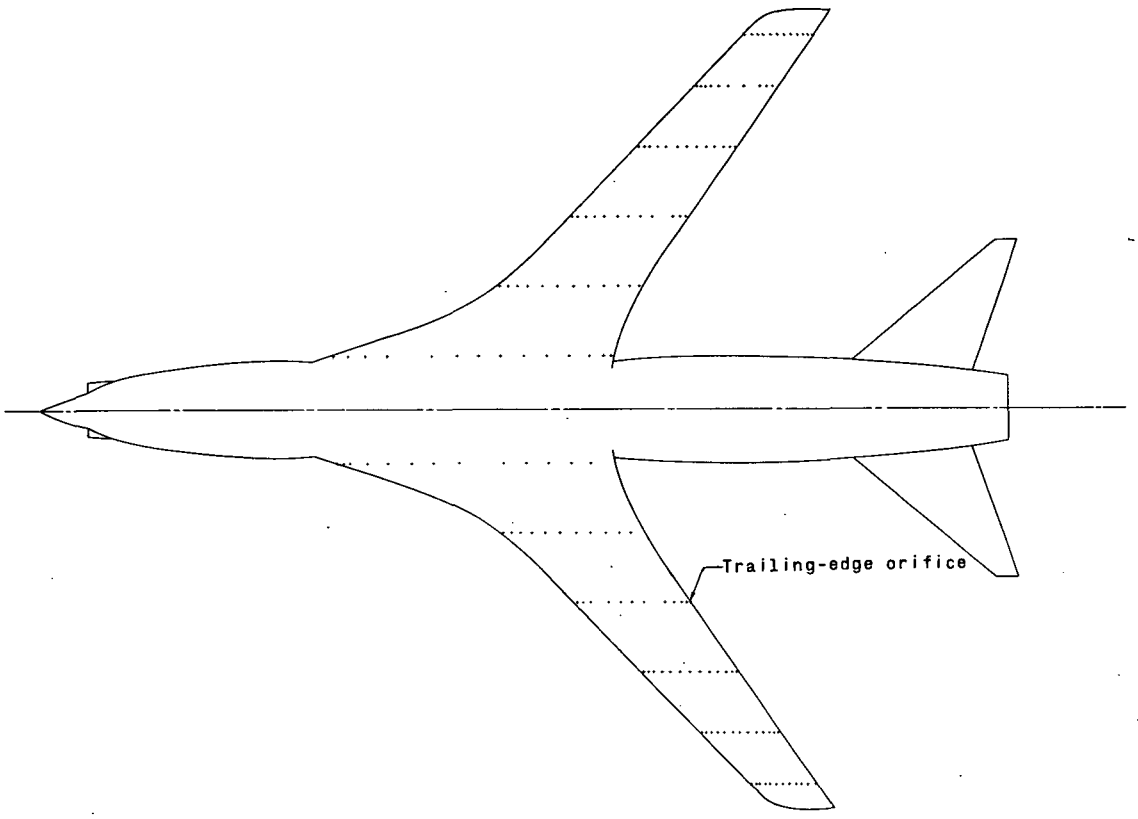

Wing orifice location, $\frac{x}{c}$, at semispan station, $\frac{y}{b/2}$, of –					
0.133 (c = 22.614 (8.903))	0.307 (c = 19.883 (7.828))	0.480 (c = 17.160 (6.756))	0.653 (c = 14.442 (5.686))	0.804 (c = 12.070 (4.752))	0.933 (c = 10.043 (3.954))
Right-wing upper surface					
-0.658	-0.021	0.023	0.025	0.022	0.018
-.565	.035	.068	.079	.075	.077
-.452	.105	.134	.133	.129	.209
-.311	.178	.209	.214	.201	.293
-.023	.286	.294	.295	.294	.396
.133	.396	.404	.407	.397	.494
.272	.514	.497	.502	.495	.590
.416	.618	.599	.601	.594	.693
.565	.733	.700	.698	.693	.777
.713	.835	.864	.780	.784	.861
.854	.919	.926	.863	.856	.918
.960	.987		.923	.926	.972
1.074			.977	.977	
1.122					
Left-wing lower surface					
-0.658	-0.022	0.024	0.025	0.019	0.020
-.615	.038	.075	.074	.066	.076
-.572	.101	.137	.130	.214	.136
-.462	.185	.297	.214	.292	.221
-.329	.289	.400	.298	.403	.295
-.172	.398	.498	.397	.489	.396
-.030	.519	.604	.501	.594	.497
.128	.620	.705	.603	.700	.597
.418	.737	.785	.703	.786	.702
.564	.831	.859	.784	.858	.786
.710	.914	.922	.868	.919	.864
.857	.986	.967	.923	.967	.985
.976	1.012	1.000	.972		
1.072					

(b) Location of pressure orifices.

Figure 1.- Continued.

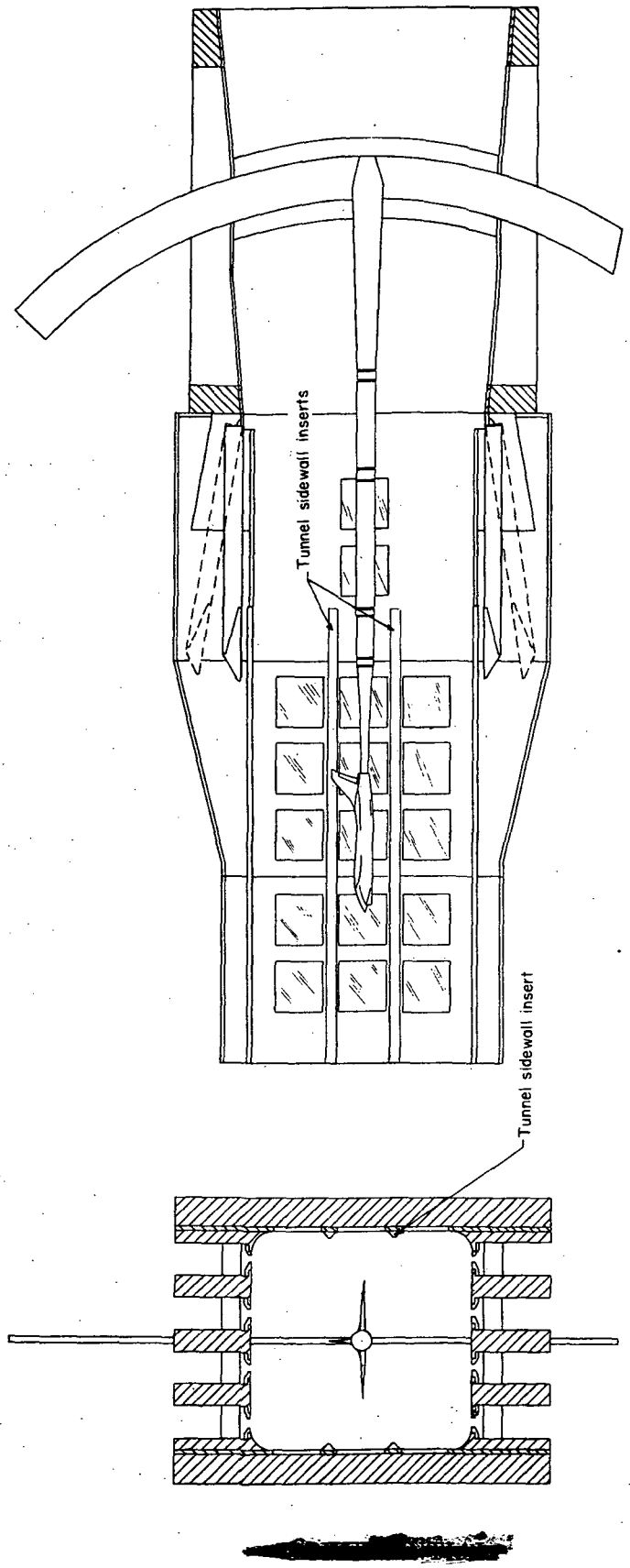

(c) Sketch of tunnel test section with sidewall inserts.

Figure 1.- Concluded.

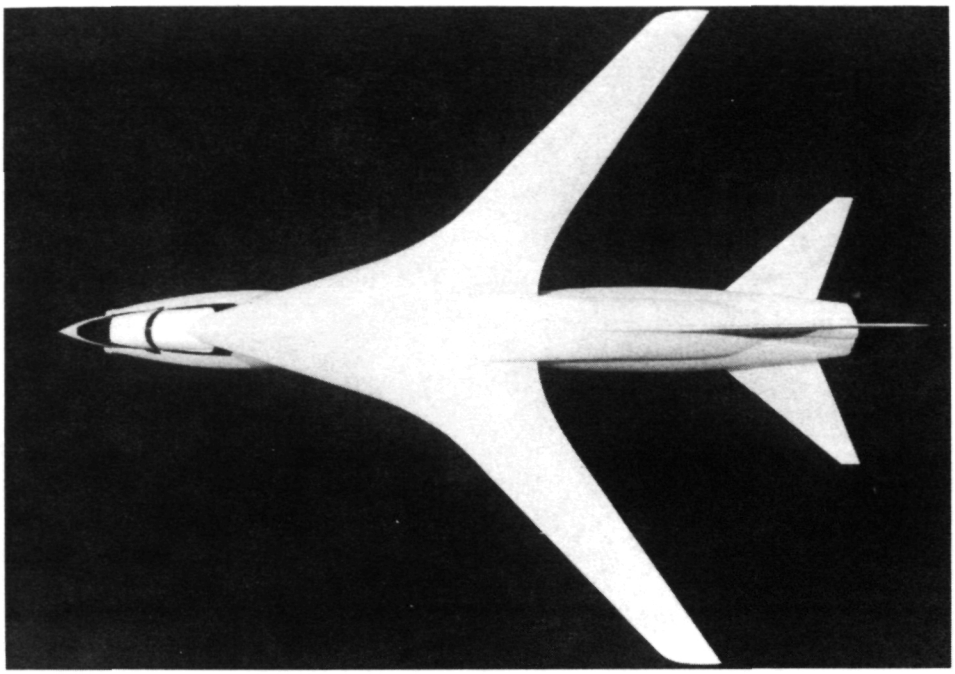

L-70-3988

(a) Top view.

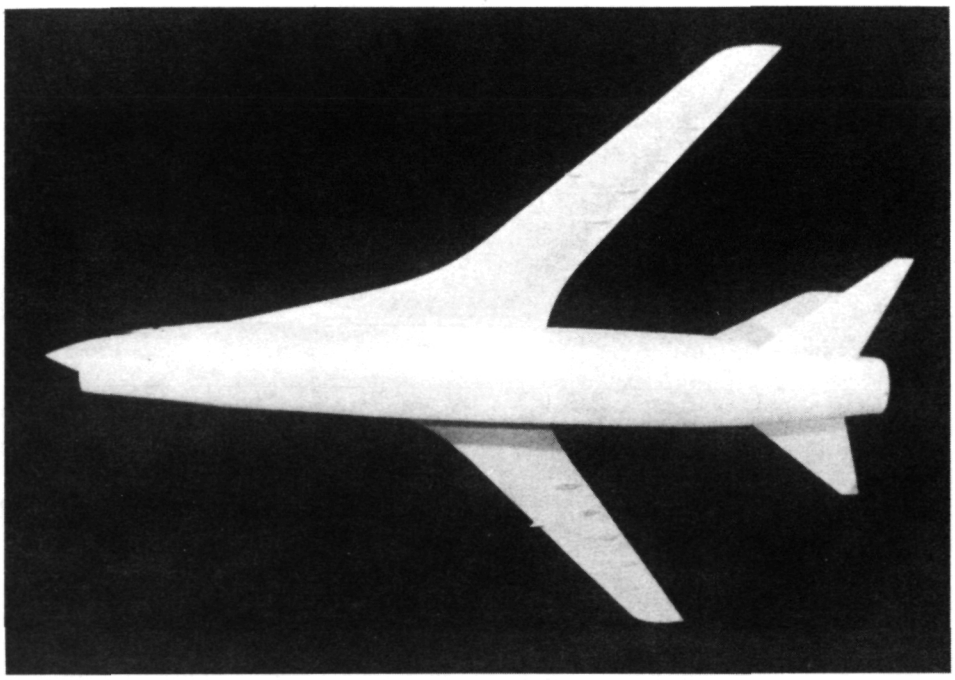

L-70-3990

(b) Three-quarter bottom view.

Figure 2.- The 0.087-scale wind-tunnel model.

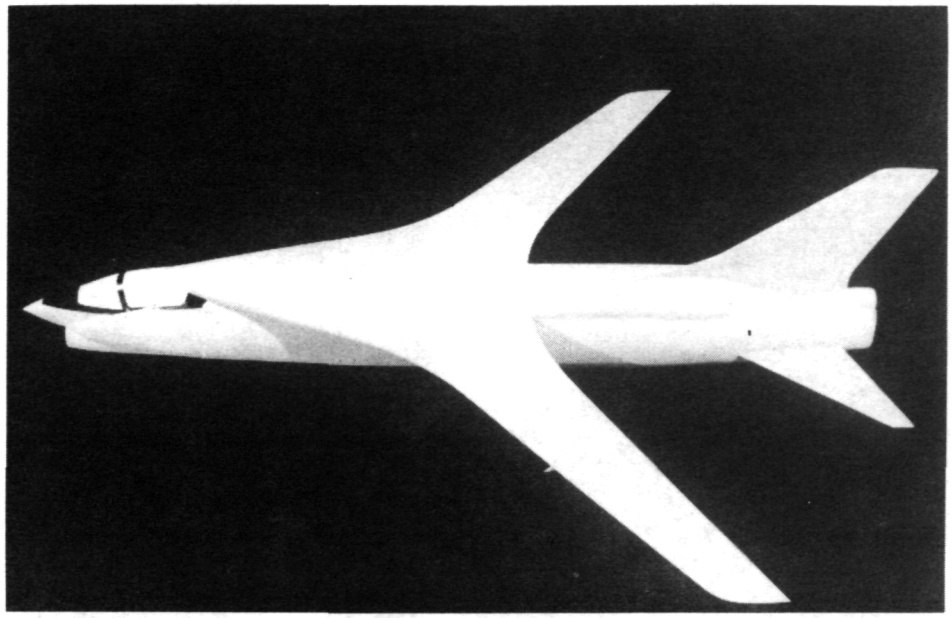

L-70-3992

(c) Three-quarter top view.

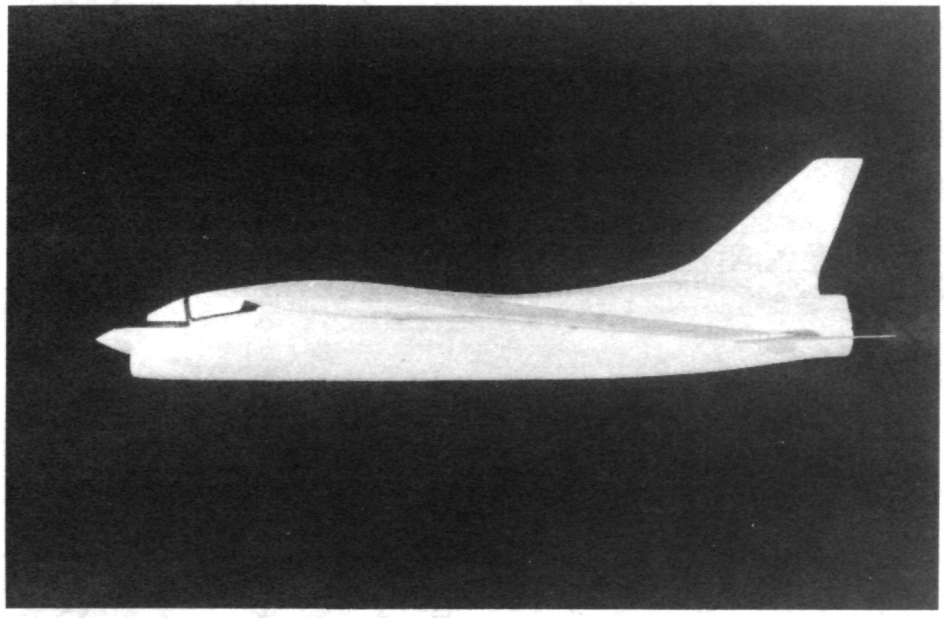

L-70-3987

(d) Side view.

Figure 2.- Concluded.

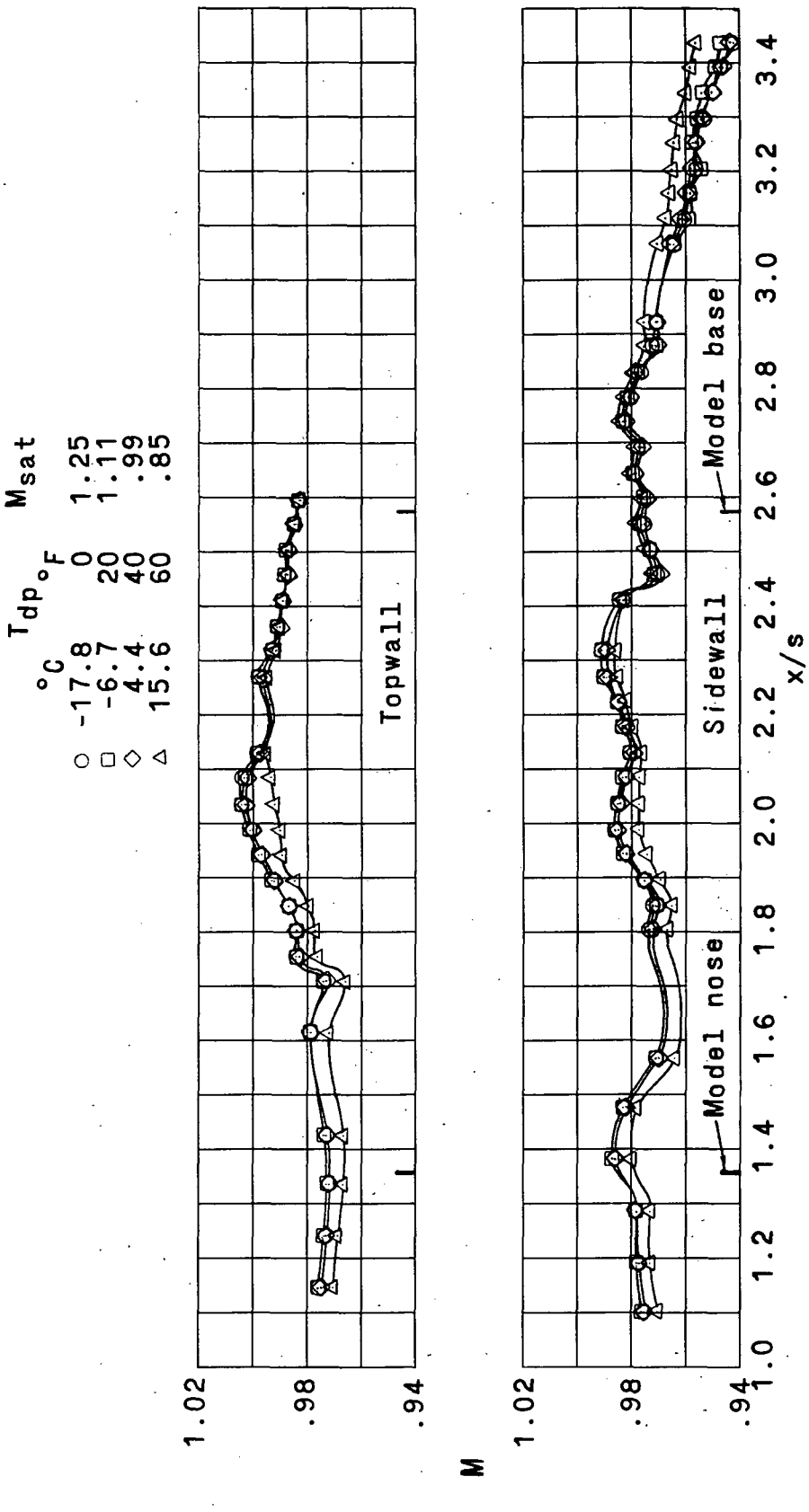

Figure 3.- Variation with wind-tunnel dewpoint of Mach number distribution axially along wall of test section.
$M_\infty = 0.980$; $T_t = 48.9^\circ$ C (120° F); $\alpha = 3.30^\circ$.

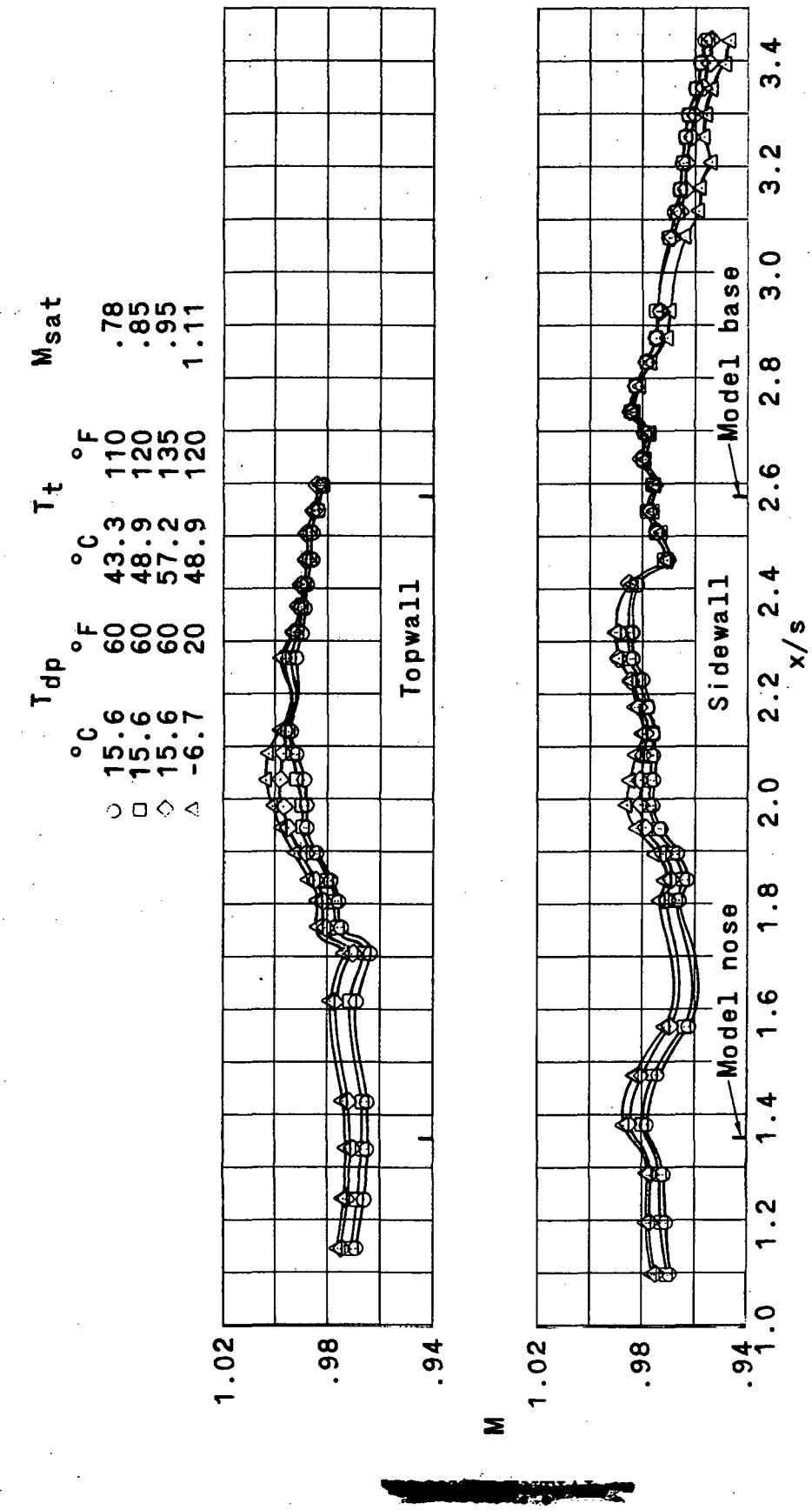

Figure 4.- Variation with wind-tunnel stagnation temperature of Mach number distribution axially along wall of test section (T_{dp} = 15.6° C (60° F)), and comparison with distribution negligibly affected by humidity. M_∞ = 0.980; α = 3.30°.

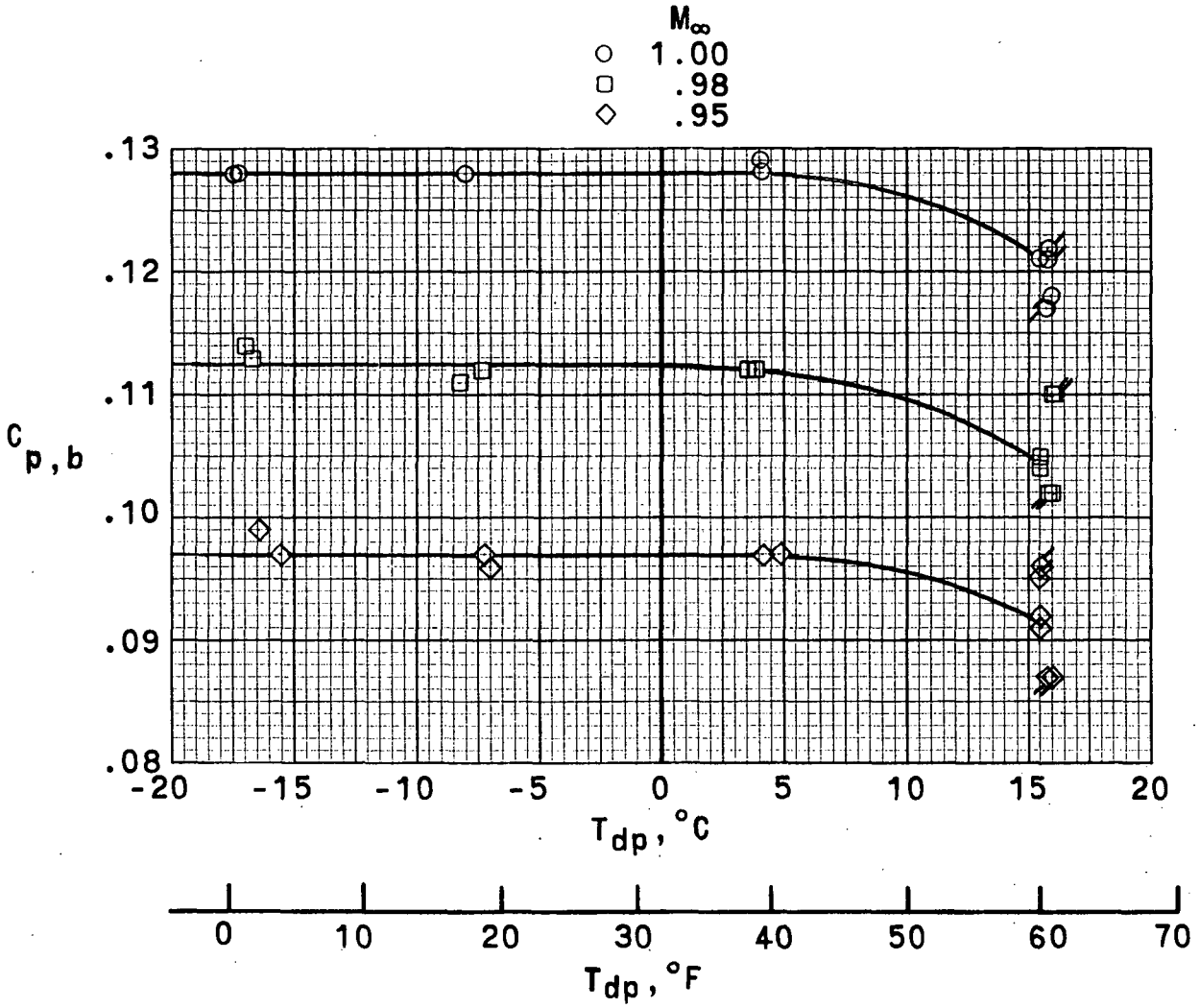

Figure 5.- Effect of wind-tunnel humidity on base pressure. $\alpha = 0^{\circ}$; $T_t = 48.9^{\circ}$ C (120° F); upward ticks on symbols, $T_t = 57.2^{\circ}$ C (135° F); downward ticks on symbols, $T_t = 43.3^{\circ}$ C (110° F).

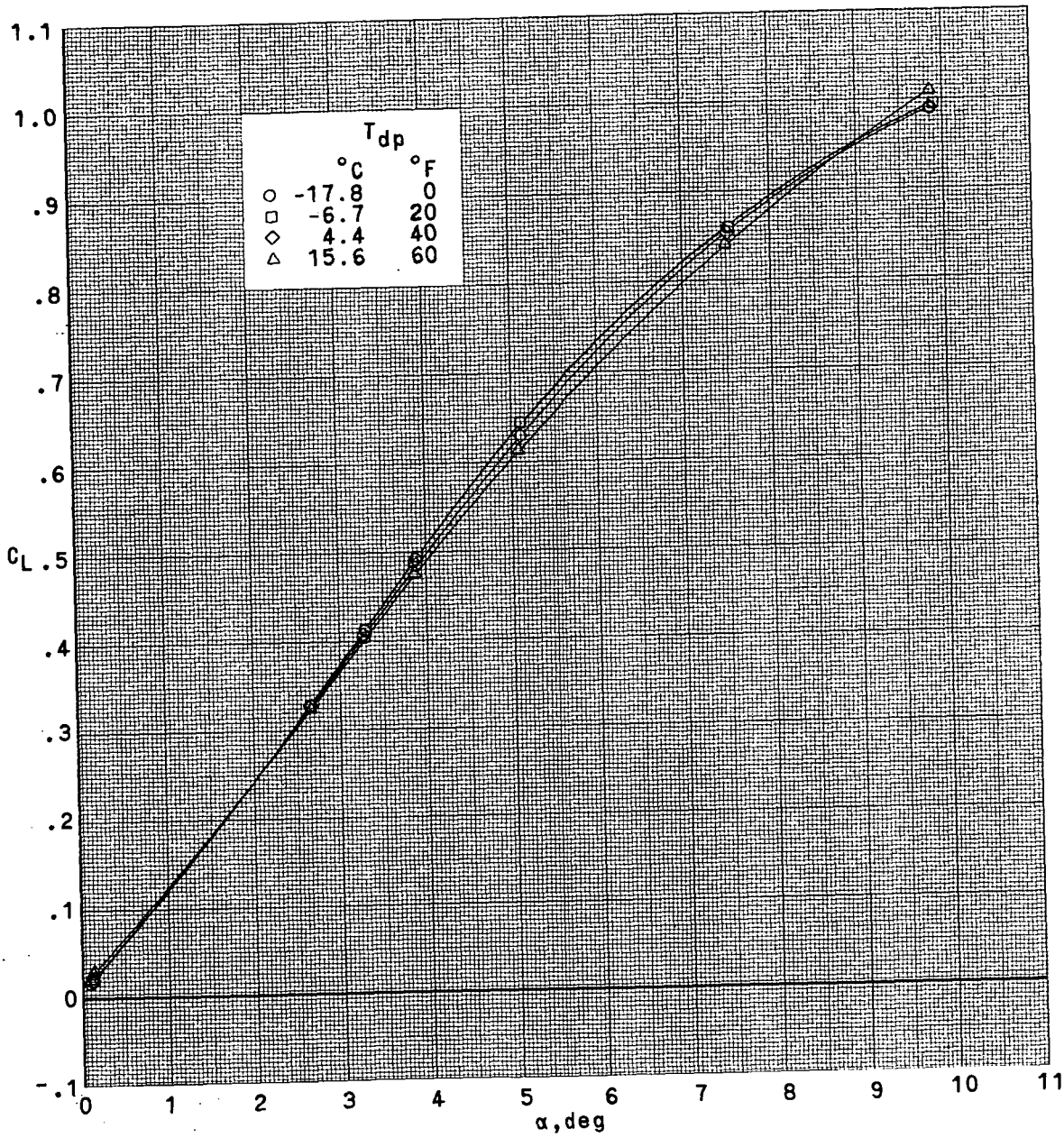

(a) $M_\infty = 0.95$.

Figure 6.- Effect of wind-tunnel dewpoint on the longitudinal aerodynamic characteristics. $T_t = 48.9^o$ C (120^o F).

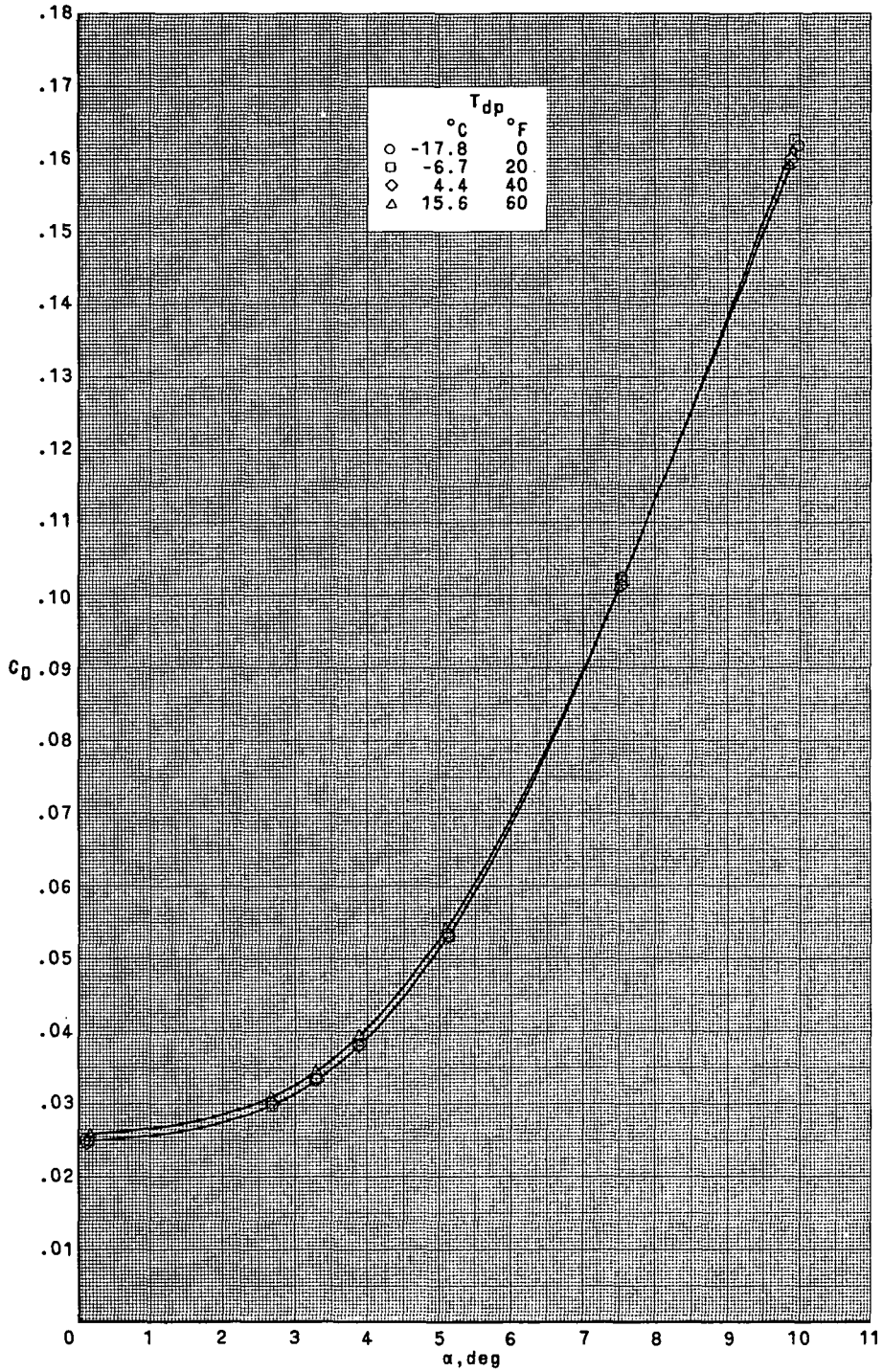

(a) $M_\infty = 0.95$. Continued.

Figure 6.- Continued.

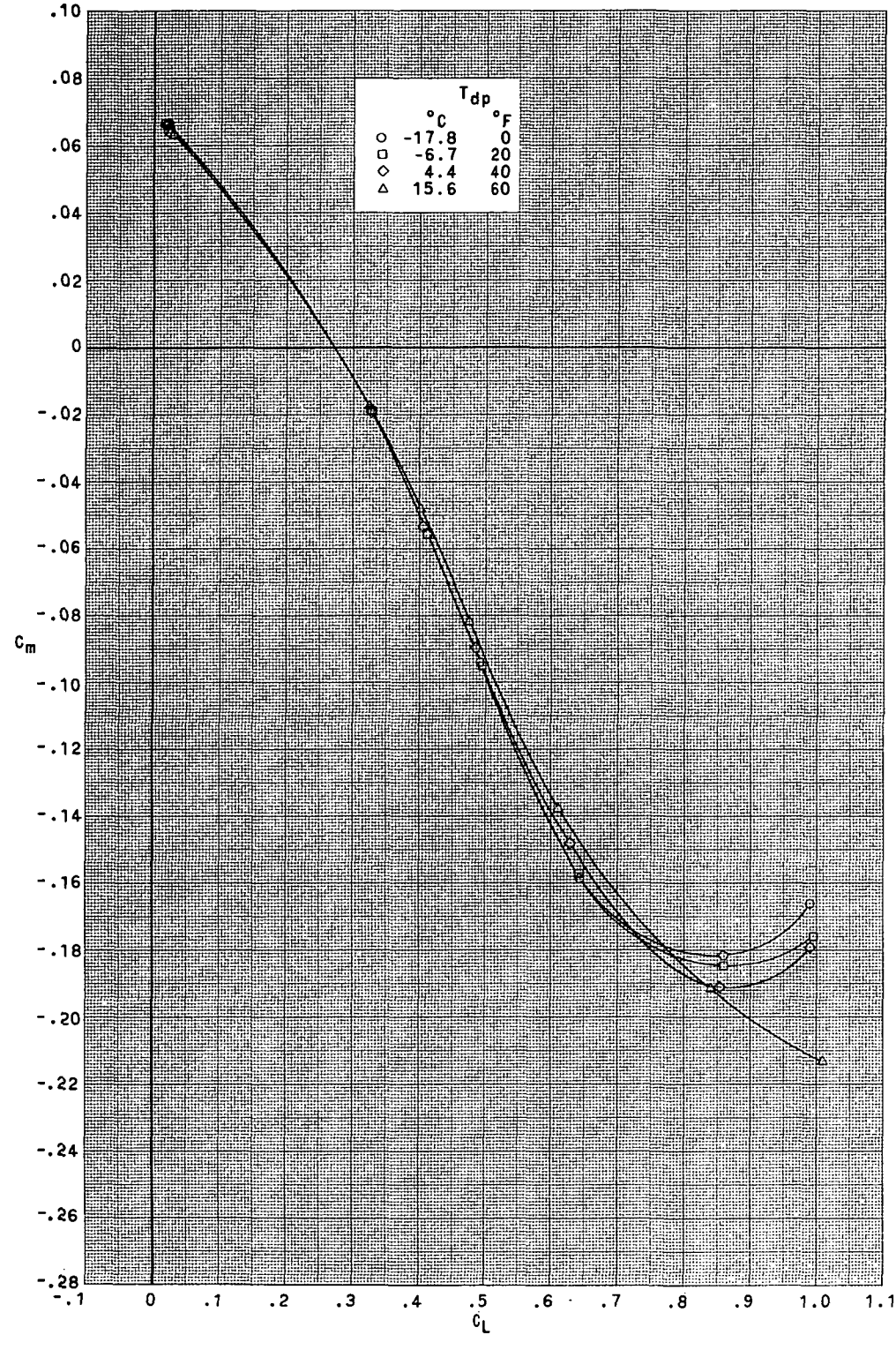

(a) $M_\infty = 0.95$. Continued.

Figure 6.- Continued.

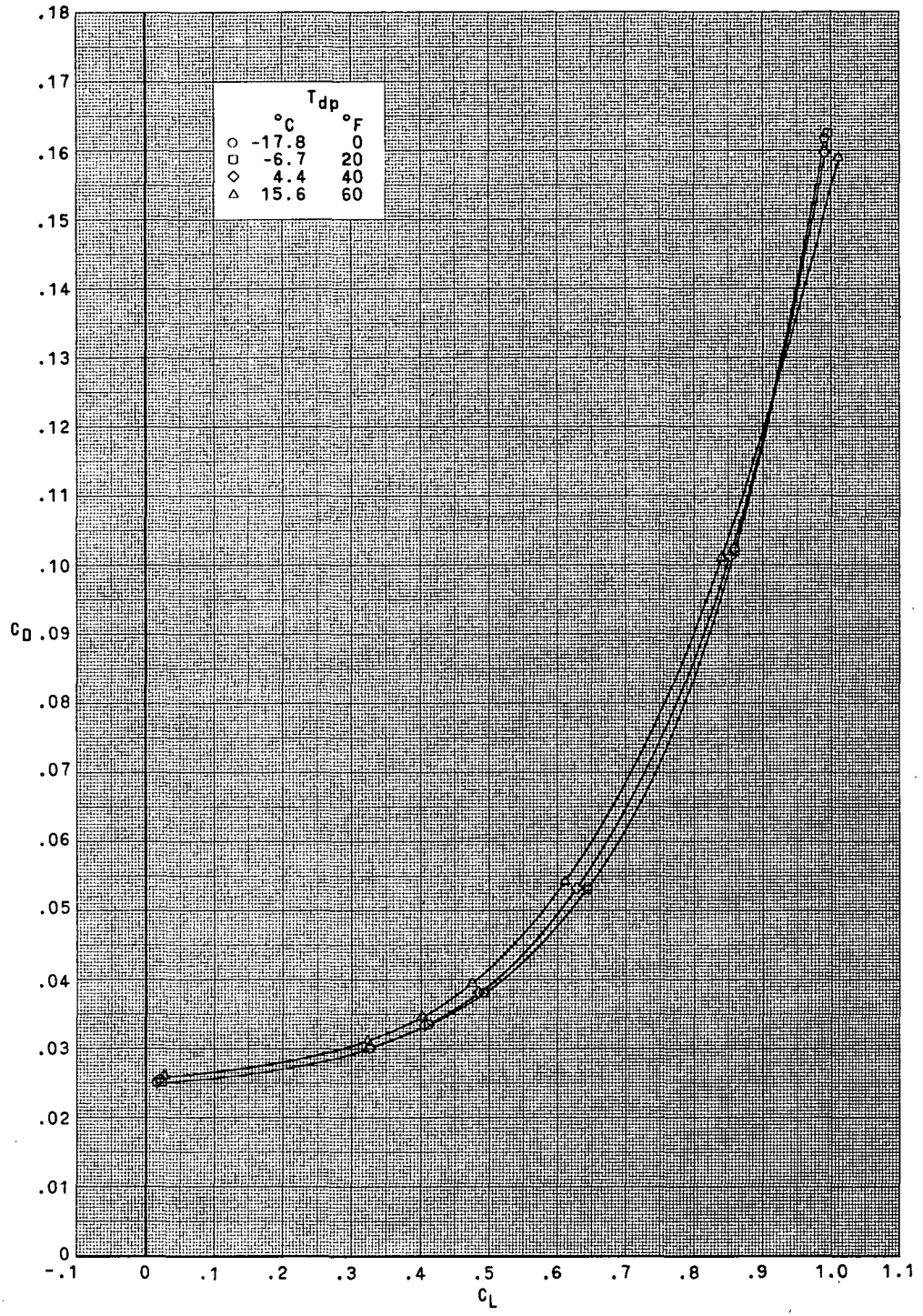

(a) $M_\infty = 0.95$. Concluded.

Figure 6.- Continued.

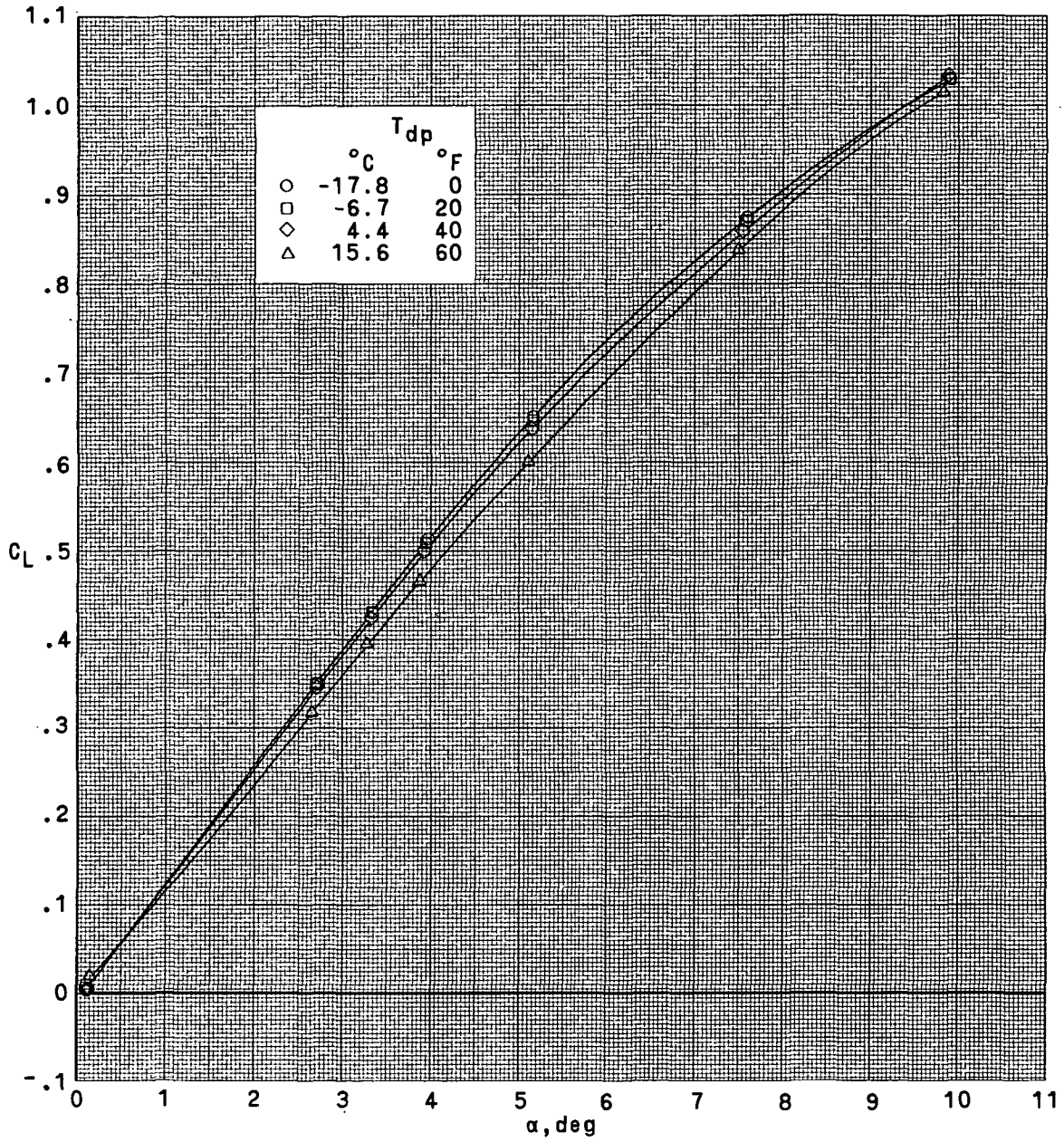

(b) $M_\infty = 0.98$.

Figure 6.- Continued.

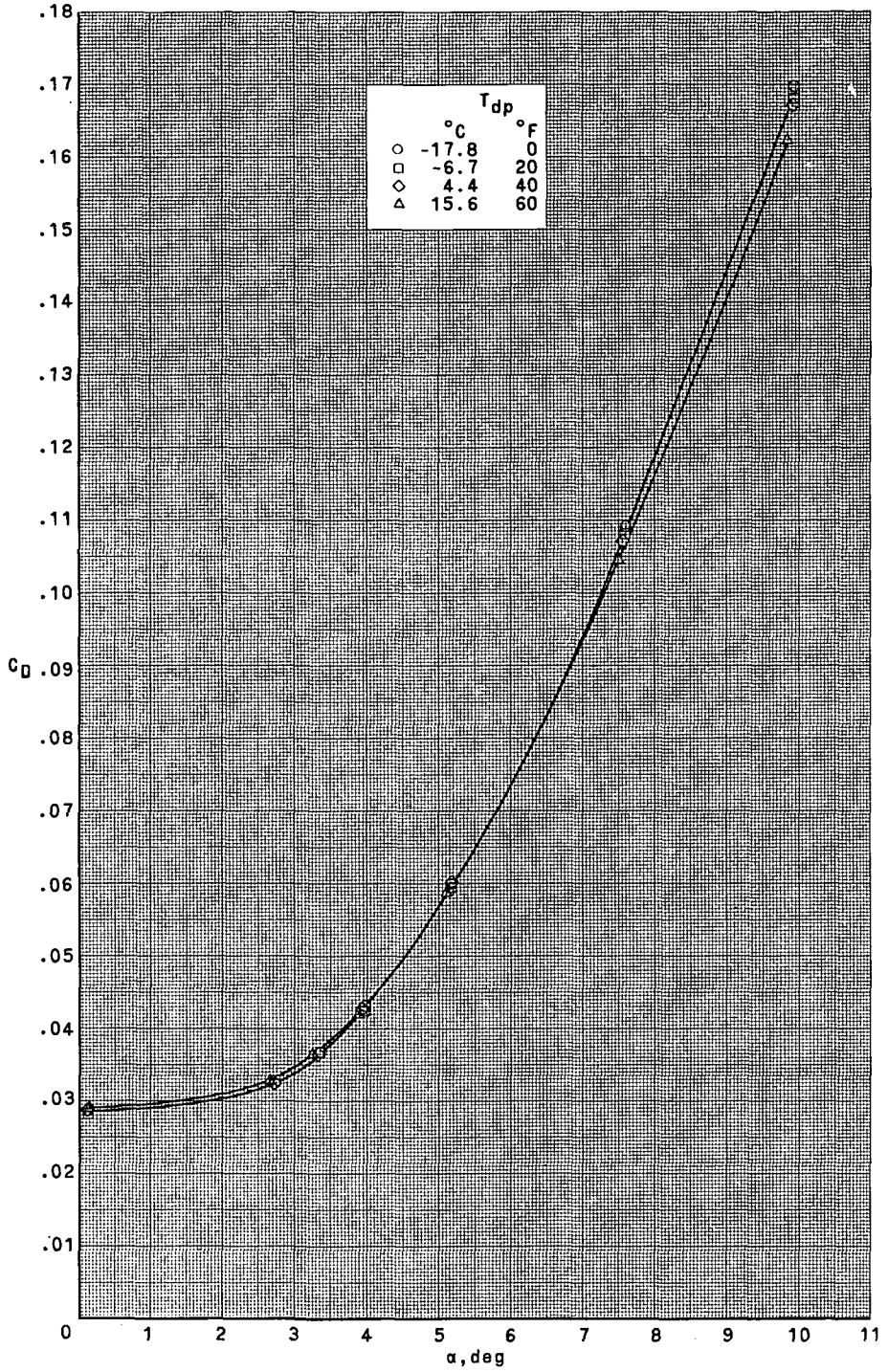

(b) M_∞ = 0.98. Continued.

Figure 6.- Continued.

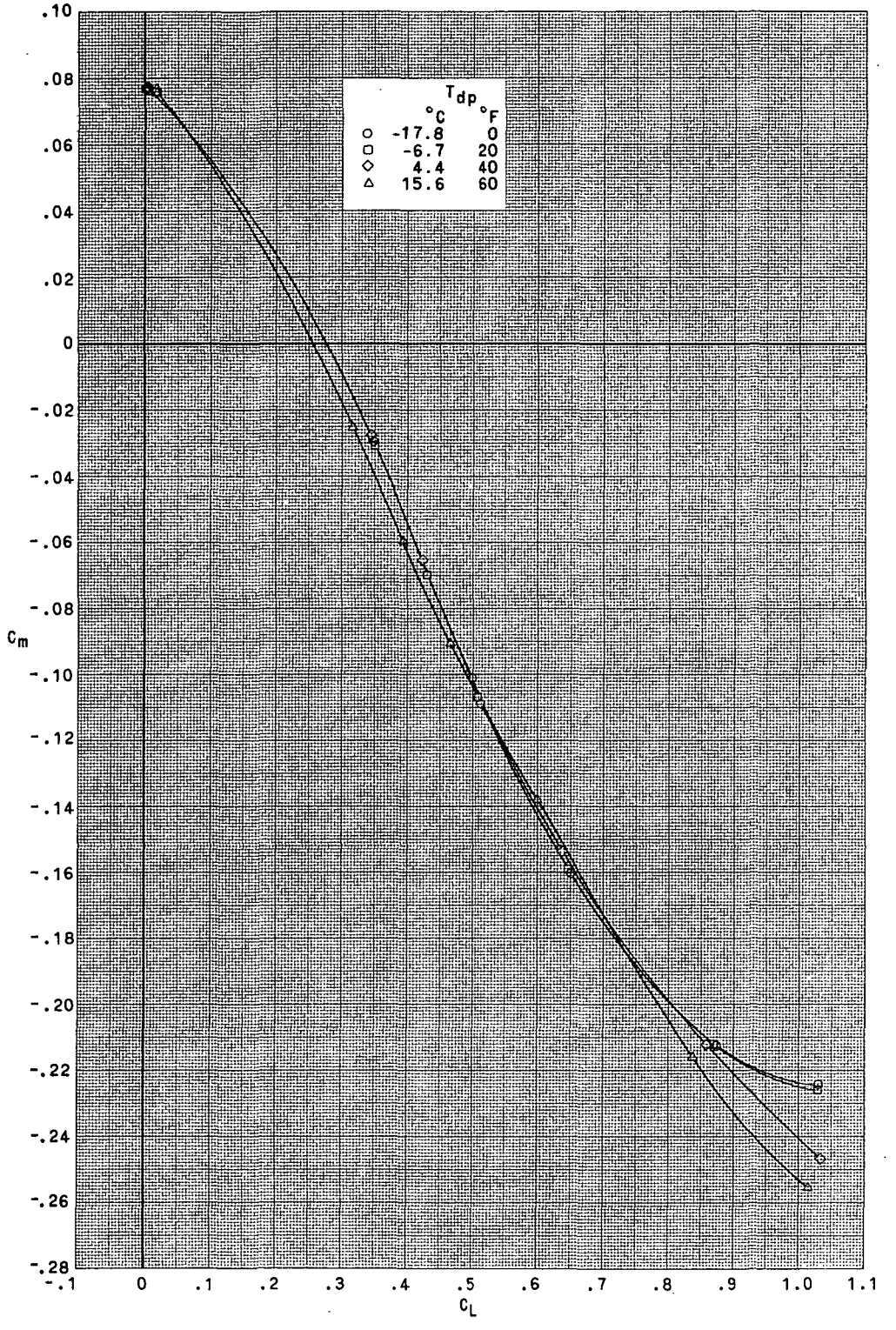

(b) $M_\infty = 0.98$. Continued.

Figure 6.- Continued.

[redacted]

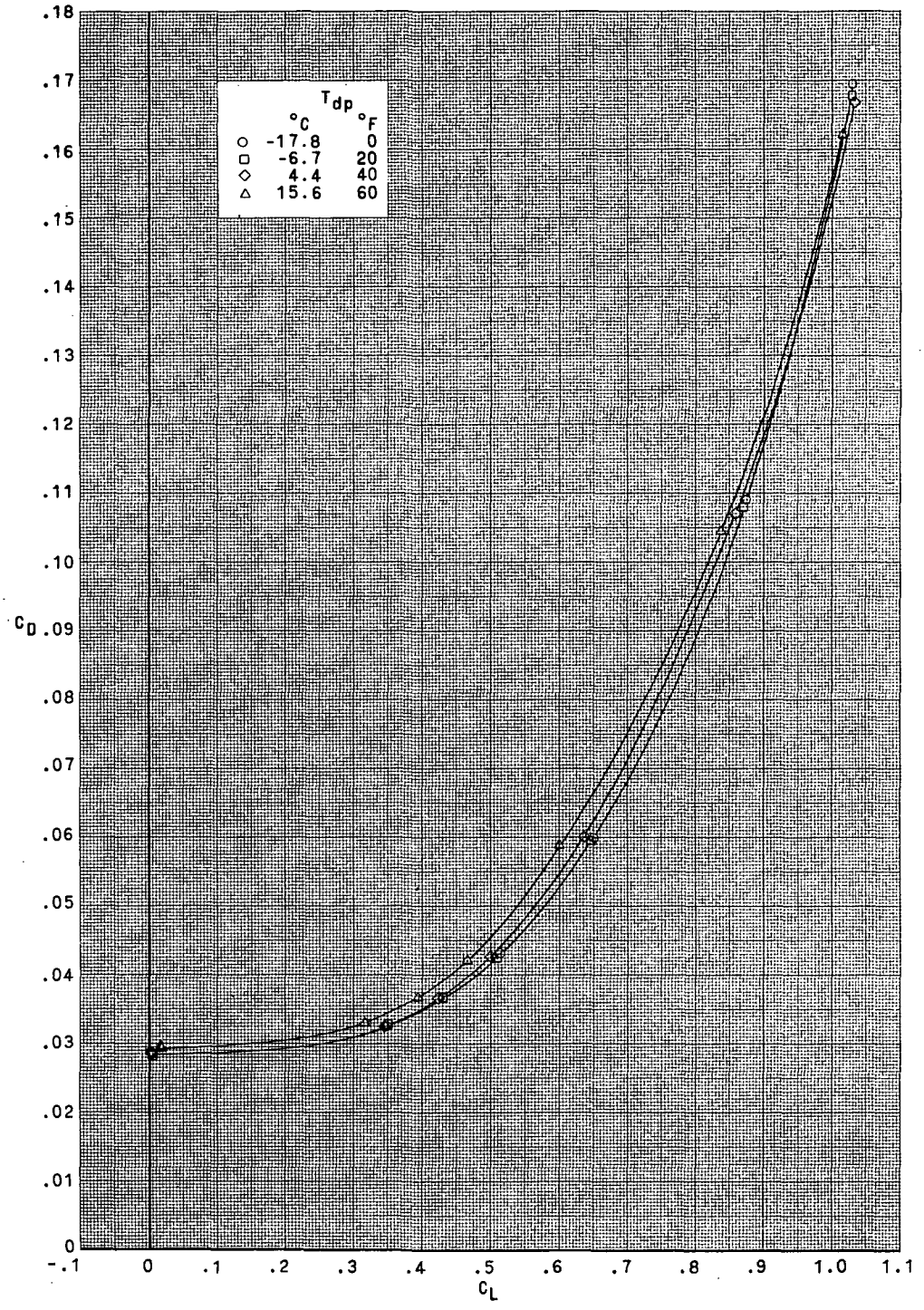

(b) $M_\infty = 0.98$. Concluded.

Figure 6.- Continued.

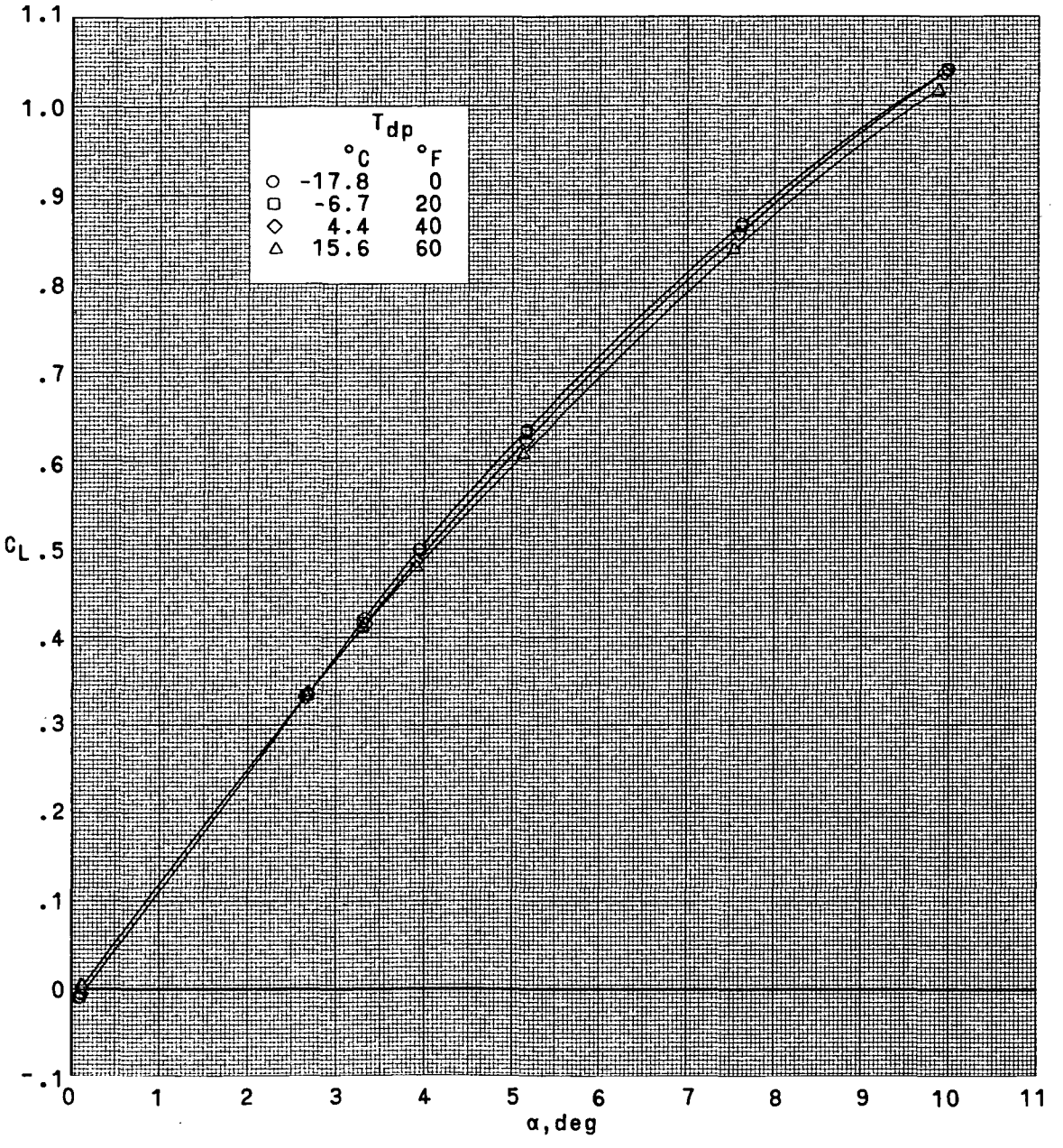

(c) $M_\infty = 1.00$.

Figure 6.- Continued.

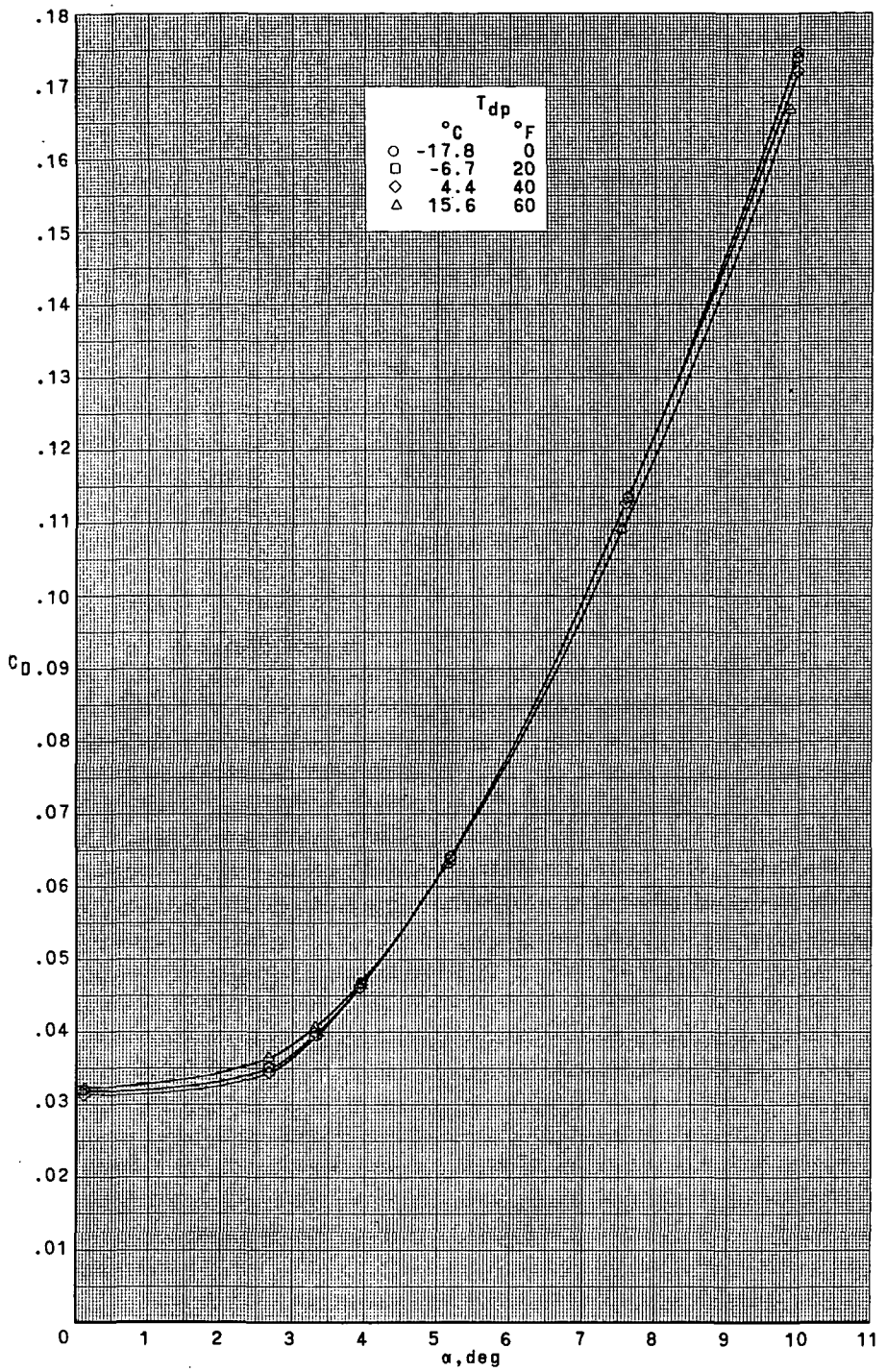

(c) M_∞ = 1.00. Continued.

Figure 6.- Continued.

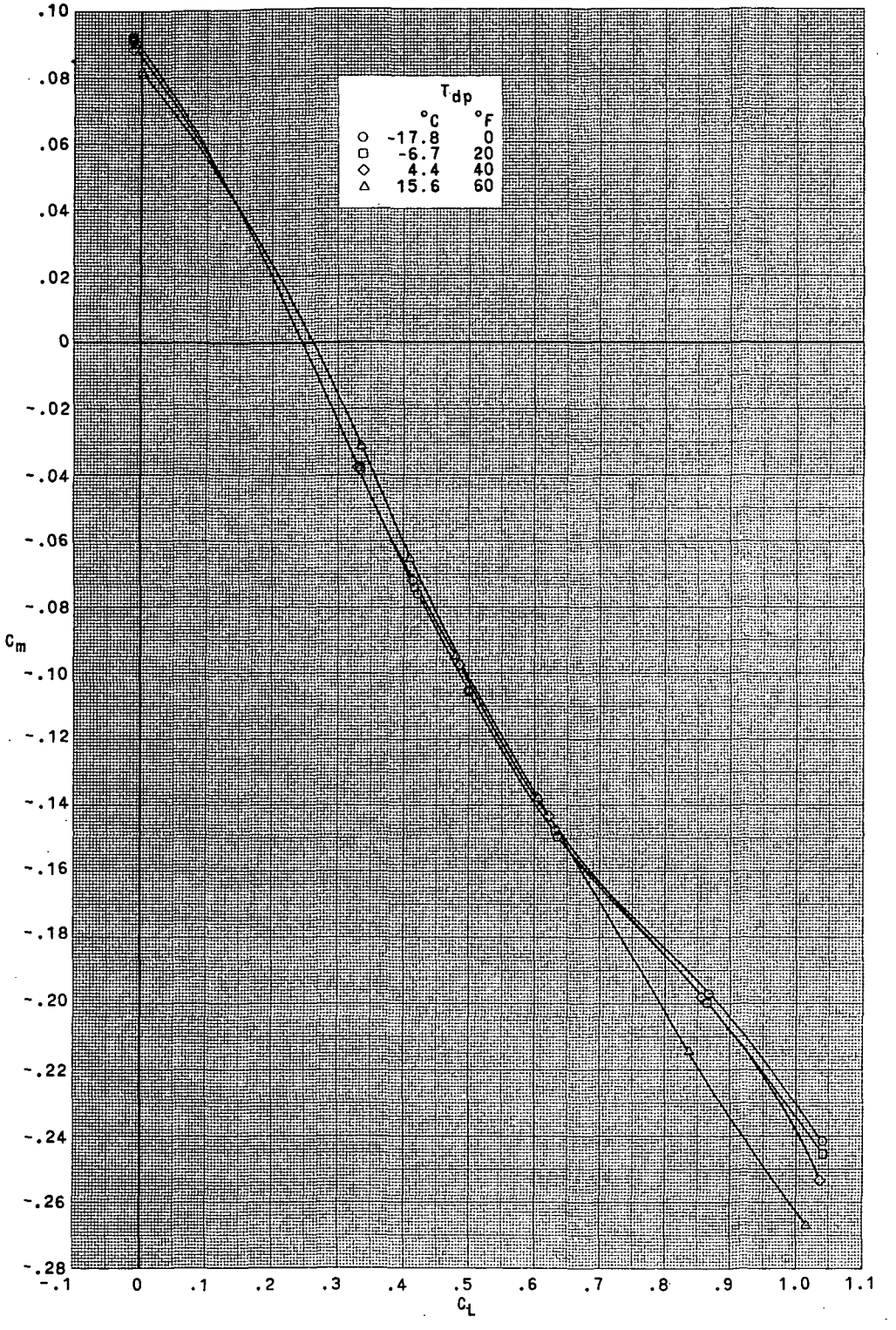

(c) $M_\infty = 1.00$. Continued.

Figure 6.- Continued.

[redacted]

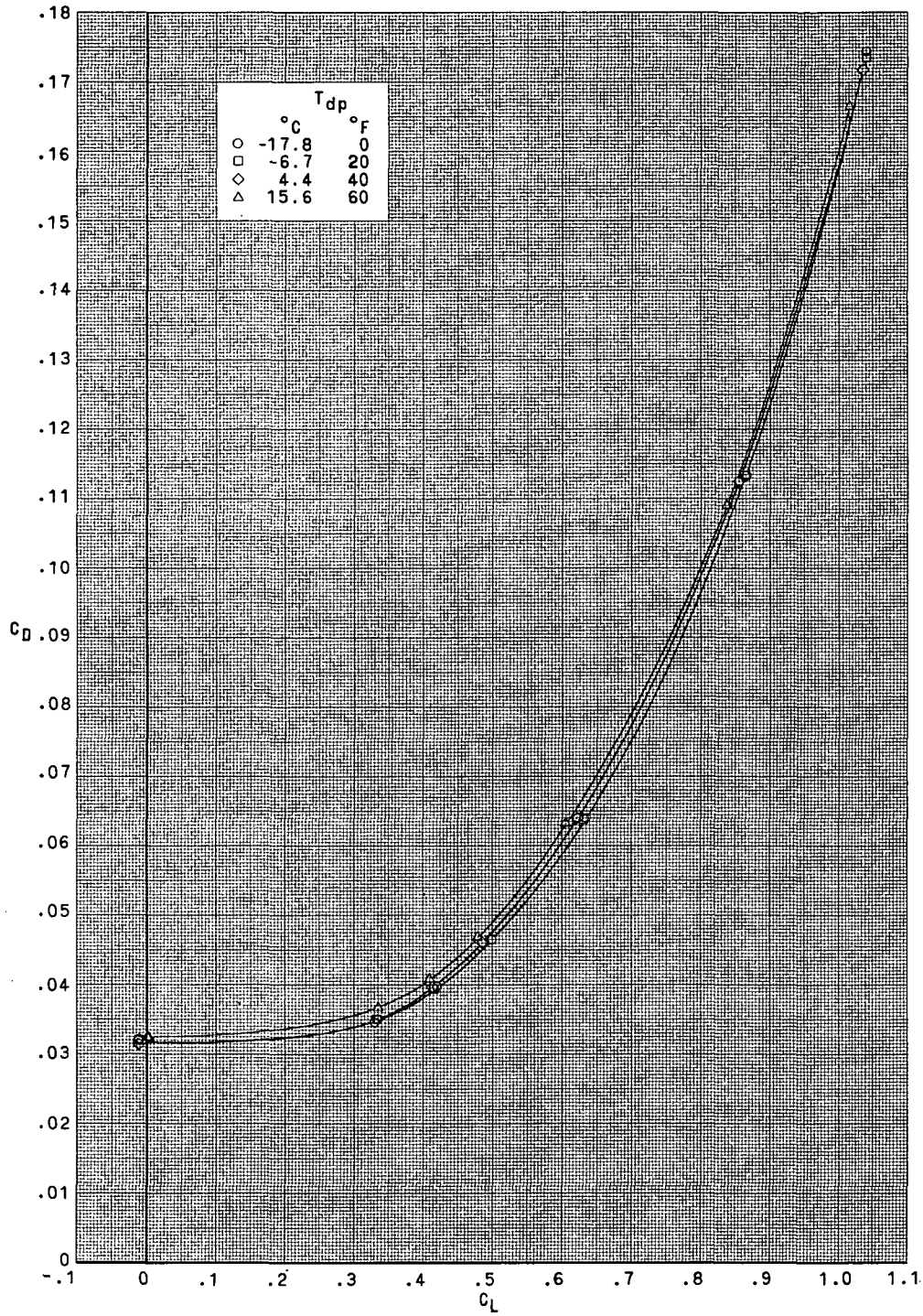

(c) $M_\infty = 1.00$. Concluded.

Figure 6.- Concluded.

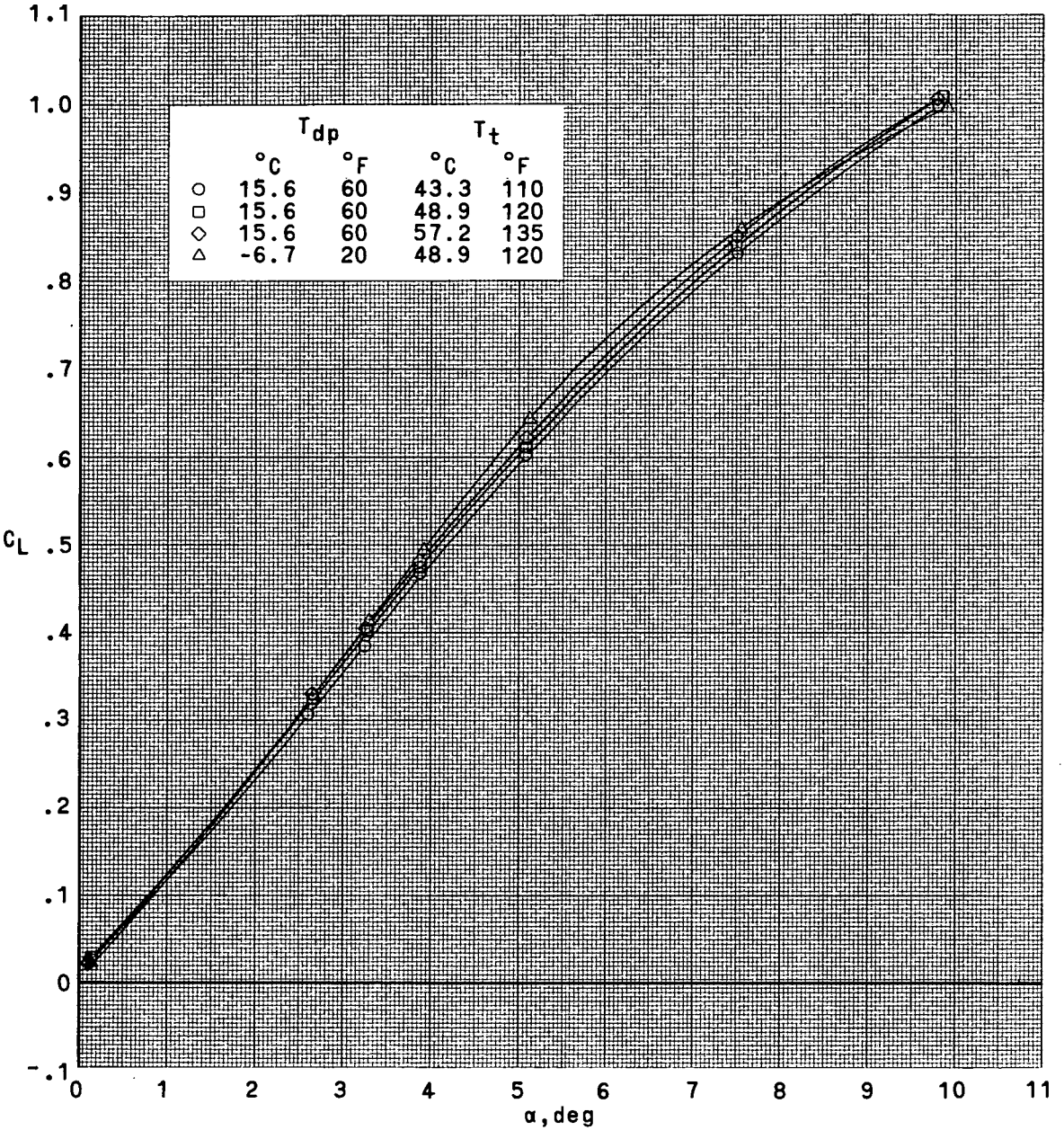

(a) $M_\infty = 0.95$.

Figure 7.- Effect of wind-tunnel stagnation temperature on the longitudinal aerodynamic characteristics at a tunnel dewpoint of 15.6° C (60° F).

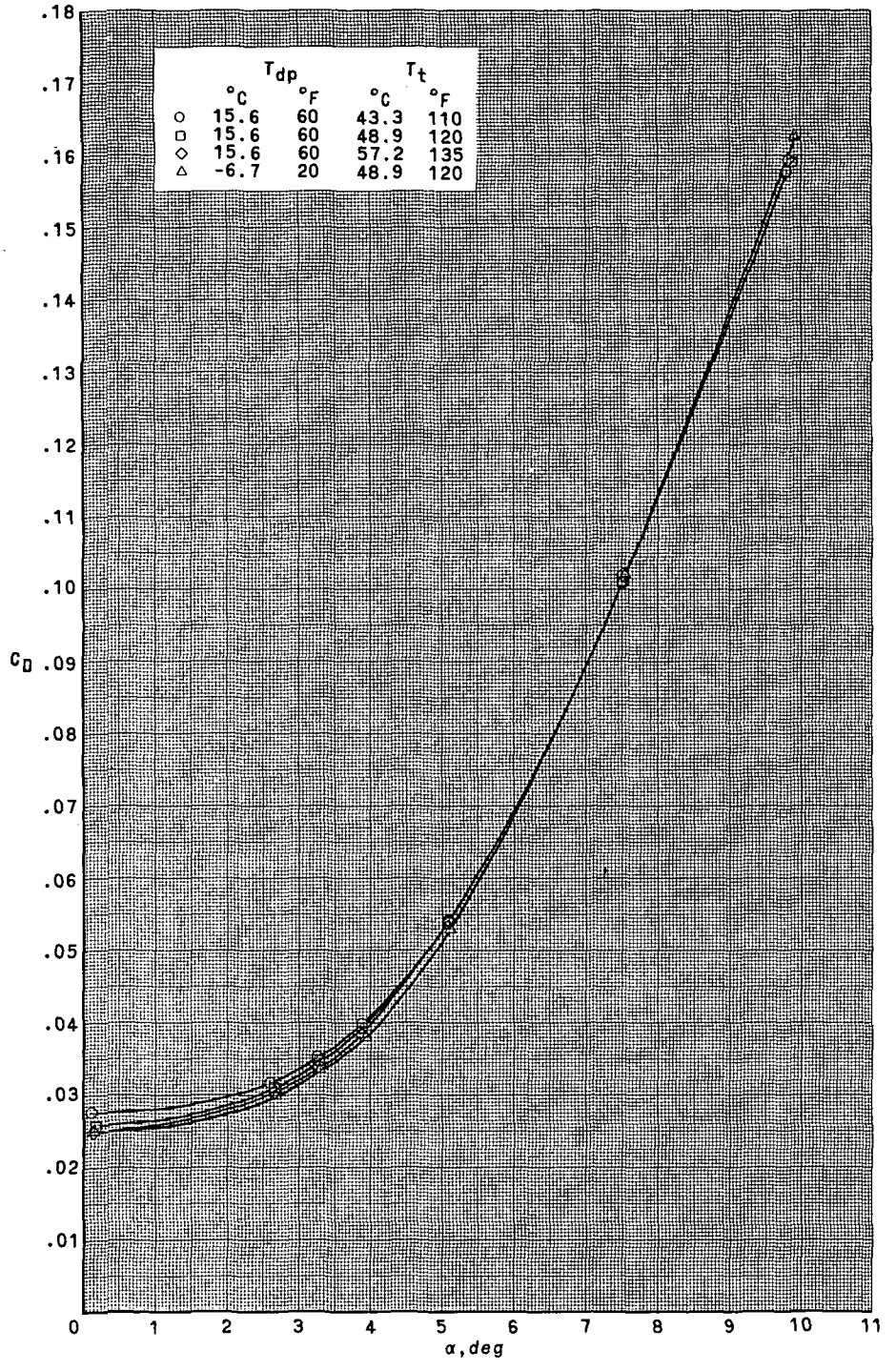

(a) $M_\infty = 0.95$. Continued.

Figure 7.- Continued.

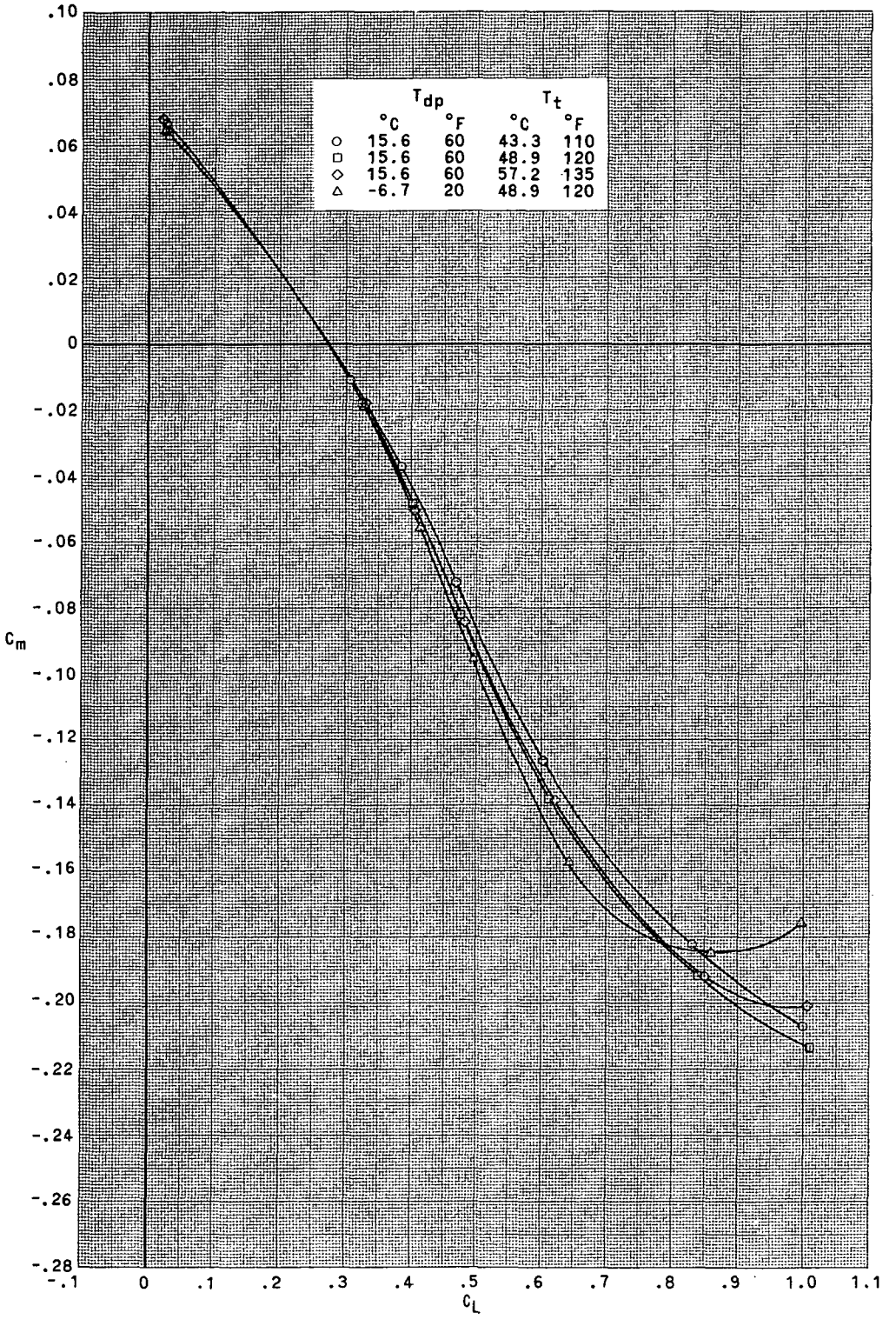

(a) $M_\infty = 0.95$. Continued.

Figure 7.- Continued.

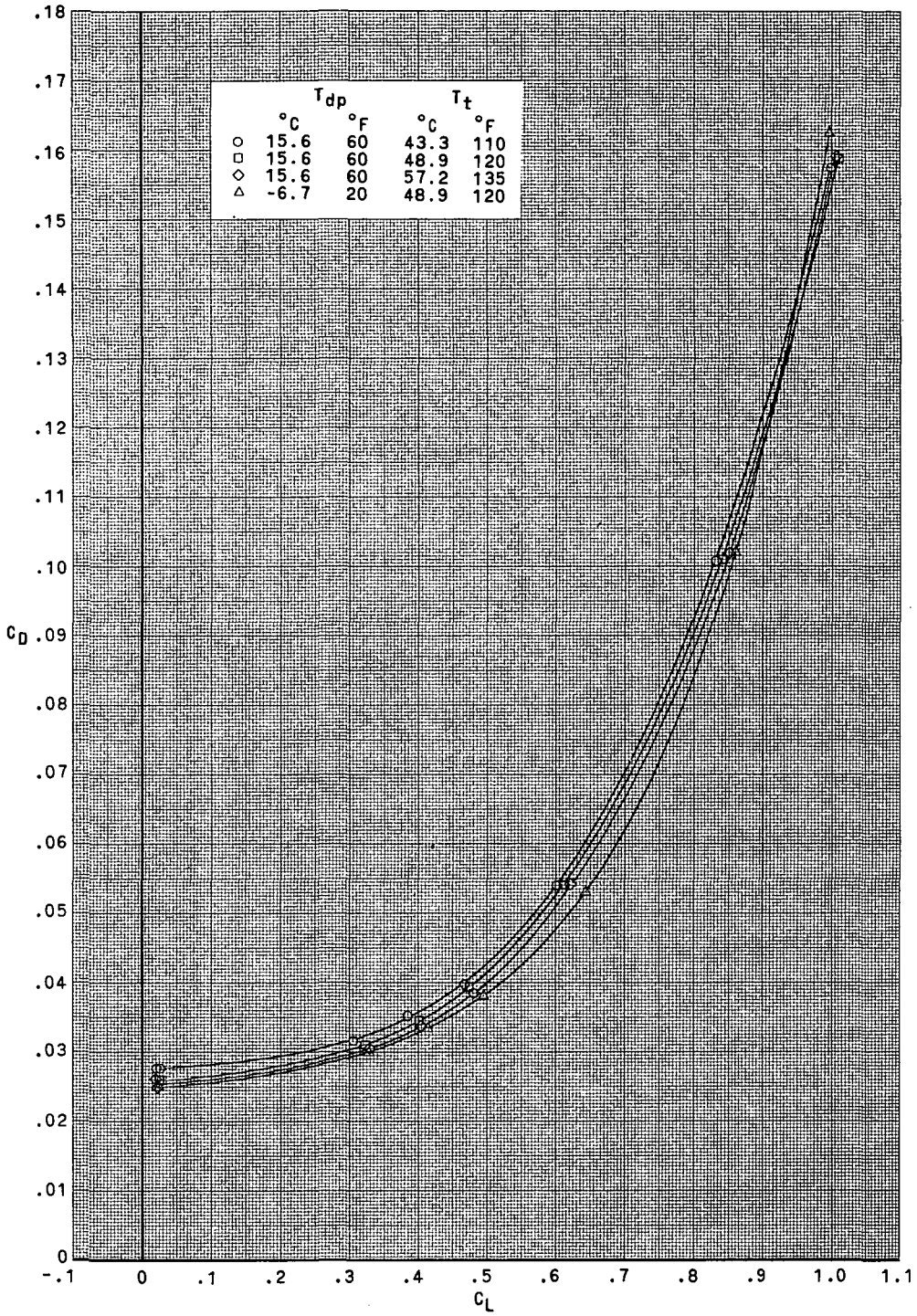

(a) $M_\infty = 0.95$. Concluded.

Figure 7.- Continued.

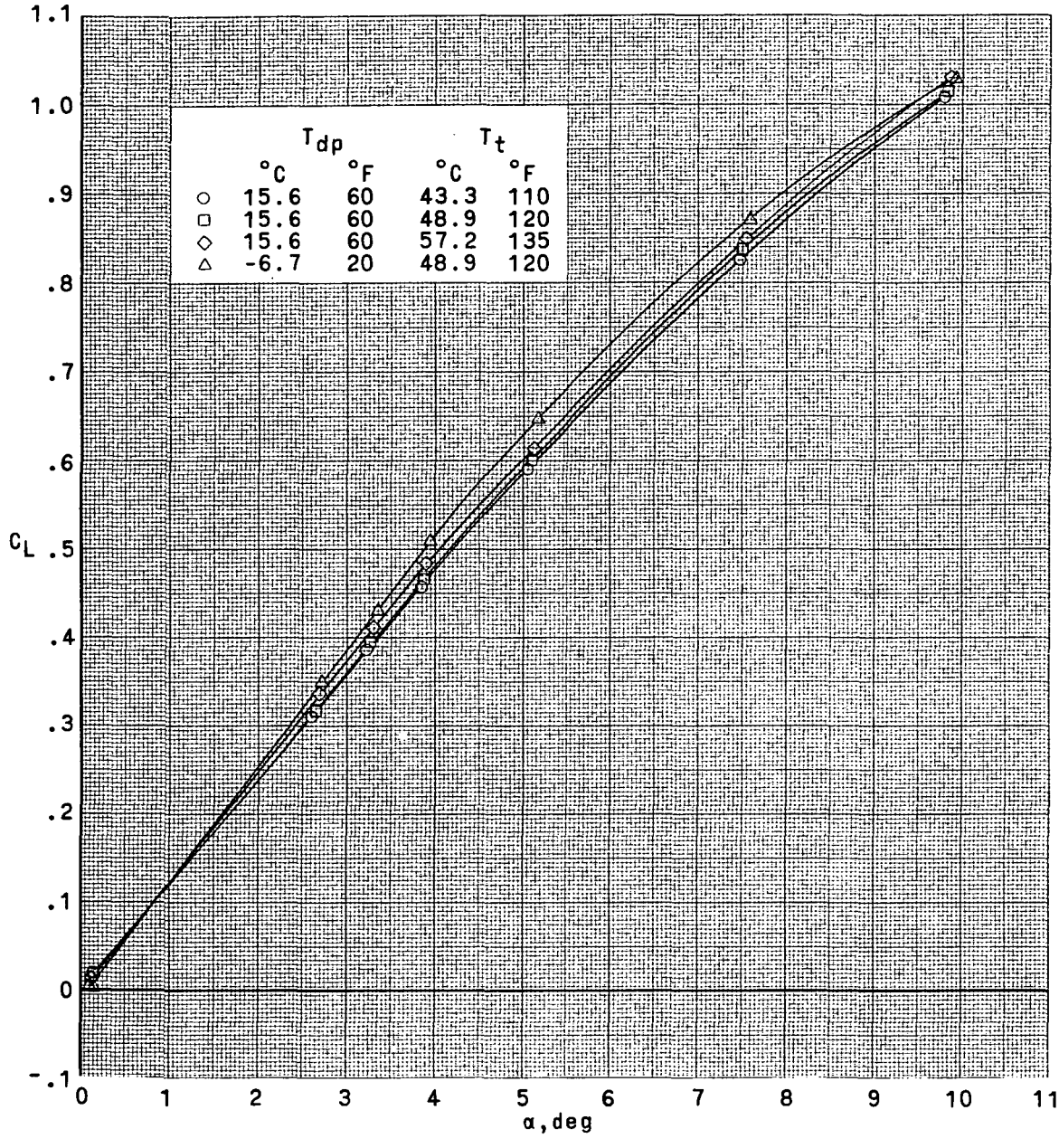

(b) $M_\infty = 0.98$.

Figure 7.- Continued.

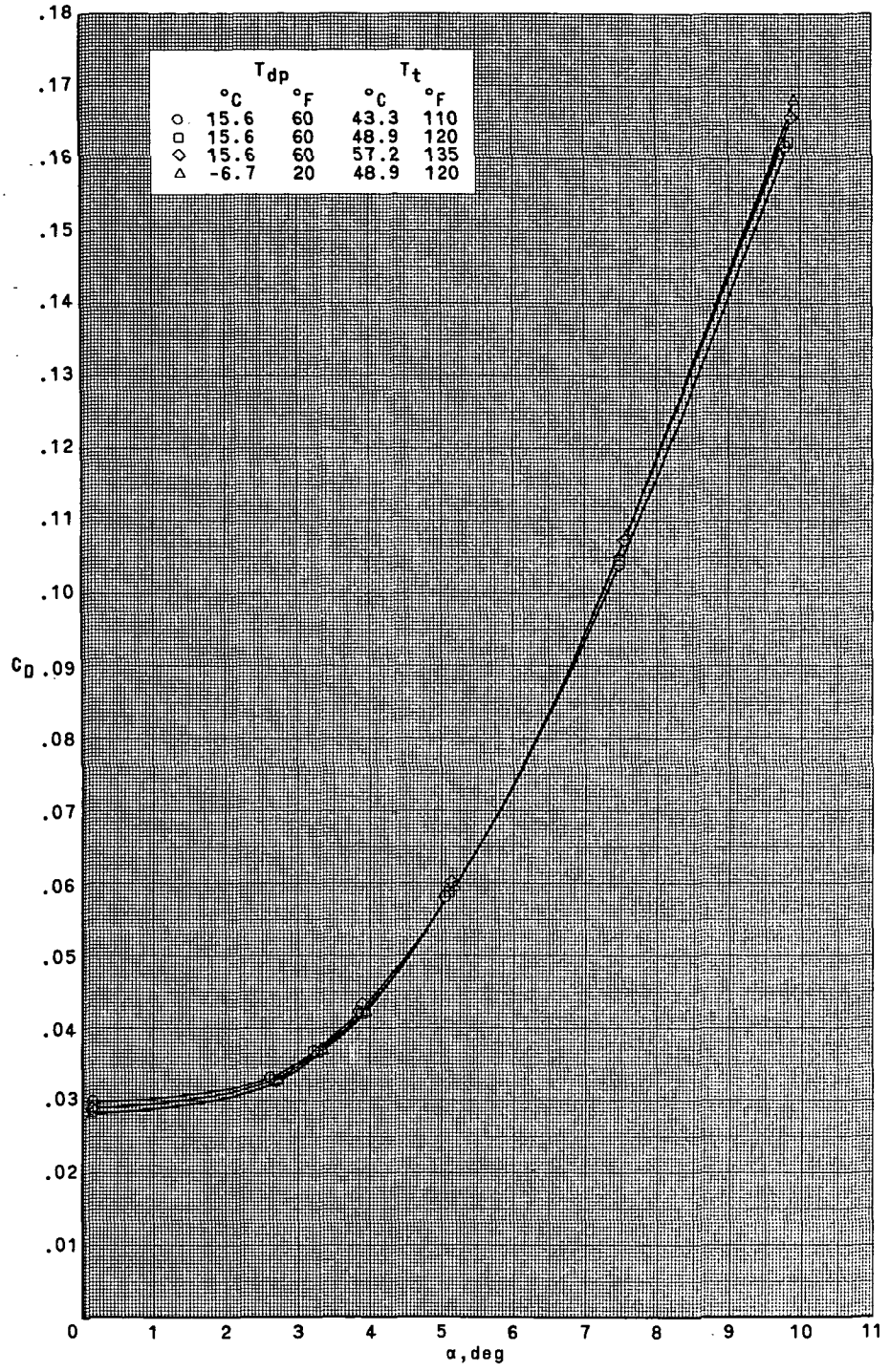

(b) $M_\infty = 0.98$. Continued.

Figure 7.- Continued.

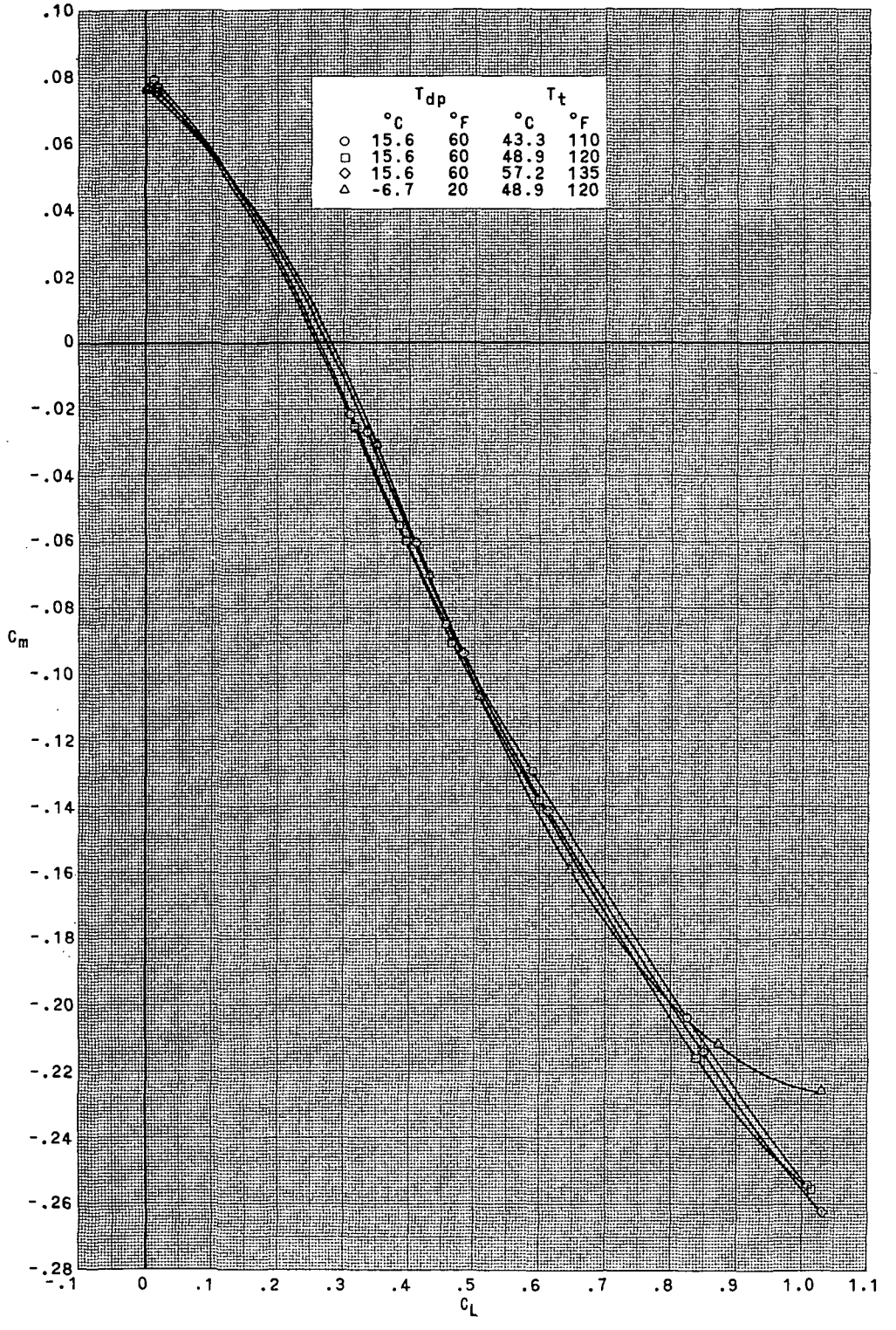

(b) $M_\infty = 0.98$. Continued.

Figure 7.- Continued.

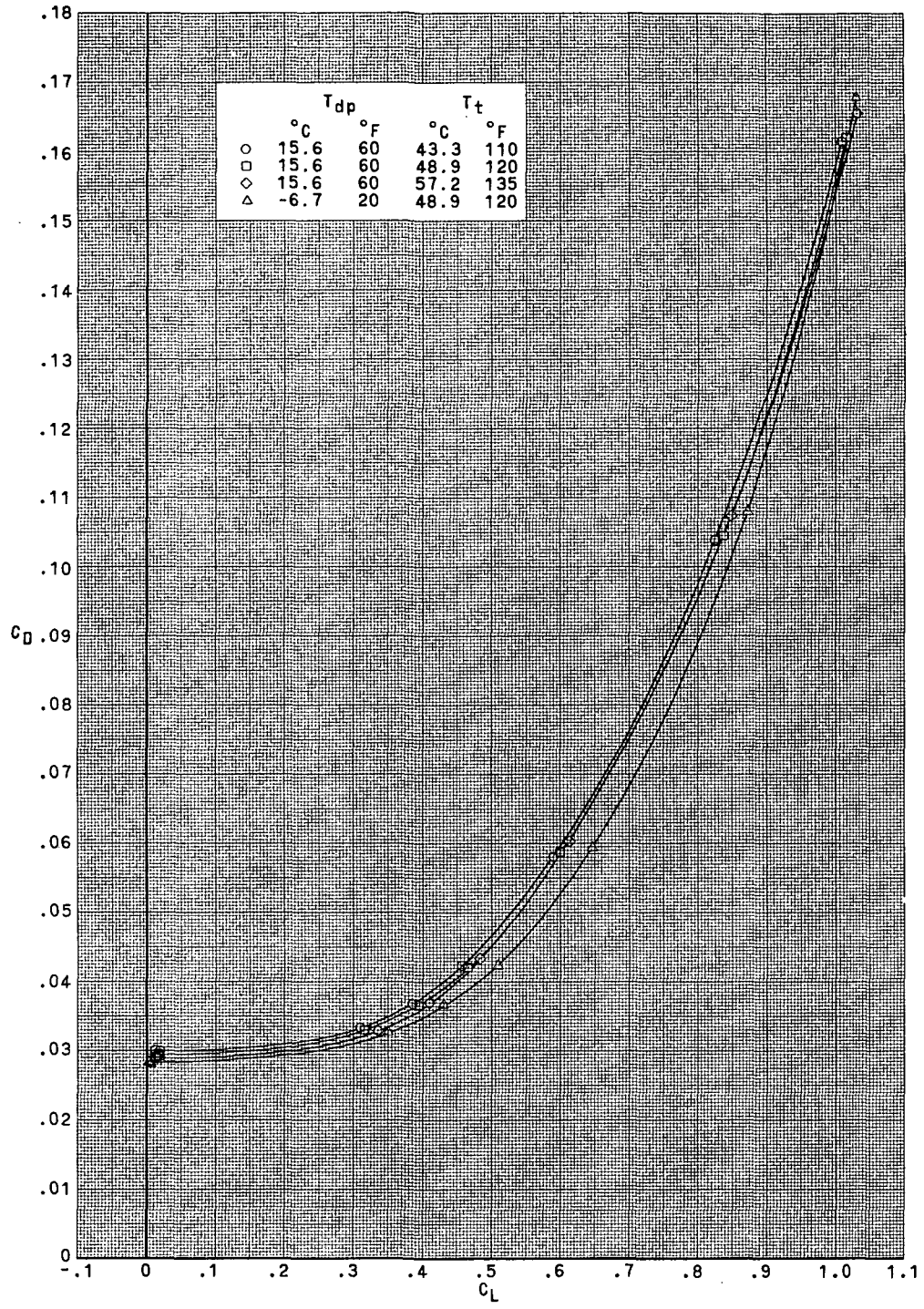

(b) $M_\infty = 0.98$. Concluded.

Figure 7.- Continued.

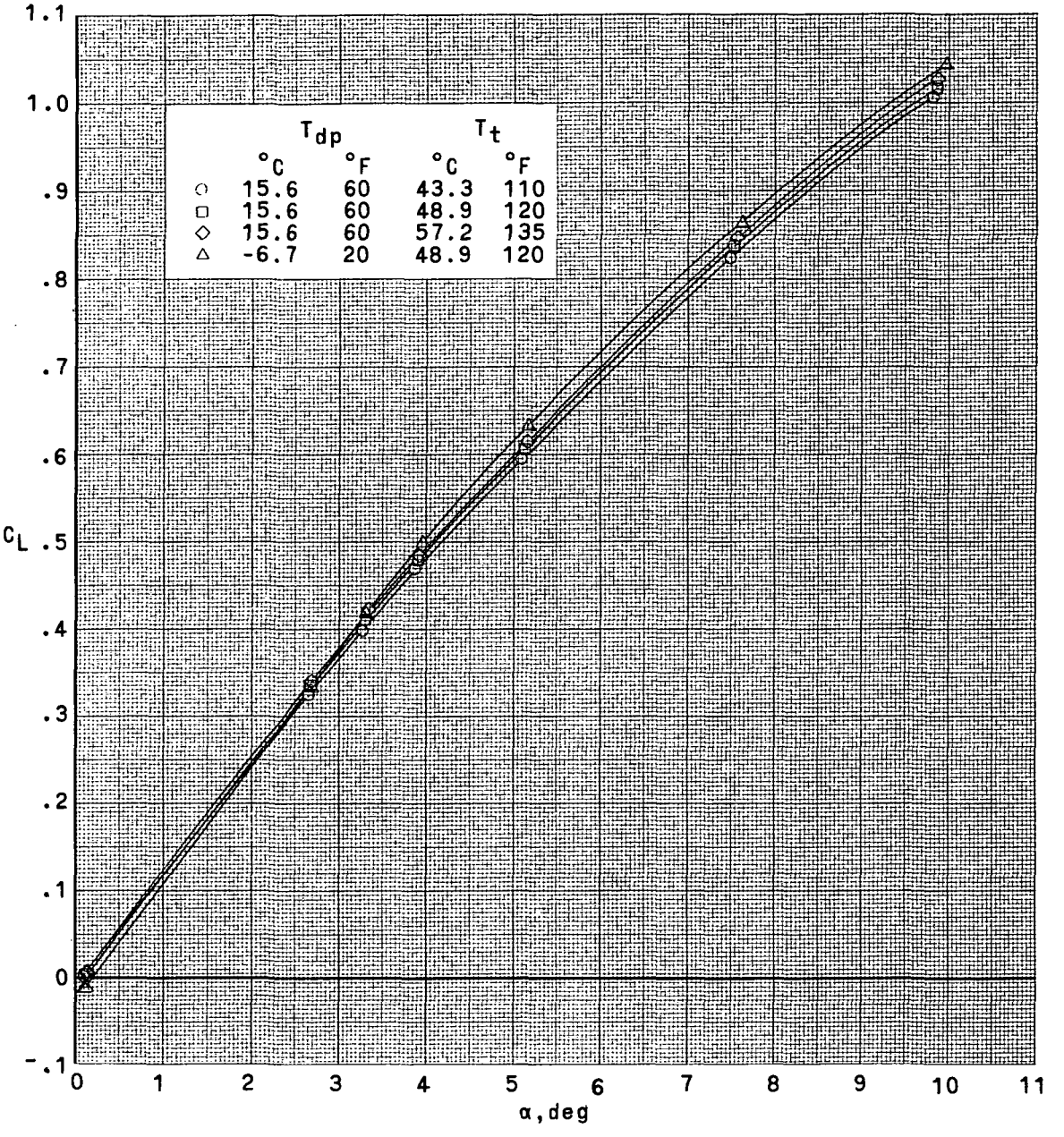

(c) $M_\infty = 1.00$.

Figure 7.- Continued.

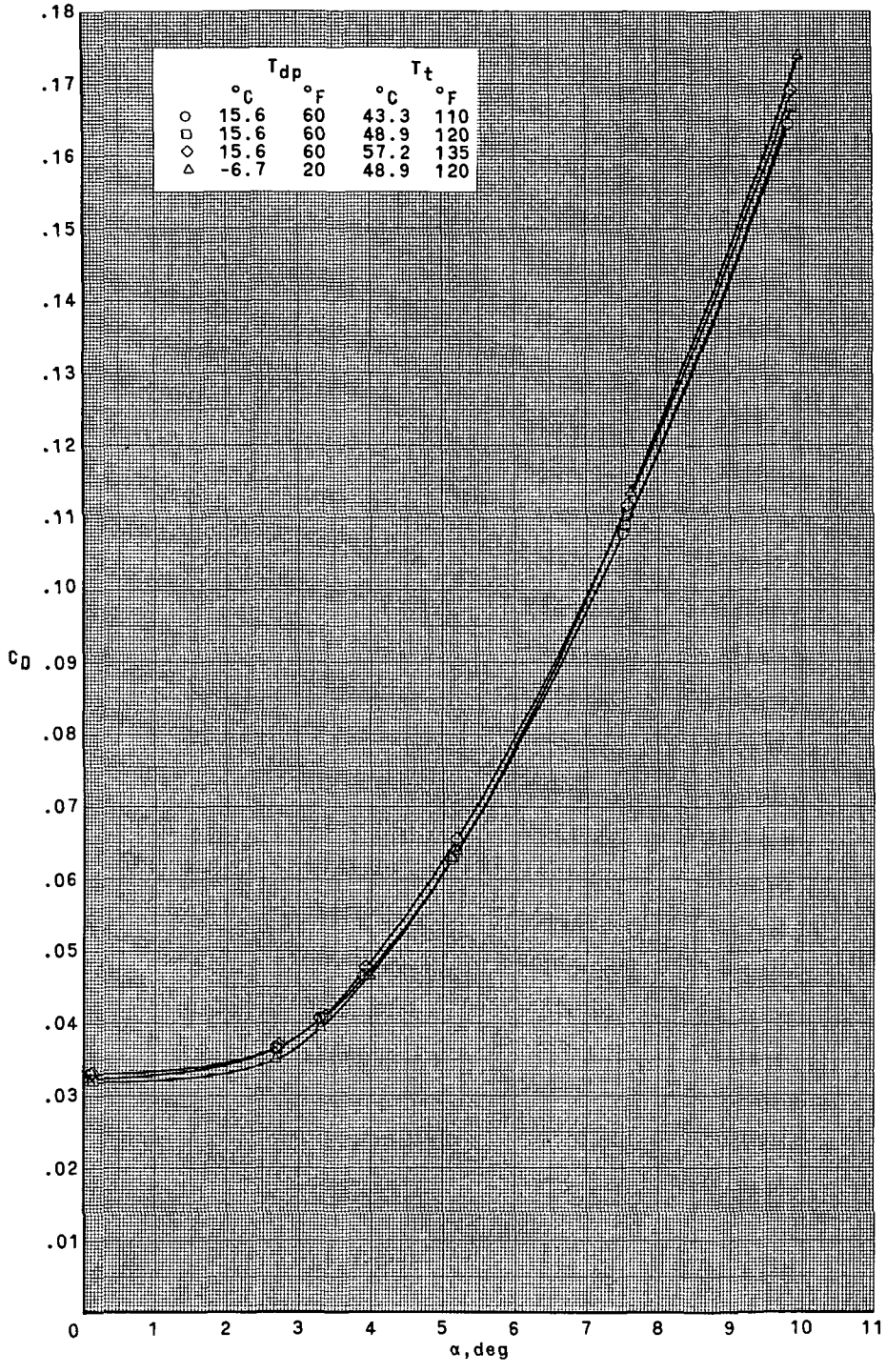

(c) M_∞ = 1.00. Continued.

Figure 7.- Continued.

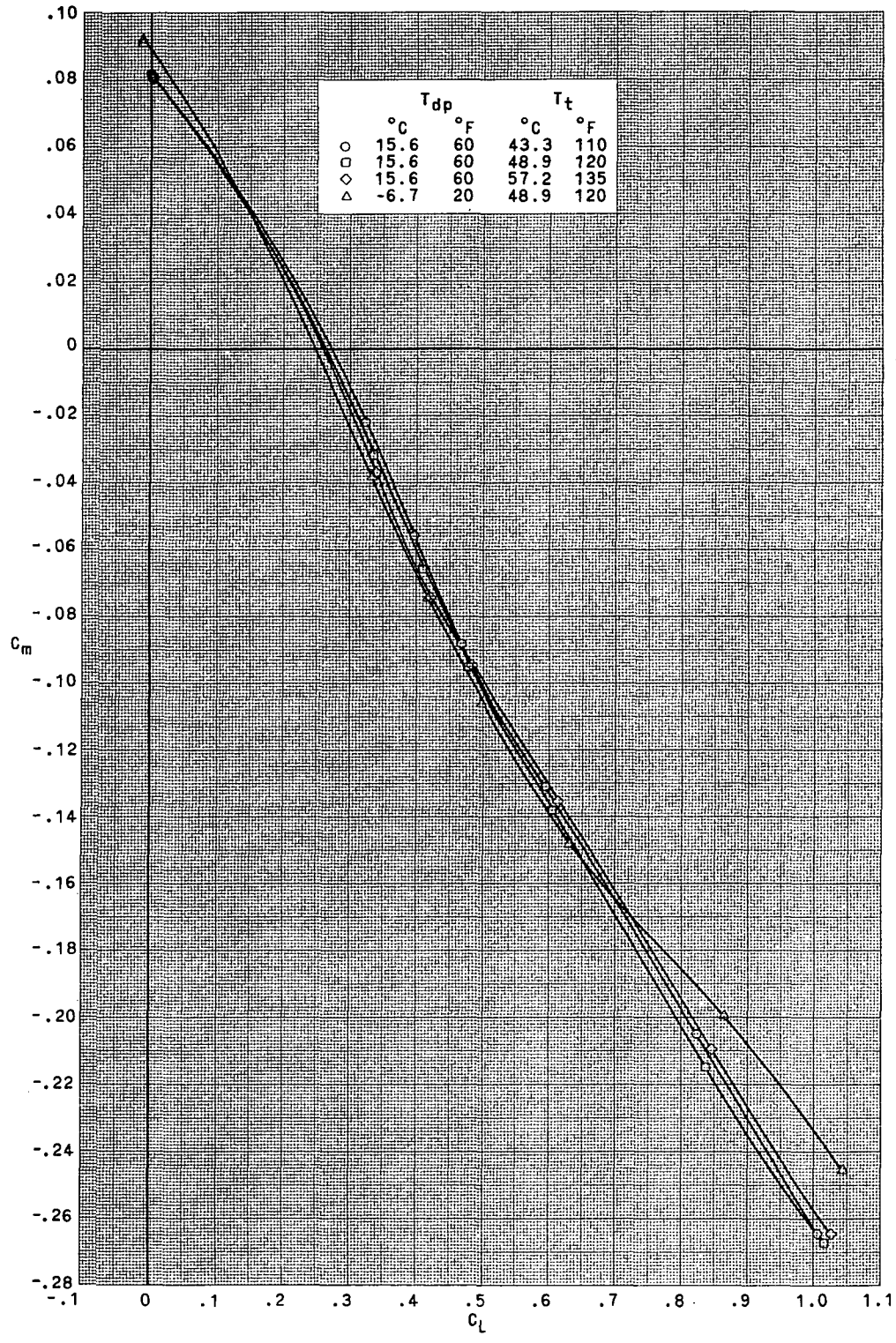

(c) $M_\infty = 1.00$. Continued.

Figure 7.- Continued.

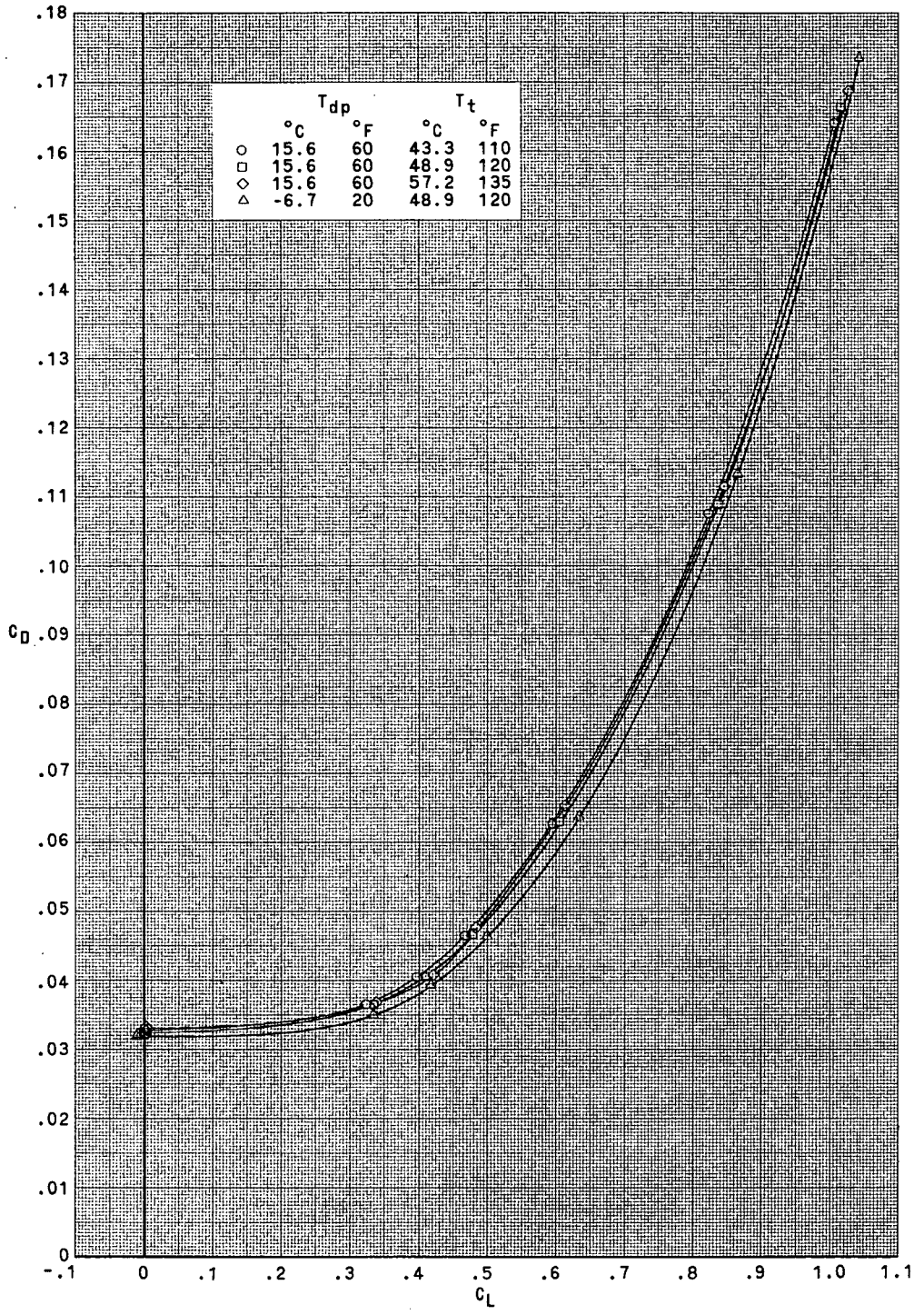

(c) $M_\infty = 1.00$. Concluded.

Figure 7.- Concluded.

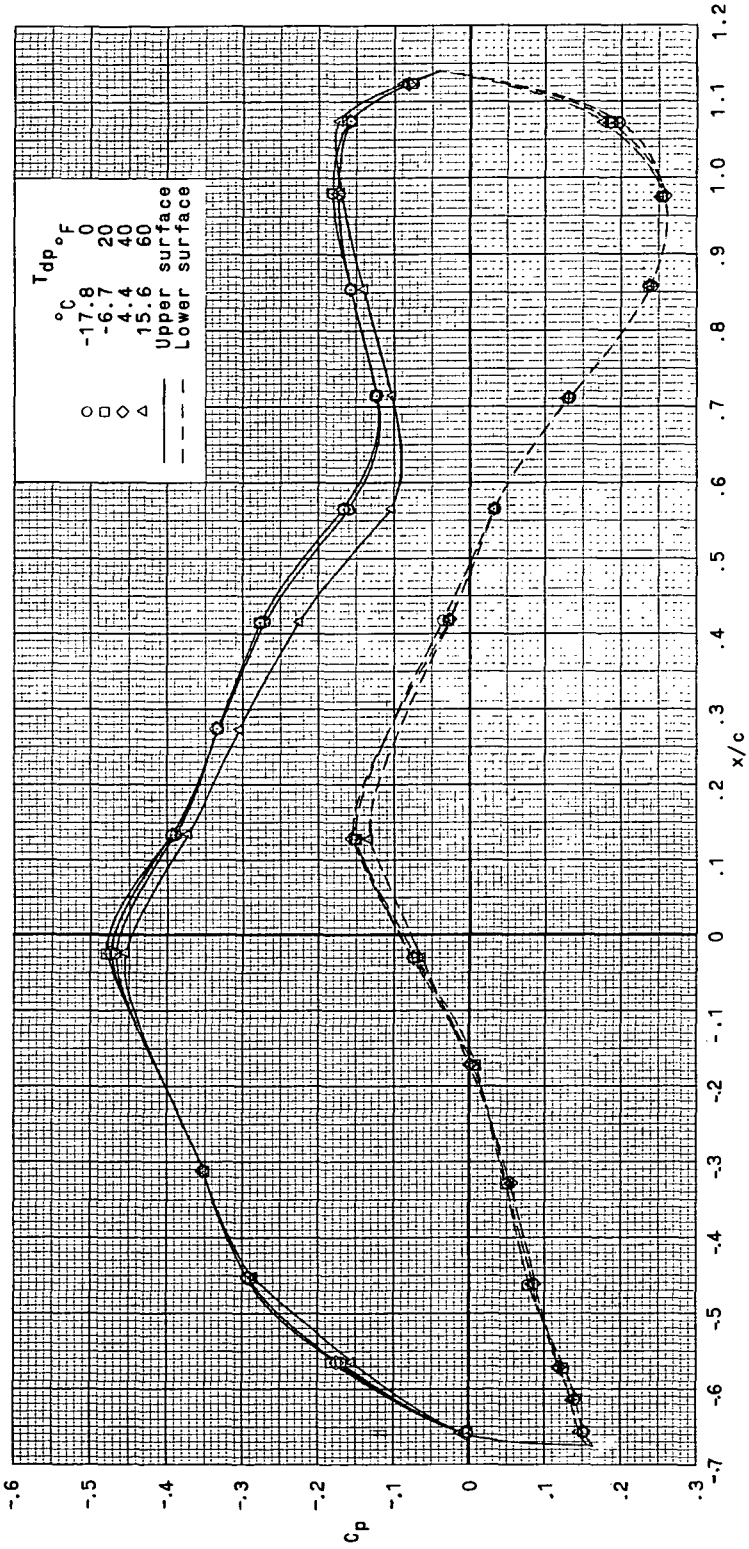

(a) c = 22.61 cm (8.903 in.); 13.3-percent-semispan station.

Figure 8.- Effect of wind-tunnel dewpoint on wing streamwise-chord pressure distributions at $\alpha = 5.2^{\circ}$. $M_{\infty} = 0.980$; $T_t = 48.9^{\circ}$ C (120° F).

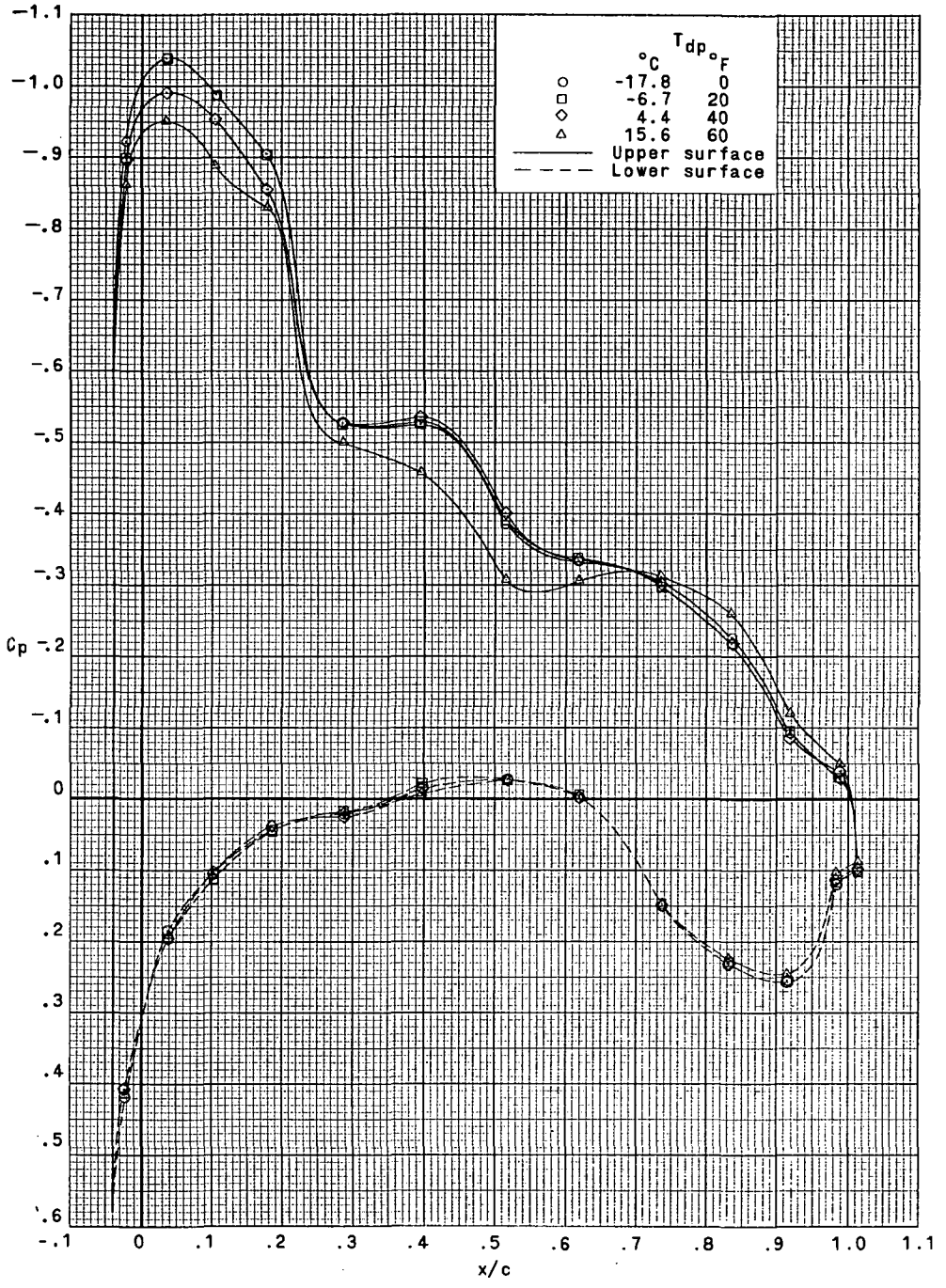

(b) c = 19.88 cm (7.828 in.); 30.7-percent-semispan station.

Figure 8.- Continued.

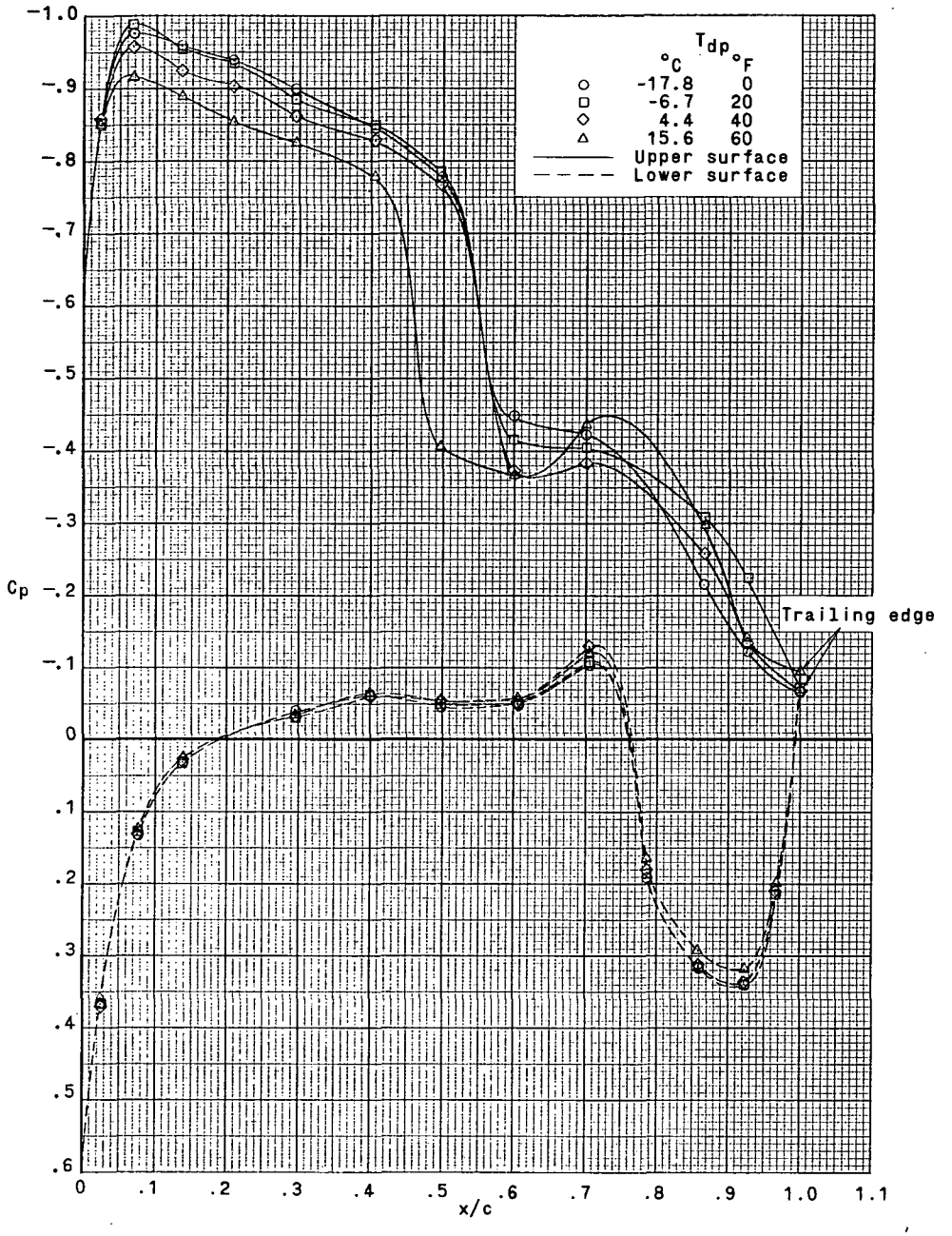

(c) c = 17.16 cm (6.756 in.); 48.0-percent-semispan station.

Figure 8.- Continued.

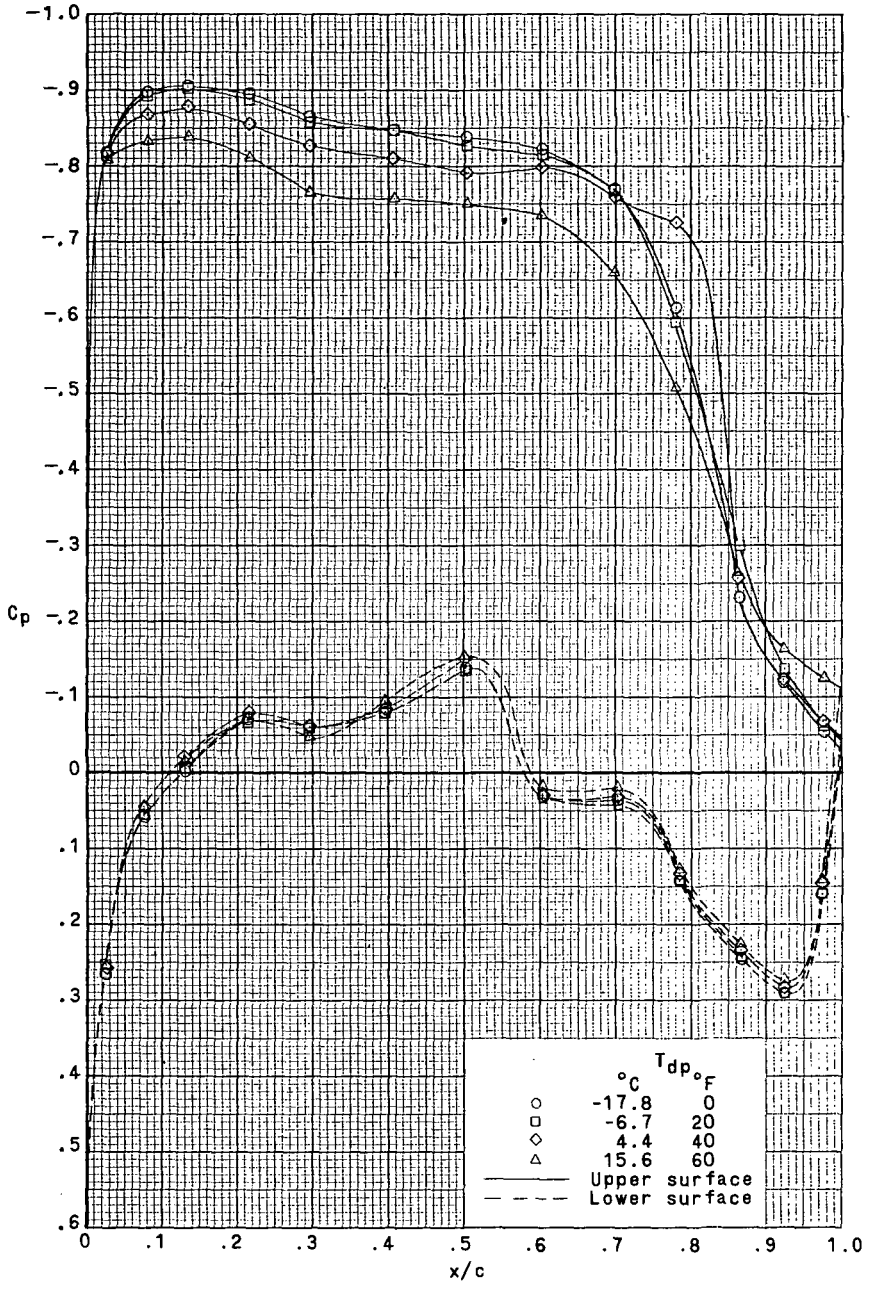

(d) c = 14.44 cm (5.686 in.); 65.3-percent-semispan station.

Figure 8.- Continued.

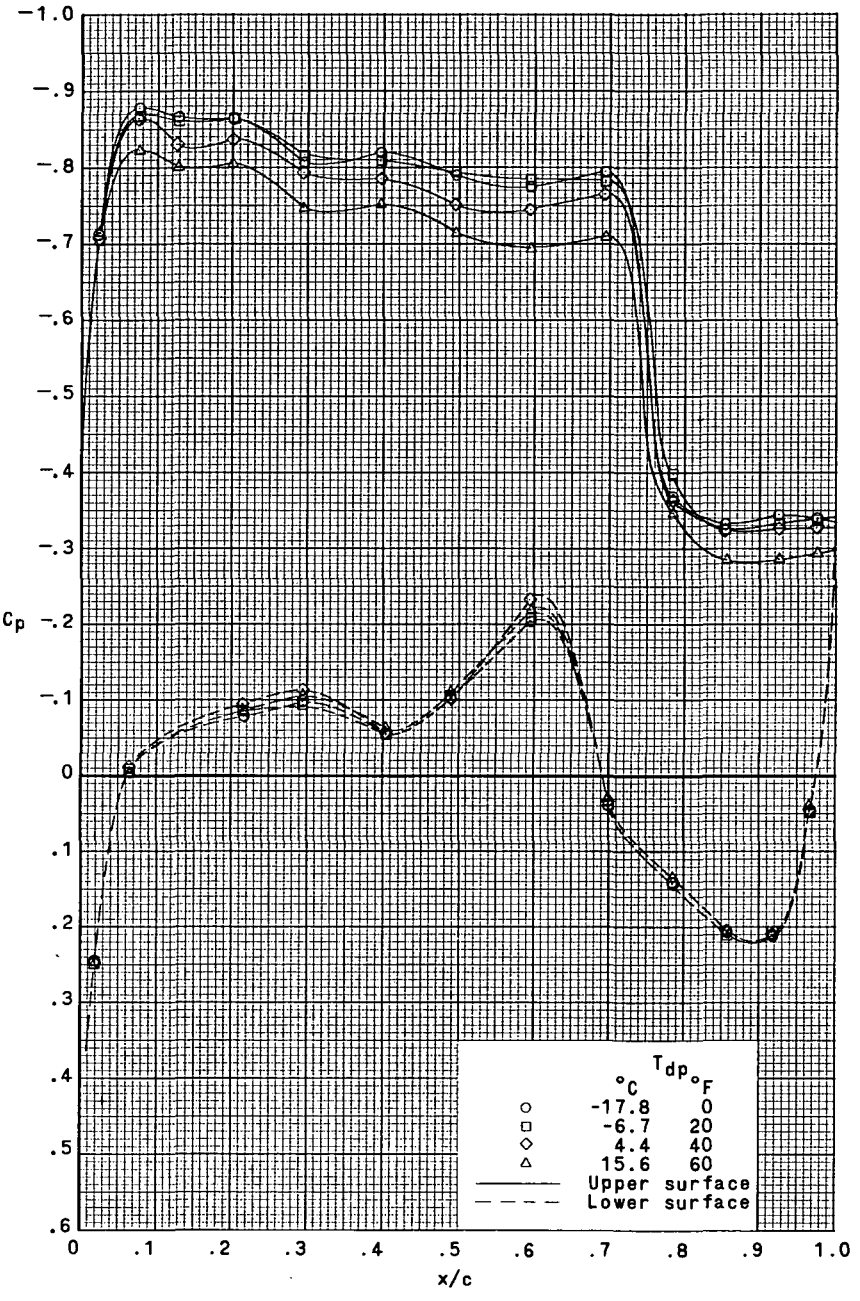

(e) c = 12.07 cm (4.752 in.); 80.4-percent-semispan station.

Figure 8.- Continued.

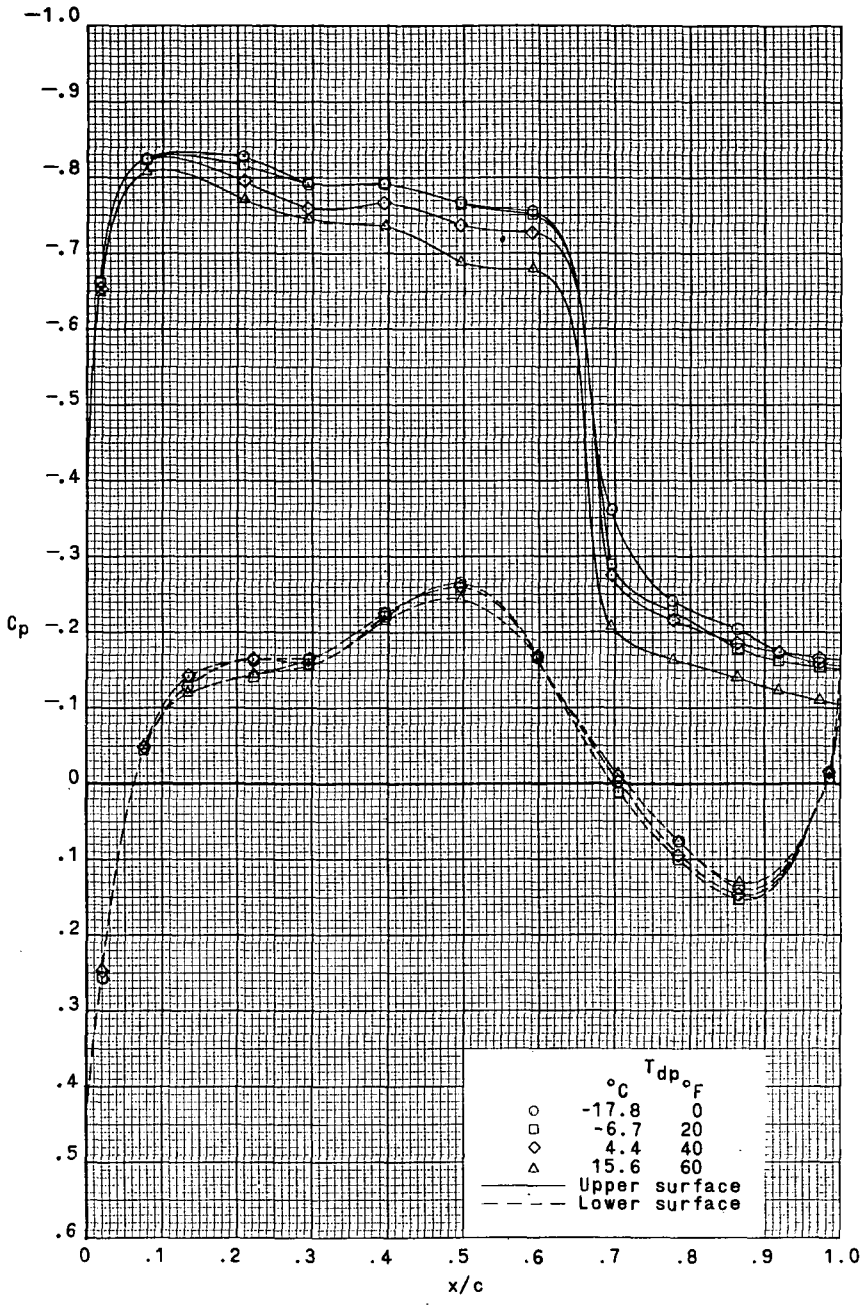

(f) c = 10.04 cm (3.954 in.); 93.3-percent-semispan station.

Figure 8.- Concluded.

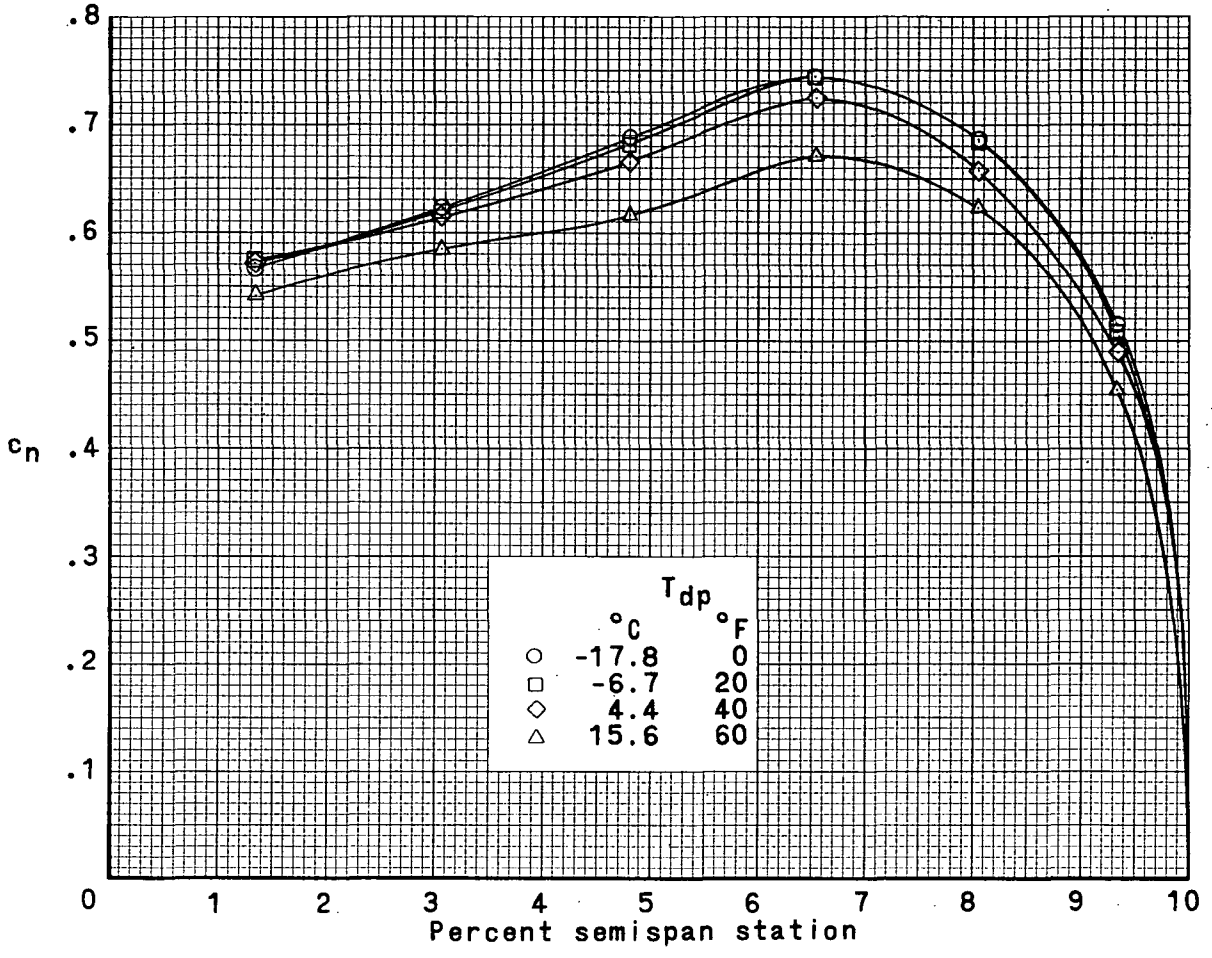

Figure 9.- Effect of wind-tunnel dewpoint on wing span load distribution at $\alpha = 5.2^{o}$. $M_{\infty} = 0.980$; $T_t = 48.9^{o}$ C (120^{o} F).

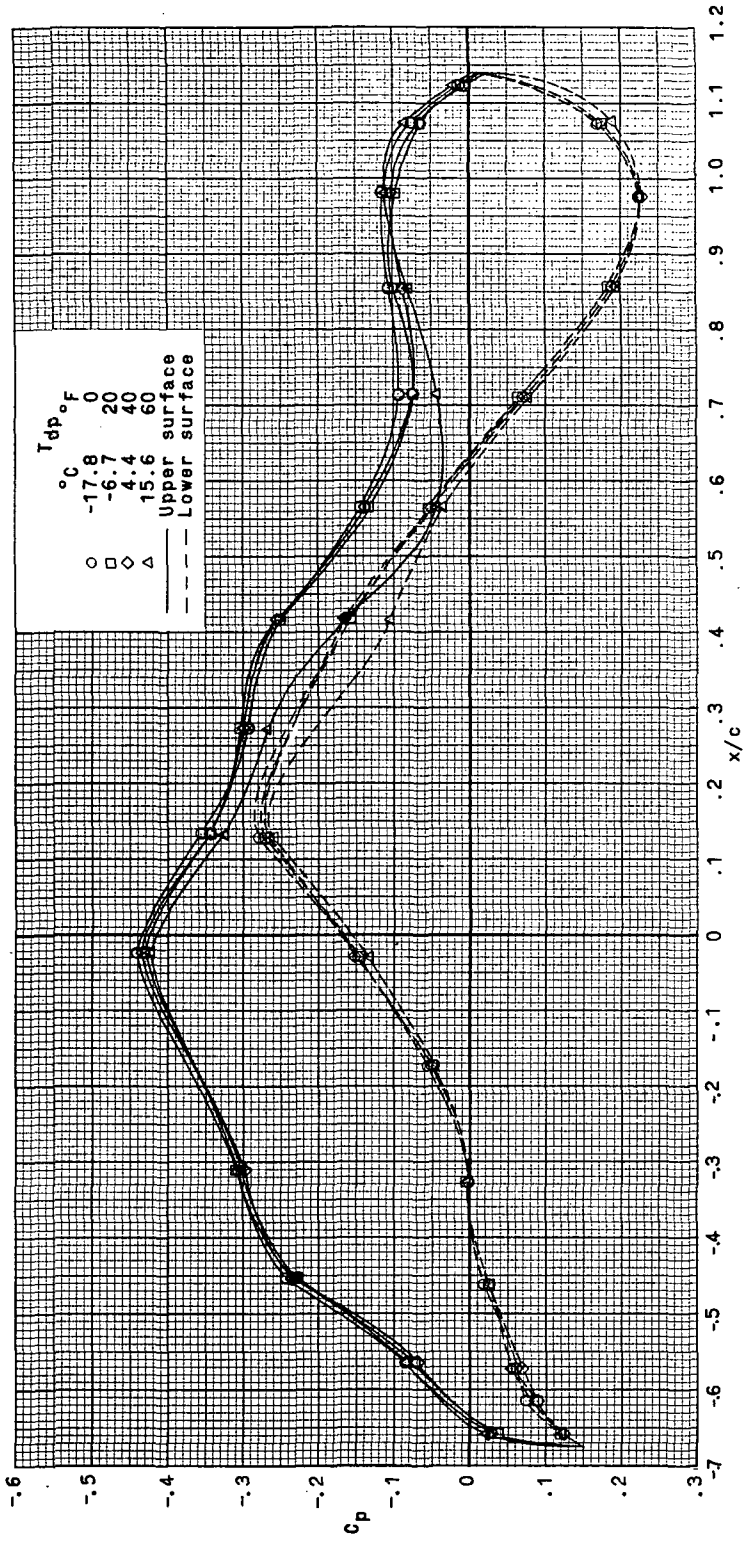

(a) c = 22.61 cm (8.903 in.); 13.3-percent-semispan station.

Figure 10.- Effect of wind-tunnel dewpoint on wing streamwise-chord pressure distributions at $\alpha = 2.7^{\circ}$. $M_{\infty} = 0.980$; $T_t = 48.9^{\circ}$ C (120° F).

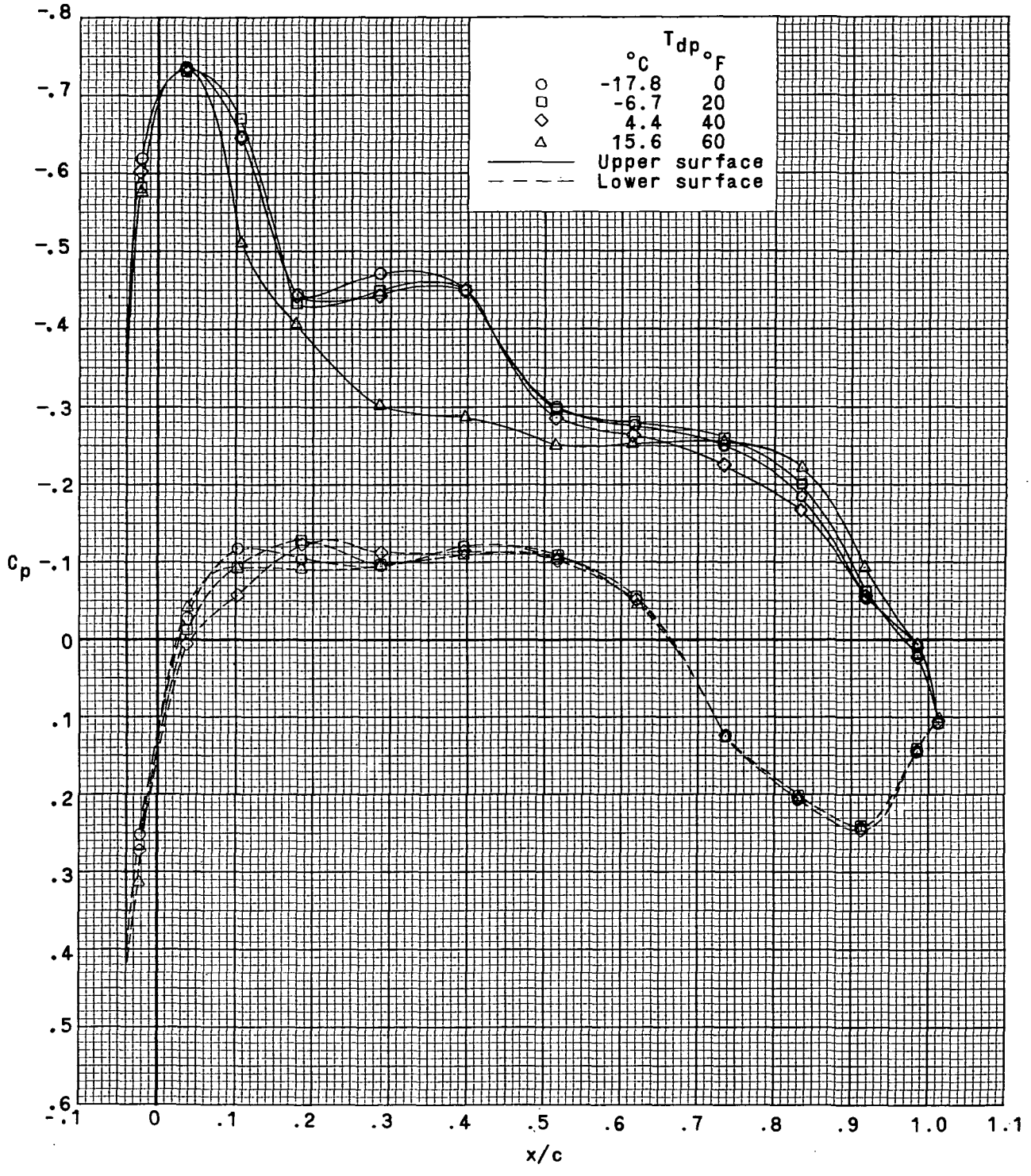

(b) c = 19.88 cm (7.828 in.); 30.7-percent-semispan station.

Figure 10.- Continued.

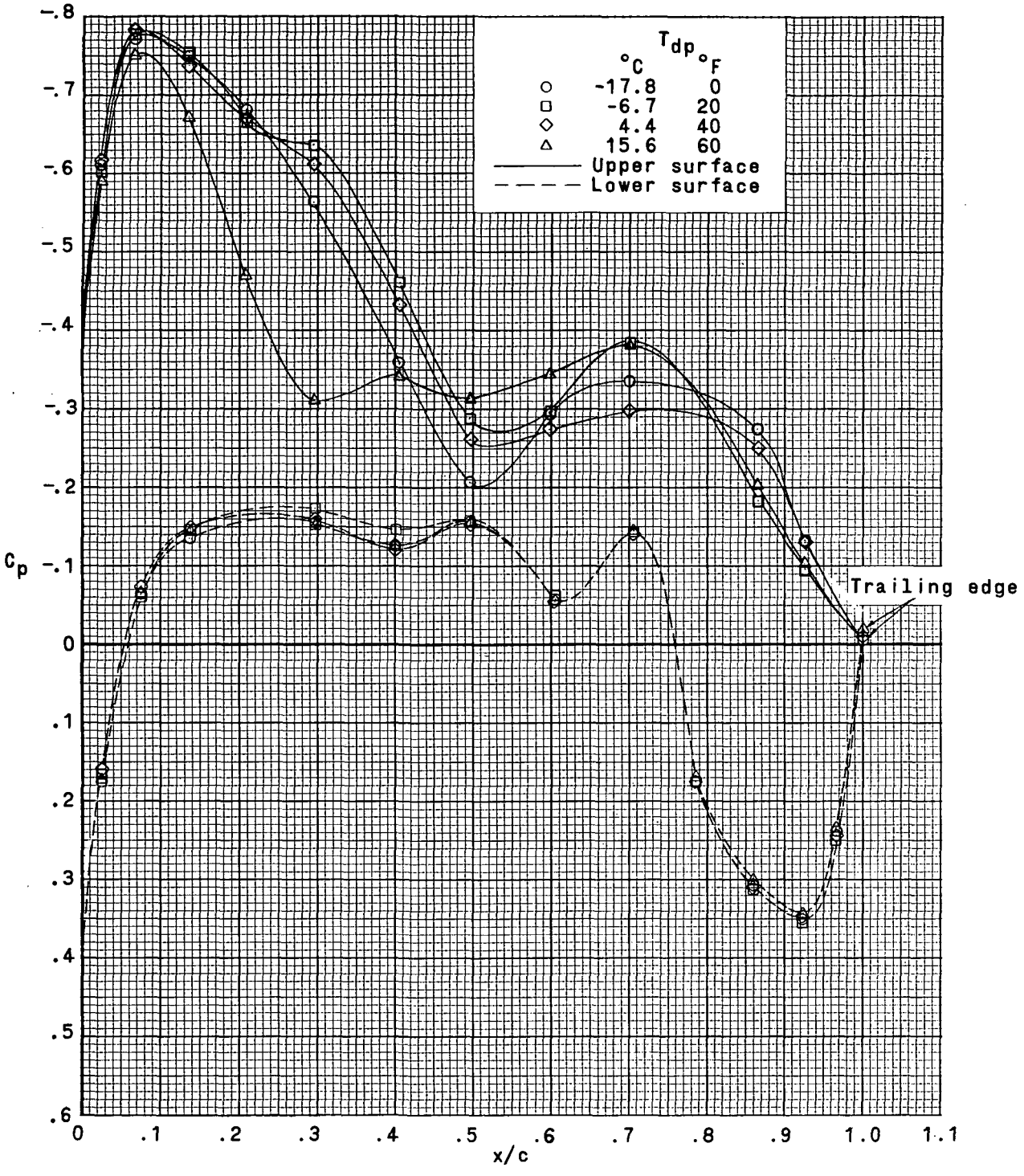

(c) c = 17.16 cm (6.756 in.); 48.0-percent-semispan station.

Figure 10.- Continued.

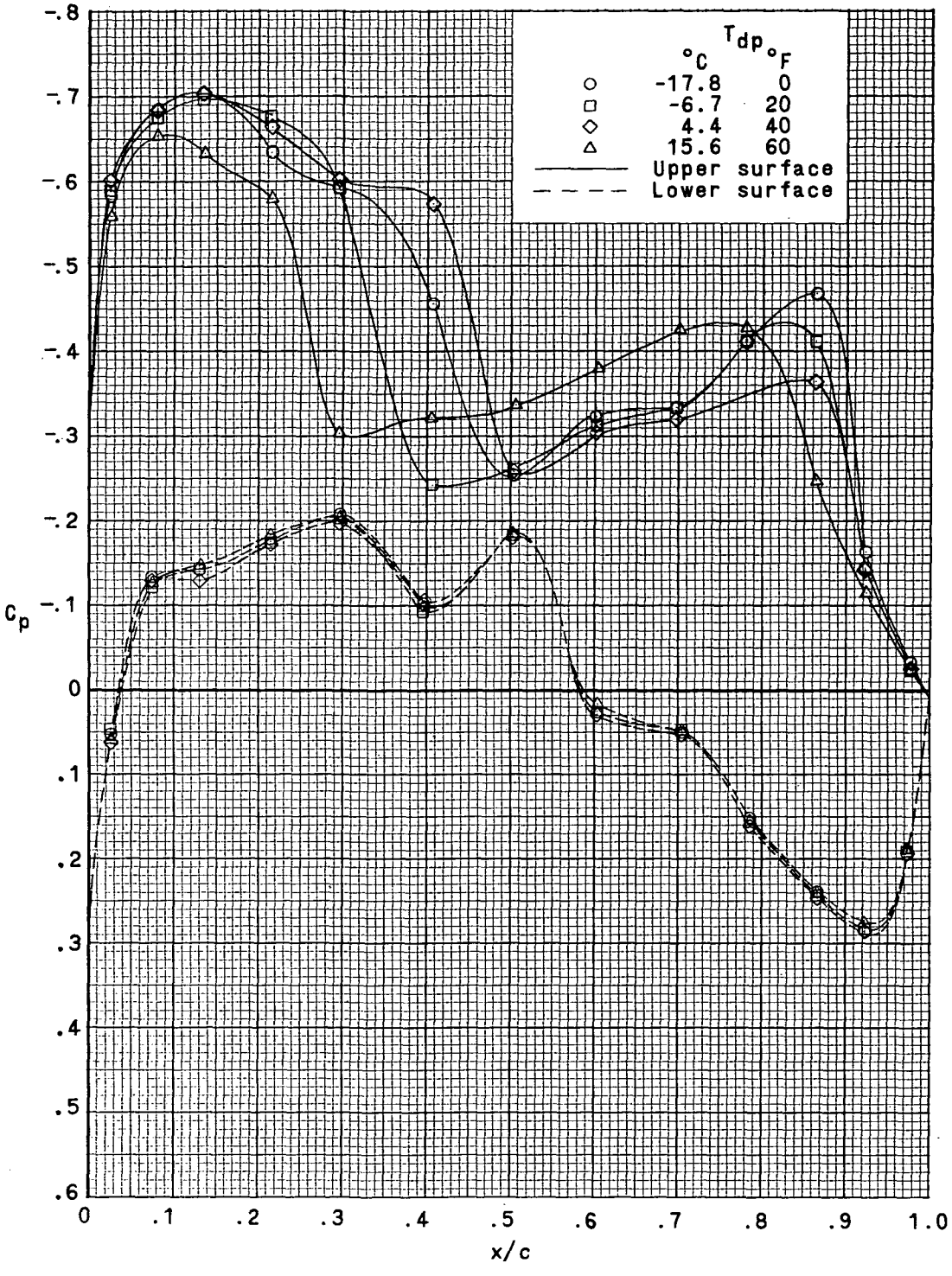

(d) c = 14.44 cm (5.686 in.); 65.3-percent-semispan station.

Figure 10.- Continued.

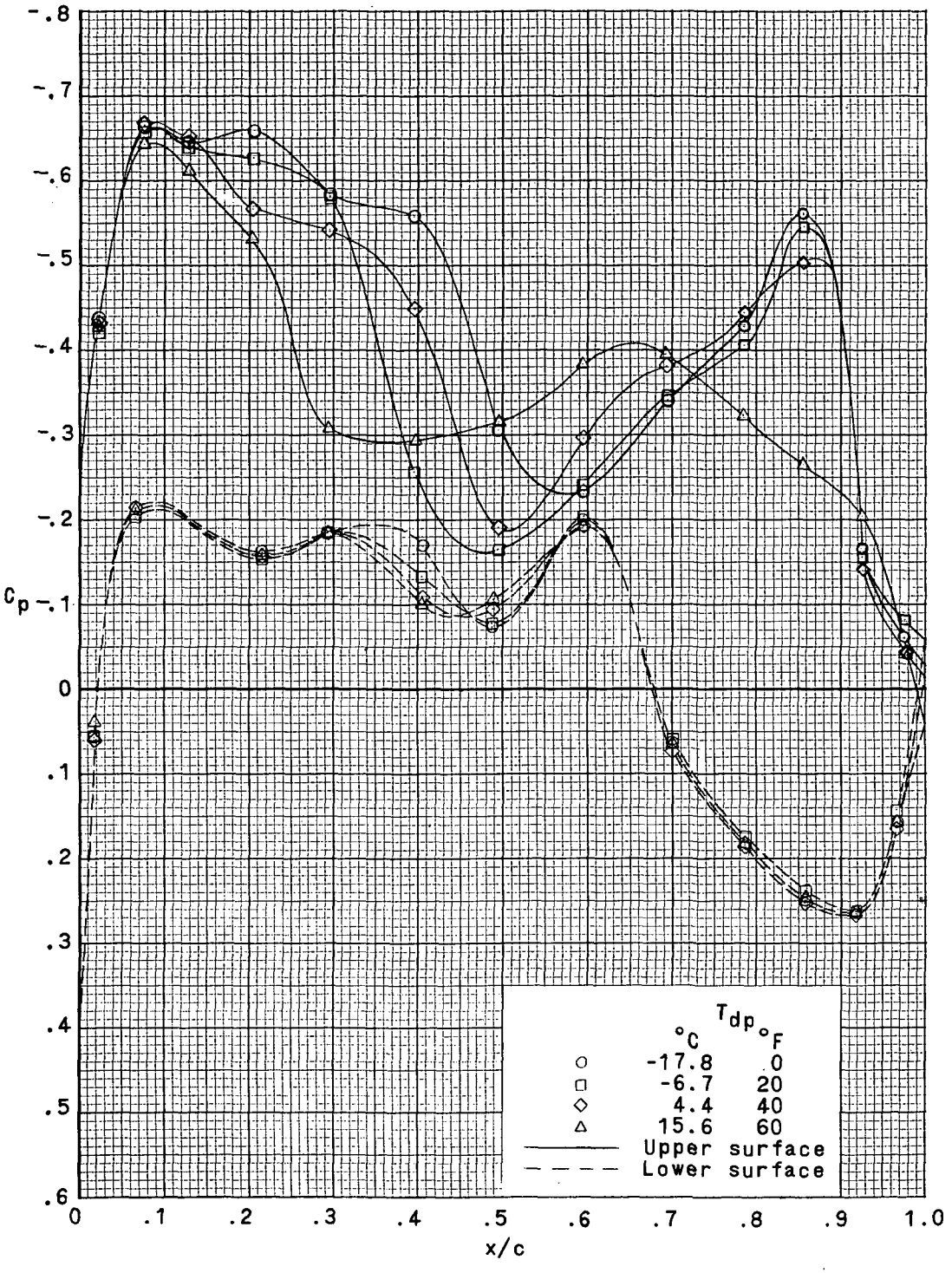

(e) c = 12.07 cm (4.752 in.); 80.4-percent-semispan station.

Figure 10.- Continued.

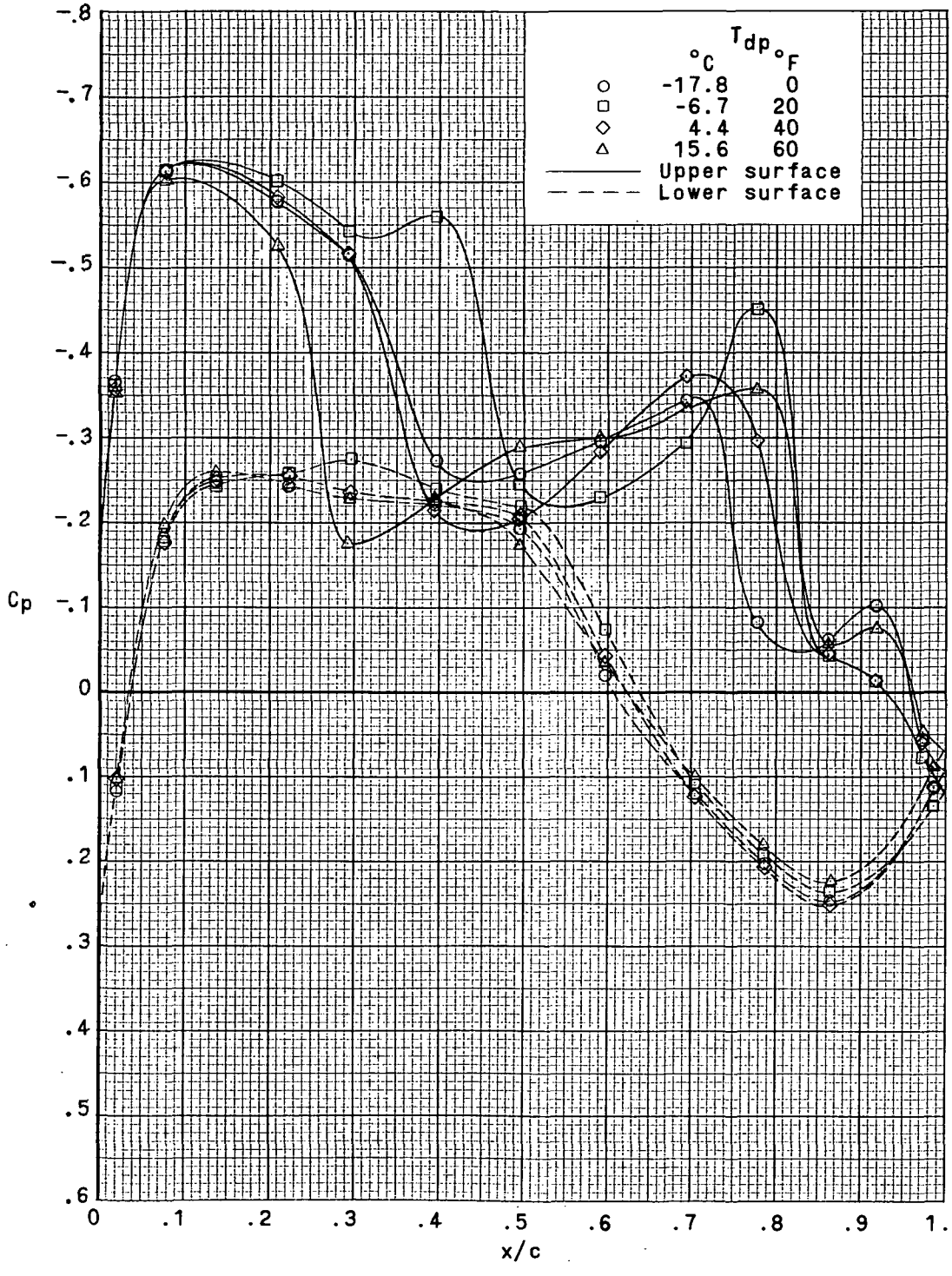

(f) c = 10.04 cm (3.954 in.); 93.3-percent-semispan station.

Figure 10.- Concluded.

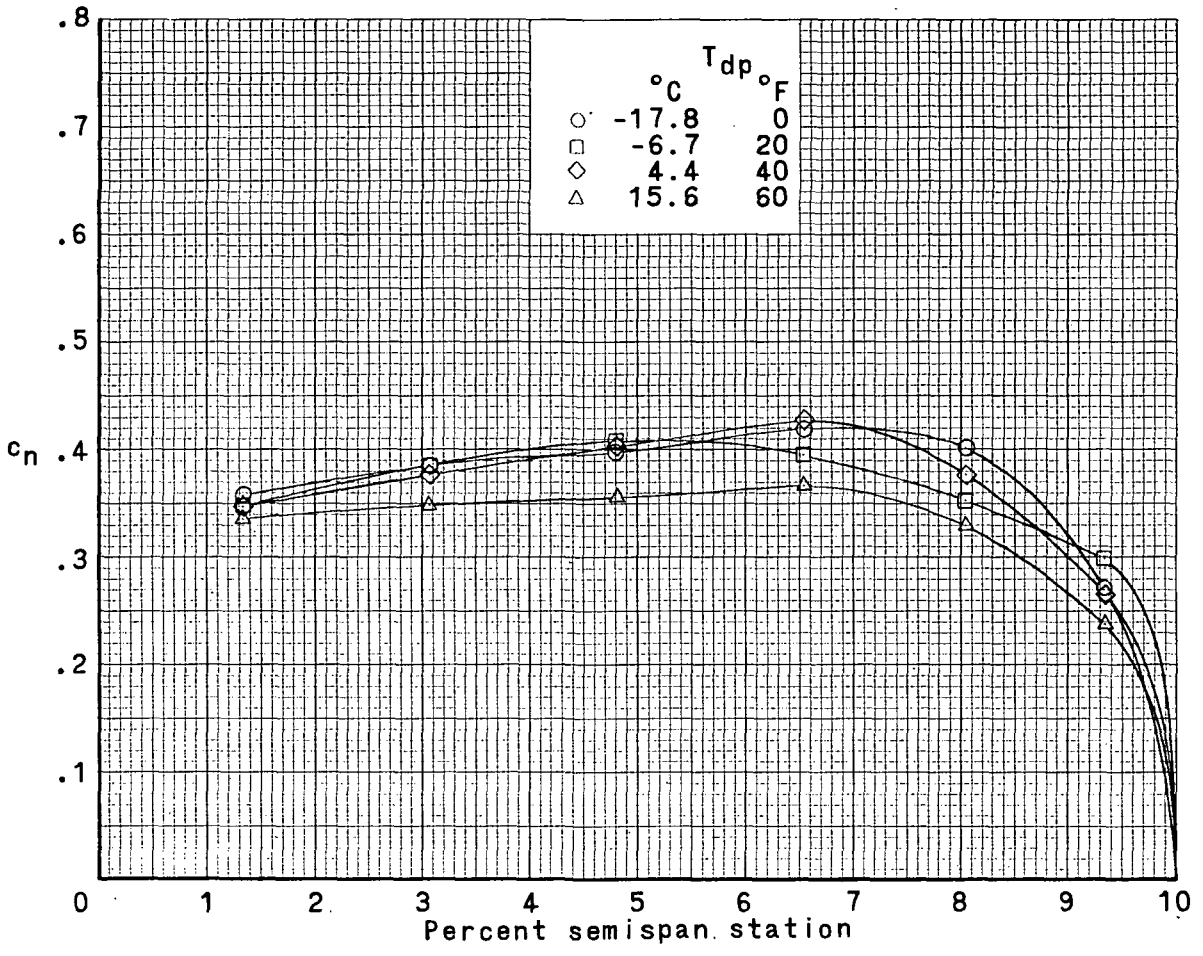

Figure 11.- Effect of wind-tunnel dewpoint on wing span load distribution at $\alpha = 2.7^{\circ}$. $M_{\infty} = 0.980$; $T_t = 48.9^{\circ}$ C (120° F).

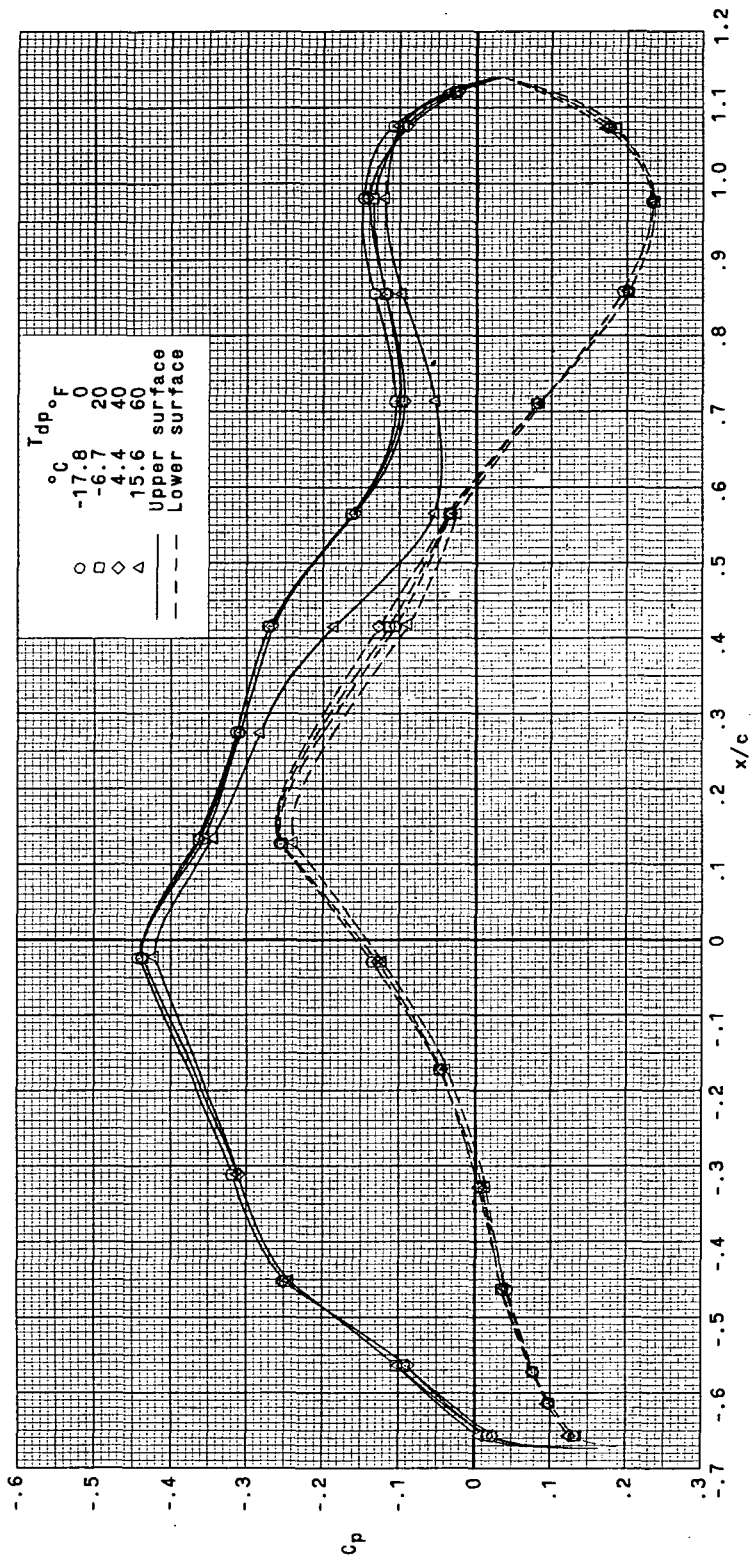

(a) c = 22.61 cm (8.903 in.); 13.3-percent-semispan station.

Figure 12.- Effect of wind-tunnel dewpoint on wing streamwise-chord pressure distributions at $\alpha = 3.3^{\circ}$. $M_{\infty} = 0.980$; $T_t = 48.9^{\circ}$ C (120° F).

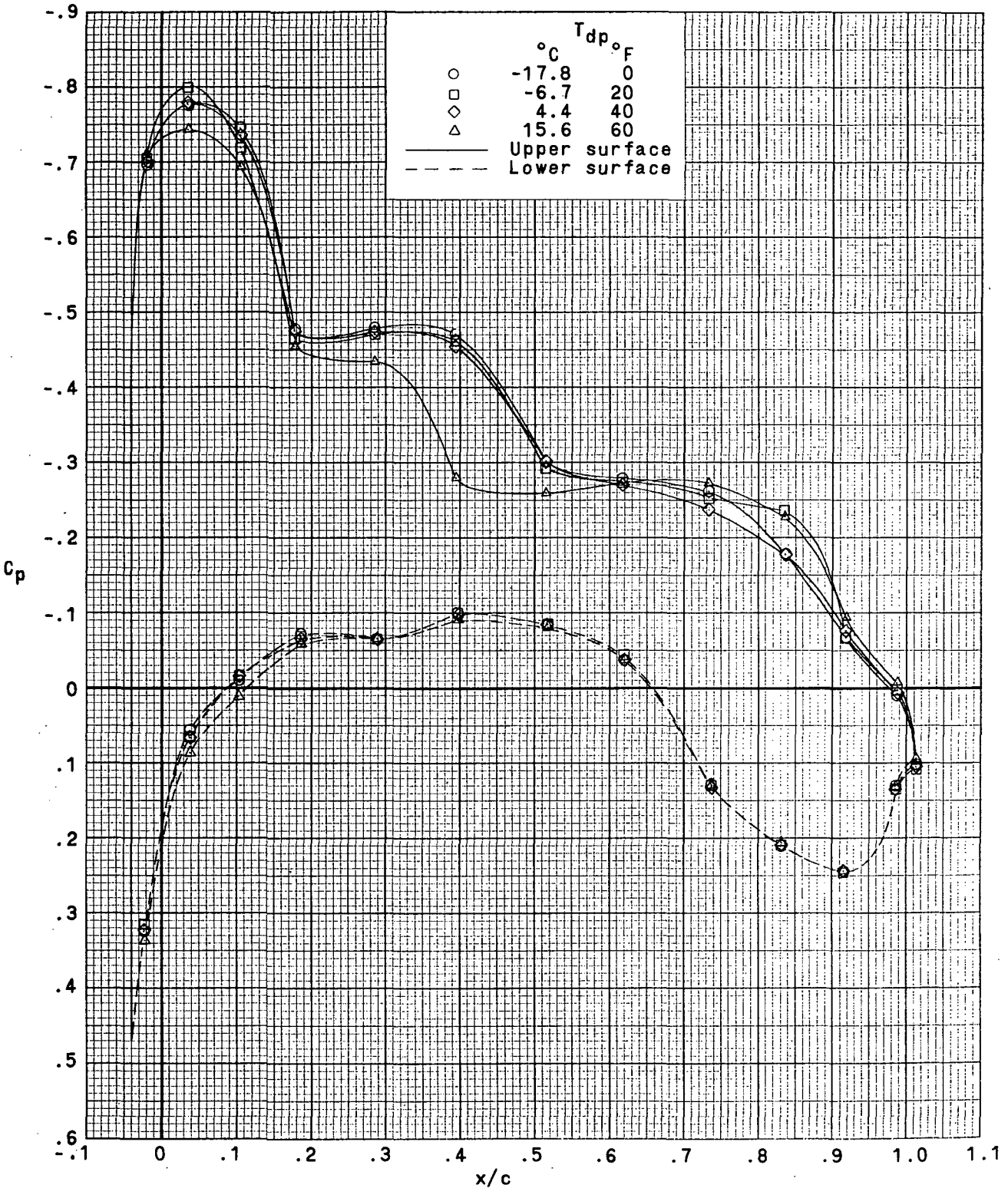

(b) c = 19.88 cm (7.828 in.); 30.7-percent-semispan station.

Figure 12.- Continued.

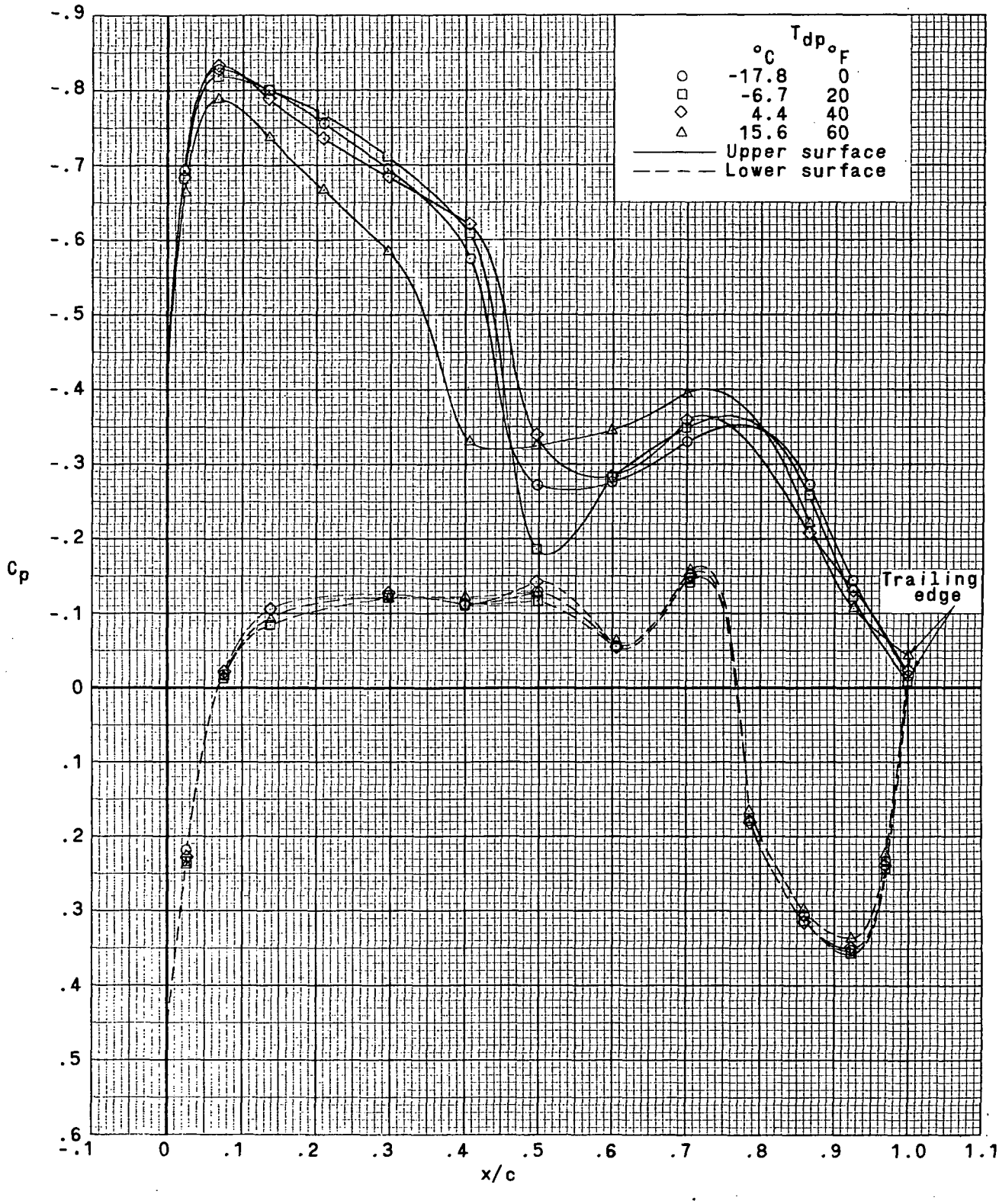

(c) c = 17.16 cm (6.756 in.); 48.0-percent-semispan station.

Figure 12.- Continued.

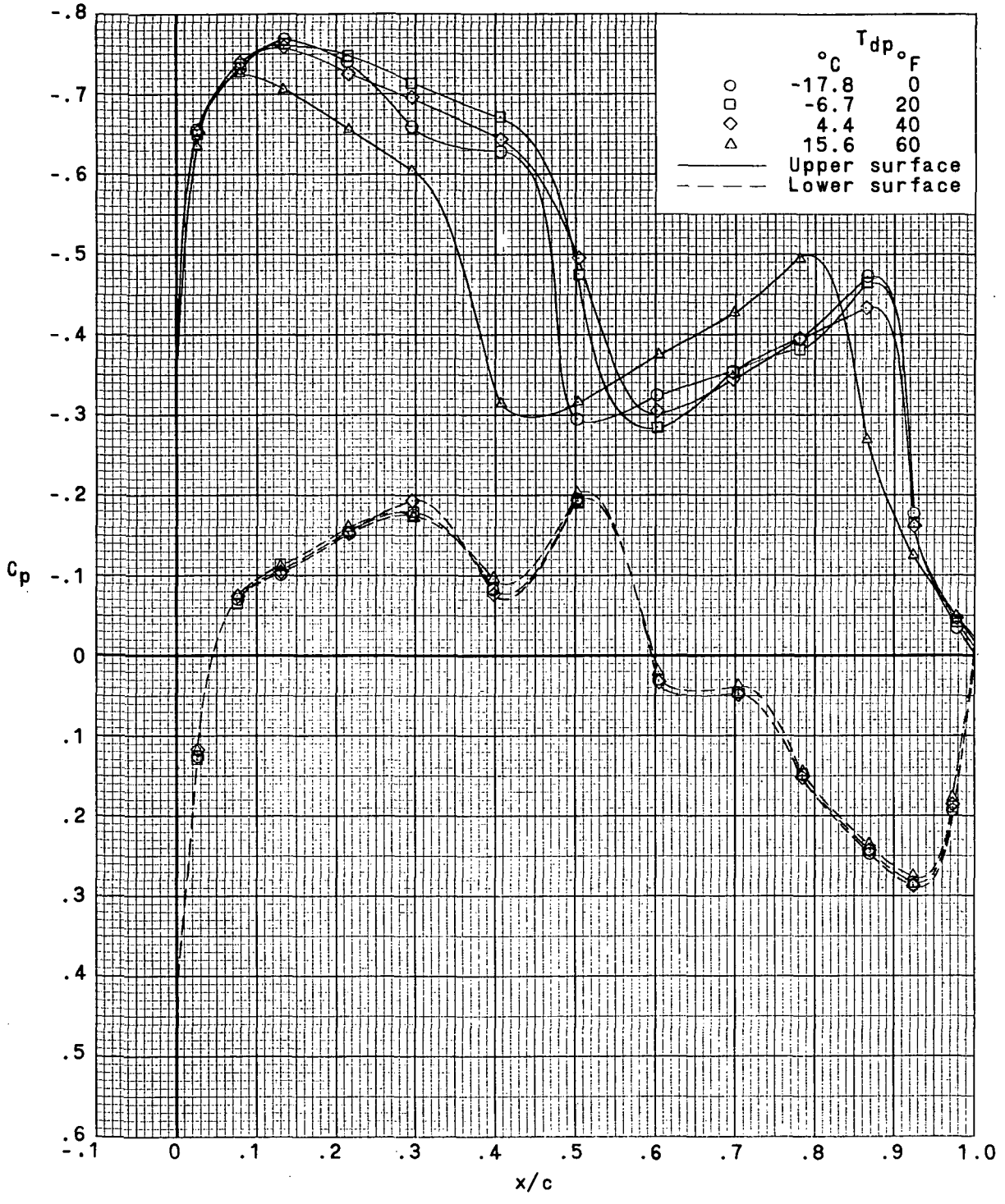

(d) c = 14.44 cm (5.686 in.); 65.3-percent-semispan station.

Figure 12.- Continued.

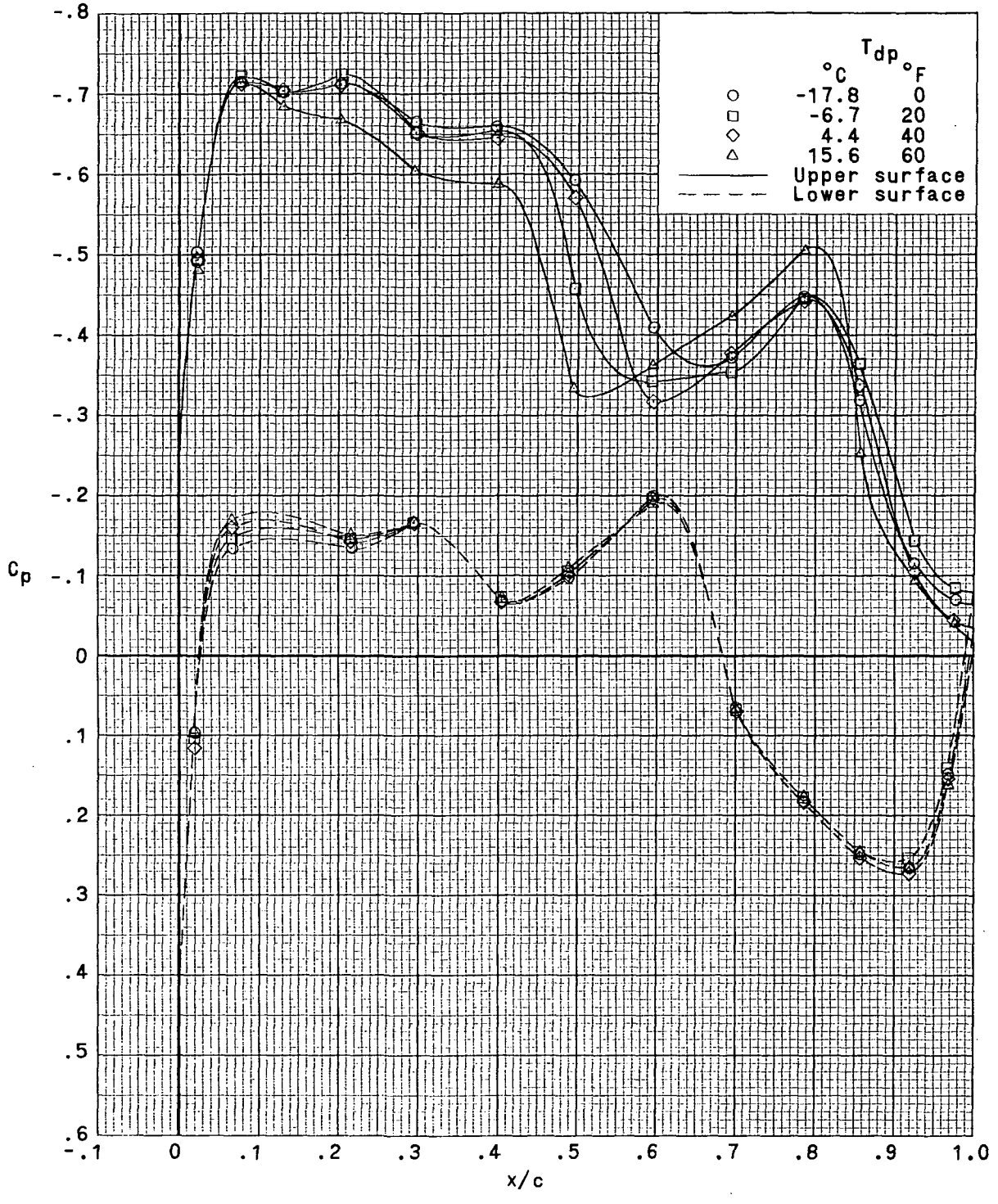

(e) c = 12.07 cm (4.752 in.); 80.4-percent-semispan station.

Figure 12.- Continued.

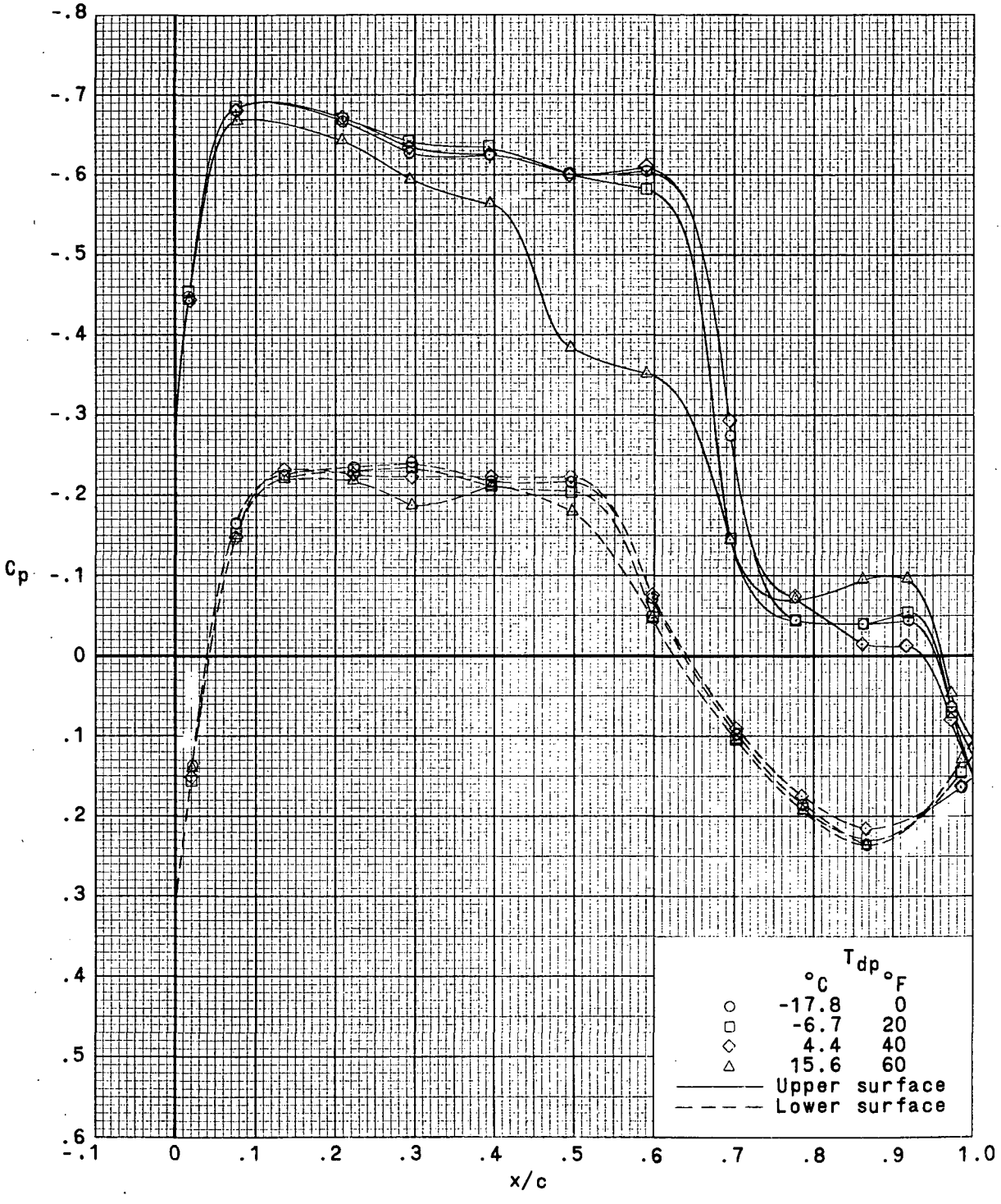

(f) c = 10.04 cm (3.954 in.); 93.3-percent-semispan station.

Figure 12.- Concluded.

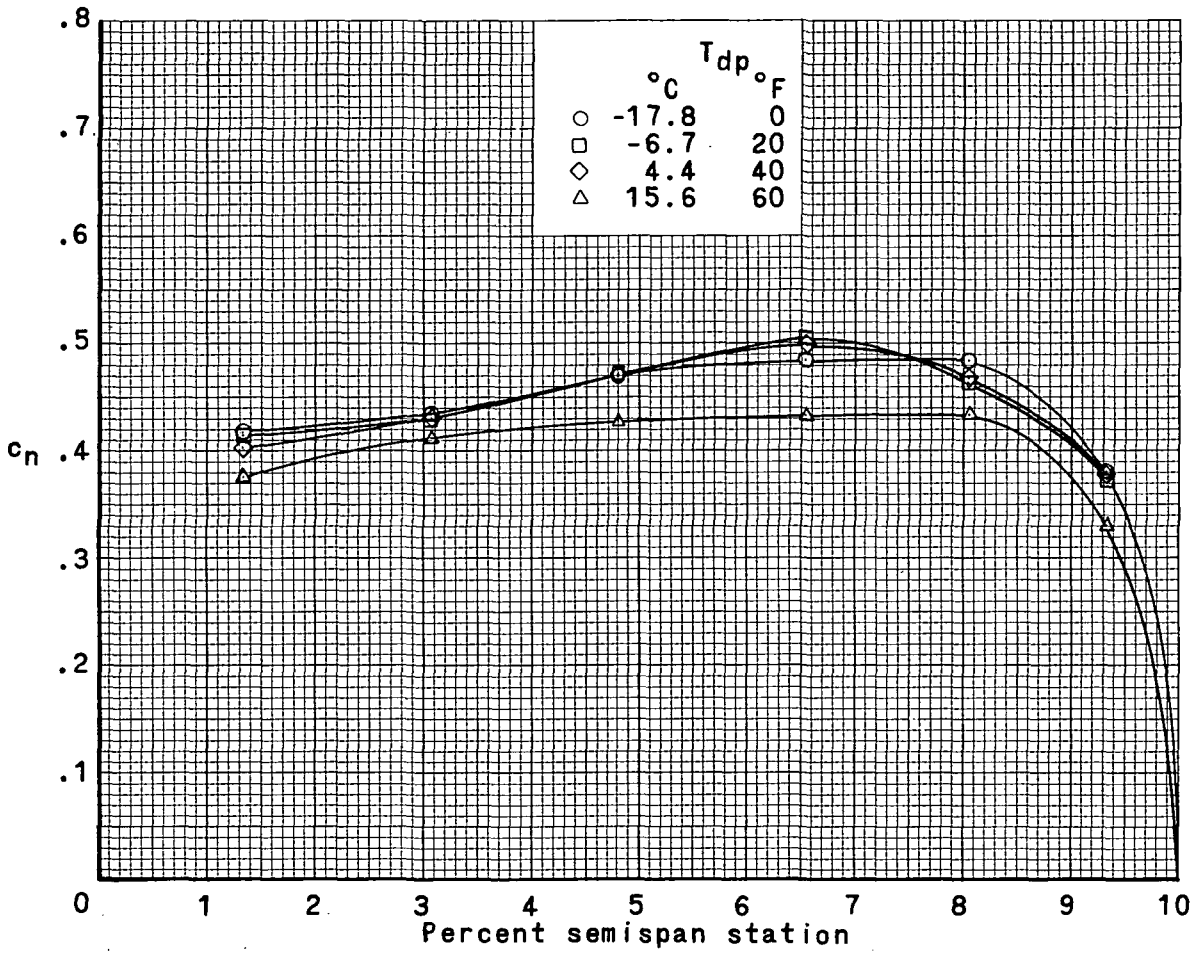

Figure 13.- Effect of wind-tunnel dewpoint on wing span load distribution at $\alpha = 3.3^{o}$. $M_{\infty} = 0.980$; $T_t = 48.9^{o}$ C (120^{o} F).

[redacted]

[redacted]

1. Report No. NASA TM X-2618	2. Government Accession No.	3. Recipient's Catalog No.
4. Title and Subtitle INVESTIGATION AT NEAR-SONIC SPEED OF SOME EFFECTS OF HUMIDITY ON THE LONGITUDINAL AERODYNAMIC CHARACTERISTICS OF AN NASA SUPERCRITICAL WING RESEARCH AIRPLANE MODEL (U)		5. Report Date August 1972 6. Performing Organization Code
7. Author(s) Frank L. Jordan, Jr.		8. Performing Organization Report No. L-8220
9. Performing Organization Name and Address NASA Langley Research Center Hampton, Va. 23365		10. Work Unit No. 767-73-01-04 11. Contract or Grant No.
12. Sponsoring Agency Name and Address National Aeronautics and Space Administration Washington, D.C. 20546		13. Type of Report and Period Covered Technical Memorandum 14. Sponsoring Agency Code

15. Supplementary Notes

16. Abstract

An investigation has been conducted in the Langley 8-foot transonic pressure tunnel to determine the effects of humidity at near-sonic speed on the longitudinal aerodynamic characteristics and wing pressure distributions of an area-rule research airplane model with an NASA supercritical wing. Effects of dewpoint at the normal tunnel operating stagnation temperature of 48.9° C (120° F) and effects of stagnation temperature at a relatively high dewpoint of 15.6° C (60° F) were investigated. The test tunnel stagnation pressure was 101 325 N/m^2 (1 atmosphere).

17. Key Words (Suggested by Author(s))

Wind-tunnel humidity effects at near-sonic speed
Supercritical wing

19. Security Classif. (of this report)	20. Securi
[redacted] Group 4	Uncl

GROUP 4
Downgraded at 3 year intervals; declassified after 12 years

within missio

"The aeronautical and space activities of the United States shall be conducted so as to contribute . . . to the expansion of human knowledge of phenomena in the atmosphere and space. The Administration shall provide for the widest practicable and appropriate dissemination of information concerning its activities and the results thereof."

— NATIONAL AERONAUTICS AND SPACE ACT OF 1958

NASA SCIENTIFIC AND TECHNICAL PUBLICATIONS

TECHNICAL REPORTS: Scientific and technical information considered important, complete, and a lasting contribution to existing knowledge.

TECHNICAL NOTES: Information less broad in scope but nevertheless of importance as a contribution to existing knowledge.

TECHNICAL MEMORANDUMS: Information receiving limited distribution because of preliminary data, security classification, or other reasons.

CONTRACTOR REPORTS: Scientific and technical information generated under a NASA contract or grant and considered an important contribution to existing knowledge.

TECHNICAL TRANSLATIONS: Information published in a foreign language considered to merit NASA distribution in English.

SPECIAL PUBLICATIONS: Information derived from or of value to NASA activities. Publications include conference proceedings, monographs, data compilations, handbooks, sourcebooks, and special bibliographies.

TECHNOLOGY UTILIZATION PUBLICATIONS: Information on technology used by NASA that may be of particular interest in commercial and other non-aerospace applications. Publications include Tech Briefs, Technology Utilization Reports and Notes, and Technology Surveys.

Details on the availability of these publications may be obtained from:

SCIENTIFIC AND TECHNICAL INFORMATION OFFICE

NATIONAL AERONAUTICS AND SPACE ADMINISTRATION

Washington, D.C. 20546